UNIVERSIDADE DE SÃO PAULO
INSTITUTO DE FÍSICA DE SÃO CARLOS

GABRIEL AUGUSTO DAS NEVES

Higher-order QCD in the decay Higgs to two photons

São Carlos

2021

GABRIEL AUGUSTO DAS NEVES

Higher-order QCD in the decay Higgs to two photons

Dissertation presented to the Graduate Program in Physics at the Instituto de Física de São Carlos, Universidade de São Paulo to obtain the degree of Master of Science.

Concentration area: Theoretical and Experimental Physics

Advisor: Prof. Dr. Diogo Rodrigues Boito

Original Version

São Carlos

2021

Neves, Gabriel Augusto das
Higher-order QCD in the decay Higgs to two photons / Gabriel Augusto das Neves; advisor Diogo Rodrigues Boito -- São Carlos 2021.
98 p.

Dissertation (Master's degree - Graduate Program in Theoretical and Experimental Physics) -- Instituto de Física de São Carlos, Universidade de São Paulo - Brasil , 2021.

1. Higgs boson. 2. Perturbative QCD. 3. Large- beta 0. 4. High-energy physics. I. Boito , Diogo Rodrigues, advisor. II. Title.

FOLHA DE APROVAÇÃO

Gabriel Augusto das Neves

Dissertação apresentada ao Instituto de Física de São Carlos da Universidade de São Paulo para obtenção do título de Mestre em Ciências. Área de Concentração: Física Básica.

Aprovado(a) em: 08/04/2021

Comissão Julgadora

Dr(a). Diogo Rodrigues Boito

Instituição: (IFSC/USP)

Dr(a). Adriano Antonio Natale

Instituição: (UNESP/São Paulo)

Dr(a). Orlando Luis Goulart Peres

Instituição: (UNICAMP/Campinas)

ACKNOWLEDGEMENTS

- Agradeço à minha família (Silvana, Pedro e Poliana) por todo o suporte durante todos os momentos da minha vida, principalmente durante os maus momentos. Muito obrigado mãe, pai e Pô.
- Agradeço à Anelisa pelo apoio às viagens. Muito obrigado, *vó*.
- I would like to thank Marina for her love, friendship and for helping me in my personal growth.
- I would like to thank Diogo for his patience and all the teachings (since my Scientific Initiation); my Masters dissertation was a roller coaster and he always tried to figure a way out of the dead ends.
- I would like to thank Jan Piclum for his hospitality, patience and all the teachings.
- Thanks a lot to Rep Zeppelin (and aggregates) for all the good times, laughs, teachings, Bavárias and crazy stories.
- I would like to thank Bilu for useful discussions, mainly the ones about life.
- I would like to thank Pestana for very useful physics discussions.
- I would like to thank IFSC for all their support during my undergraduation and Master dissertation.
- I would like to thank the Particle Physics Group at the University of Siegen for their cordiality during my stay there.
- I would like to thank FAPESP for the financial support of this dissertation (PROCESS 2018/12305-4).

Without you, this work would not be finished.

ABSTRACT

NEVES, G. A. **Higher-order QCD in the decay Higgs to two photons**. 2021. 98 p. Dissertation (Masters in Science) - Instituto de Física de São Carlos, Universidade de São Paulo, São Carlos, 2021

In the absence of direct observation of Physics Beyond Standard Model at the LHC, precise tests of the theory require increasing accuracy. The decay width of the Higgs boson into photons is known, incompletely, at the 5-loop level, i.e. N4LO in the strong coupling, α_s^4, while the exact knowledge of the QCD corrections is up to N2LO or the 3-loop level. In this work, we calculated, for the first time, the effect due to higher-order QCD corrections in the decay $H \to \gamma\gamma$ through the so-called large-β_0 limit, in which the corrections from the leading-n_f terms are known to all orders in α_s. The analysis of the series' singularities in Borel space enable us to study, in a semi-qualitative way, the series behaviour with respect to variations of the renormalization scale. Furthermore, we calculated the Borel sum due to the contribution of the leading-n_f diagrams, trying to understand the significance of the diagrams which are sub-leading in n_f, and the optimal renormalization energy scale to compute the QCD corrections of $\Gamma(H \to \gamma\gamma)$. Finally, we estimated the magnitude of the next QCD correction as well as the error due to truncation of the series with the known perturbative corrections in QCD.

Keywords: Higgs boson. Perturbative QCD. Large-β_0. High-energy physics.

RESUMO

NEVES, G. A. **QCD perturbativa em ordens altas no decaimento Higgs em dois fótons**. 2021. 98 p. Dissertação (Mestrado em Ciências) - Instituto de Física de São Carlos, Universidade de São Paulo, São Carlos, 2021

Na ausência de observação direta de física além do modelo padrão no LHC, testes precisos da teoria requerem precisão cada vez maior. A largura de decaimento do bóson de Higgs em fótons é conhecida, de forma incompleta, até quarta ordem no acoplamento forte, α_s^4, enquanto o conhecimento exato das correções é conhecido até segunda ordem (N2LO). Neste trabalho, calculamos, pela primeira vez, os efeitos devidos a correções de QCD de ordens superiores no decaimento $H \to \gamma\gamma$ através do chamado limite large-β_0, no qual as correções advindas dos termos dominantes em n_f são conhecidas em todas as ordens em α_s. A análise das singularidades da série no espaço de Borel nos permite estudar, de forma semi-qualitativa, o comportamento da série com as variações da escala de energia. Além disso, calculamos a soma de Borel da série devido à contribuição dos diagramas leading-n_f, procurando entender a significância dos diagramas ignorados, i.e. o quão relevante são os diagramas sub-dominantes em n_f, e a melhor escala de energia para estimar as correções de QCD do processo $\Gamma(H \to \gamma\gamma)$. Por fim, estimamos a magnitude da próxima correção em QCD bem como o erro de truncamento da série com o conhecimento atual das correções perturbativas.

Palavras-chave: Bóson de Higgs. QCD perturbativa. Large-β_0. Física de altas energias.

LIST OF FIGURES

LIST OF TABLES

CONTENTS

1 INTRODUCTION

The Standard Model (SM) of Particle Physics is one of the greatest achievements in the history of Physics. It describes three out of the four fundamental forces in nature: Strong, Electromagnetic and Weak interactions. The only exception is gravity, which does not have a complete quantum formulation entirely consistent.

Although it is hard to stipulate an initial date, the work of Paul Dirac describing the interaction between matter and radiation in the late 20s[1] initiated the study of fundamental particle interactions. The construction of the SM went throughout the 20th century with contributions from several of the greatest physicists of all times: Fermi[2], Feynman, Schwinger and Tomonaga (who developed Quantum Electrodynamics (QED) to be the most precise theory in physics to date[3–5]), Yang and Mills (who developed a gauge theory for non-Abelian groups transformations[6]), Glashow, Weinberg and Salam (who combined electromagnetic and weak interactions[7–9]), Englert, Brout and Higgs (who developed a mechanism for allowing massive gauge bosons[10,11]), Fritzsch, Gell-Mann and Leutwyler (who supported QCD and the existence of quarks which combined themselves into color singlets to give rise to the plethora of observed particles[12,13]) among others.

Alongside the theoretical progress, experimental particle physics developed enormously and the various accelerators built around the world provided experimental evidence that the theory under construction was sound. Particle after particle, the fundamental constituents of the SM were discovered enhancing with that the model's status as a solid theoretical framework.

However, one of its main ingredients — the Higgs boson — remained unobserved. The particle which enables all massive content in the theory (and thus its coherence) could not be observed, in spite of the international community effort — the advent of more energetic colliders was enabling the search for the Higgs boson at higher energy scales (and with increasing detection sensibility) to no avail.

This scenario changed in 2012, when the Large Hadron Collider (LHC) announced the observation of a scalar particle which was identified as the long-sought Higgs boson[14,15]. The next logical step, after its announcement, was the measurement of its properties. So far, the Higgs boson announced agrees with the one predicted theoretically more than half a century ago[14,16].

However, the experimental accuracy is increasing in a rapid pace, and thus precise theoretical calculations become a must in order to match with results obtained in the laboratory. In this context, higher-order calculations are mandatory for testing the correctness and the limits of the (now) well established Standard Model.

To obtain precise theoretical results, Quantum Chromodynamics (QCD) higher-order

calculations are very important, since strong corrections almost always dominate over the sub-leading Electroweak (EW) corrections. Unfortunately, QCD is a very involved theory and its perturbative higher-order calculations are extremely hard to compute. Thus, a viable alternative is to resort to Effective Field Theories (EFT) which try to incorporate many of the main theory aspects when applied to some limits; it is important to keep in mind that these EFTs do not have a global reach: they are intended to explain the physics in certain energy scales which in turn can augment our physics understanding and, in some cases, enable us to predict experimental results with accuracy.

One of the possible EFTs covers the scenario in which one of the masses in the problem is much heavier than the remaining scales. When this is the case, one can expand the calculation in powers of $(1/m_h^2)^p$, where m_h is the heavy scale; this expansion is intended to simplify the original calculations. Then, the resulting expression is a series in which each term presents a correction of the order of $1/m_h^2$; in the limit when we take the heavy-scale to infinity, only the leading-order term contributes. In this scenario, we say that the heavy degree of freedom (d.o.f.) was integrated out of the theory. Thus, interactions mediated by the exchange of heavy particles are interpreted as contact interactions. It is important to note that, the more the gap between the heavy scale and the remaining ones, the better the effective theory becomes: lets say that $m_l^2/m_h^2 \simeq 0.01$, with m_l a light d.o.f. in the problem; then, the leading-order (LO) term is already a very good approximation and further corrections will amount to approximately 1% of the value in the full theory.

Another interesting limit to study higher-order QCD corrections is the so-called large-β_0 limit. In this scenario, first one considers the limit in which the number of flavours in the theory goes to infinity while keeping the product $n_f\alpha_s \sim \mathcal{O}(1)$ constant. It is argued that in some cases the real scenario is not very different from the scenario where $n_f \to \infty$[17]. After that, one proceeds to the large-β_0 limit, in which $\beta_{0,f}$ — the contribution to the first β-function term due to fermions — is substituted by the full first coefficient of β, β_0. This procedure yields good qualitative insights as well as it is a good approximation in various processes[18]; Thus, through the large-β_0 limit, one can expect to understand the series behaviour at higher-orders. We note, however, that since this procedure is not an EFT (there is no matching conditions, for example), there is no guarantee of its success as well as no mathematical proof of its validity. Its theoretical status as an interesting limit of QCD is mainly based on the successful applications to several different processes[19–23]

To study the Higgs-boson properties, an interesting process is the Higgs decay into two photons, since it is one of the main channels at the LHC. Due to its low-background, it is an easily detected channel, even though it is not among the leading decay channels. In this decay, because the final particles are massless and the Higgs boson couples only to massive particles, the leading-order (LO) process already happens at the 1-loop level, mediated by fermion triangle-loops; furthermore, the transition amplitude is dominated by the top-quark loop[24], since the top-quark mass is two orders of magnitude larger than the

second-to-most heavy quark — the bottom-quark — and the Higgs coupling to fermions is proportional to the fermion mass.

In this work, we study the decay of the Higgs boson into two photons in the heavy top-quark limit — in our case, the expansion parameter is $\tau_t \equiv M_H^2/4m_t^2 \approx 0.13$, where M_H is the Higgs mass while m_t is the top mass, our heavy scale. In our analysis, we calculated the leading-n_f terms for the decay to all orders in perturbation theory in QCD, a result which is not present in the literature to the best of our knowledge. With this result, we proceeded to the large-β_0 limit, where, in our conventions, we substituted $n_f \to 6\pi\beta_0$. The analysis of the resulting series and the comparison with the original QCD series enabled us to try to answer quantitative questions as 'what is the magnitude of the next QCD correction' or 'what is the error in the perturbative truncation of the series', as well as qualitative insights about the series behaviour. Our result suggests that uncertainties due to the perturbative QCD corrections are sub-leading when compared to the uncertainties due to parameters used in the calculation of the observables (such as the strong coupling, α_s).

This work is organized as follows: in Sec. 2 we construct the Standard Model with its basic properties; in Sec. 3 we focus on the strong interaction and its peculiarities, as well as the limit in which we will perform our calculation. in Sec. 4 we analyze the Higgs sector in the SM and introduce its main features to enable us to develop our calculation. In Sec. 5 we introduce in detail the program used for the calculations; in Sec. 6 we present the results obtained as well as discussions about further calculations from the results. Finally, we end this work in Sec. 7 with the conclusions.

2 THE ELECTROWEAK STANDARD MODEL LAGRANGIAN

In this chapter we aim at developing the relevant sectors of the electroweak SM Lagrangian for this work in a concise and self-consistent way. This chapter is based on Refs.[24,25].

The SM Lagrangian contains all elementary degree of freedom. The fundamental fields are the three fermion families (shown in Tab. 1), eight gluons, g, which are the gauge bosons responsible for the strong force, the gauge bosons of the electroweak interaction, $W^{\pm}$, Z and γ, along with a scalar particle, the Higgs boson. The strong and EW interactions are constructed through the *gauge principle* applied to the Dirac Lagrangian describing the free fermions. However, due to different transformation properties between left- and right-handed fields, these fermion fields are treated as massless. In the context of the SM, to generate the masses of all massive particles — the gauge bosons $W^{\pm}$, Z and all fermions —, a new scalar particle needs to be introduced, the Higgs boson. Allowing the Higgs boson to acquire a nonzero vacuum expectation value (vev) through a self-interaction potential, one is able to spontaneously break the symmetry — which is interpreted as choosing a specific vacuum state among all possible states — and generate the masses of the $W^{\pm}$ and Z, while keeping the photon massless. Through Yukawa couplings with the fermions, the same scalar field provides mass to these particles and the mass generation in the SM is completed.

This procedure shows the central role of the Higgs boson in the theory — without it, it would be impossible to have massive particles in the SM Lagrangian. The Higgs boson then becomes an active degree of freedom of the SM and generates a new sector with its own phenomenology. The Higgs sector will be explored in Section 4.

We start this chapter with the gauge principle, introducing the Yang-Mills theory (non-Abelian, $SU(N)$ symmetry). Then we focus on the more complex structure of the EW sector, based on the $SU(2)_L \times U(1)_Y$ gauge symmetry. After the introduction of the gauge fields, we identify the known EW gauge bosons as linear combinations of the original $SU(2)_L \times U(1)_Y$ gauge fields. Finally, the Higgs boson is introduced with its mechanisms of mass generation in the theory.

2.1 The gauge principle

The gauge principle is the underlying symmetry principle in the Standard Model; it is based on the invariance of the theory under local gauge transformations. In the case of the SM, the underlying symmetry group is $SU(3)_C \times SU(2)_L \times U(1)_Y$, where the sub-index C refers to *color*, the strong interaction charge, L refers to *left-handiness*, which is the quality of the particles described by $SU(2)$ doublets, and Y refers to the hypercharge, the quantum

Table 1 – Fermions present in the SM divided into families.

Family	Leptons	Quarks
1st	ν_e, e	u, d
2nd	ν_μ, μ	c, s
3rd	ν_τ, τ	t, d

Source: By the author.

number of the $U(1)$ symmetry group. Therefore, the $SU(3)_C$ gauge invariance will give rise to the strong interactions, while the $SU(2)_L \times U(1)_Y$ gives rise to the Electroweak interaction.

When we impose the Lagrangian to be invariant under a gauge transformation, we are forced to introduce new fields in the theory interacting with the original fermion fields — the so-called gauge boson fields —, and with certain transformation properties. The reason why we need to introduce a new scalar particle in the theory, the Higgs boson, is due to the fact that the gauge principle performed on a Dirac Lagrangian only admits the introduction of massless gauge bosons, i.e., it is a perfect good symmetry for QCD and QED, where the gluons and photons do not have mass, but does not work for the weak sector of the SM, where the gauge bosons are massive[26]; the mass term for these bosons would spoil the symmetry.

In this section, we will introduce the Yang-Mills theory, which will present qualitative features which will enable us to understand the more robust EW sector of the SM Lagrangian.

2.1.1 Yang-Mills theory

The Yang-Mills theory incorporates the gauge principle for non-Abelian $SU(N)$ group transformations. Since $U(1)$ is a subgroup of $SU(N)$ and is the symmetry involved in QED, Quantum Electrodynamics is already present in the development we will present here.

Consider the Lagrangian for a massless Dirac field,

$$\mathscr{L}_f^0 = \bar{\psi} i\gamma^\mu \partial_\mu \psi. \tag{2.1}$$

Now, assume a gauge transformation in the field ψ,

$$\psi \to \psi' = U\psi, \qquad U = e^{i\theta^a T^a}, \tag{2.2}$$

where the T^a's are the generators of the underlying Lie algebra $su(N)$.[I] The properties of

[I] We represent the group by upper-case letters, while the underlying Lie algebra are represented by lower-case letters.

the special unitary group elements are such that

$$UU^\dagger = U^\dagger U = \mathbb{1}, \qquad \det(U) = 1.$$

The Lagrangian is clearly invariant under global $SU(N)$ transformations, but not under local ones: if we let θ^a to be a function of the space-time coordinate, $\theta^a(x)$, then the new Lagrangian reads

$$\mathscr{L}_f^0 \to (\mathscr{L}_f^0)' = \bar{\psi} i\gamma^\mu [iT^a(\partial_\mu \theta^a(x) + \partial_\mu]\psi. \tag{2.3}$$

Thus we introduce the *covariant derivative*, D_μ, as

$$D_\mu = \partial_\mu + igT^a G_\mu^a. \tag{2.4}$$

Note that, in this definition, we incorporated $N^2 - 1$ new vector fields G_μ^a in the theory, since $su(N)$ possess $N^2 - 1$ generators. With this new derivative, the Lagrangian

$$\mathscr{L}_f = \bar{\psi} i\gamma^\mu D_\mu \psi \tag{2.5}$$

transforms as

$$\begin{aligned} \mathscr{L}_f \to (\mathscr{L}_f)' &= \bar{\psi} U^\dagger (i\gamma^\mu [\partial_\mu + igT^a (G_\mu^a)'])U\psi \\ &= \bar{\psi} U^\dagger [i\gamma^\mu (\partial_\mu U)\psi + i\gamma^\mu U \partial_\mu \psi] - gT^a \bar{\psi} U^\dagger \gamma^\mu (G_\mu^a)' U\psi. \end{aligned} \tag{2.6}$$

The gauge principle states that *the Lagrangian needs to be invariant under local gauge transformations.* Thus, to satisfy this principle we demand that the new degrees of freedom G_μ^a transform so as to cancel the extra terms,

$$G_\mu^a \to (G_\mu^a)' = UG_\mu^a U^\dagger + \frac{i}{g} \frac{T^a}{(T^b T^b)} (\partial_\mu U) U^\dagger. \tag{2.7}$$

With these definitions, the new Lagrangian transforms under a local $SU(N)$ group element as

$$\mathscr{L}_f \to (\mathscr{L}_f)' = \bar{\psi}(i\gamma^\mu D_\mu)\psi = \mathscr{L}_f. \tag{2.8}$$

Thus, we were able to develop a Lagrangian invariant under local $SU(N)$ transformations. We begin to analyze the resulting Lagrangian by noticing that there is only one type of interaction vertex between the fermions and the gauge bosons,

$$\mathscr{L}_{Gf\bar{f}} = -gG_\mu \bar{\psi} \gamma^\mu \psi, \tag{2.9}$$

where we defined $G_\mu \equiv G_\mu^a T^a$. But, remember, we introduced new spin-1 gauge fields; if we want these spin-1 gauge fields to be real propagating fields, we must introduce a kinetic term involving at least first derivatives on G_μ^a. This process is tricky for non-Abelian fields,

because the G_μ's do not commute among themselves. To circumvent this, note that, with our definition of D_μ, we obtain the transformations for the covariant derivative such that it cancels the transformations of the fermion fields. Explicitly, the net result is

$$D_\mu \to D'_\mu = U D_\mu U^\dagger \implies [D_\mu, D_\mu] \to U[D_\mu, D_\nu]U^\dagger. \tag{2.10}$$

With this in mind, we introduce the field strength tensor, $G_{\mu\nu}$, as

$$G_{\mu\nu} = -\frac{i}{g_s}[D_\mu, D_\nu] = \partial_\mu G_\nu - \partial_\nu G_\mu + i g_s [G_\mu, G_\nu]. \tag{2.11}$$

From our definition, the contraction of the field strength tensor with itself transforms under a $SU(N)$ gauge transformation as

$$G_{\mu\nu}G^{\mu\nu} \to (G_{\mu\nu})'(G^{\mu\nu})' = U G_{\mu\nu} G^{\mu\nu} U^\dagger. \tag{2.12}$$

This is not yet invariant under $SU(N)$ transformations, but due to the cyclic property of the trace, we can construct a $SU(N)$ invariant Lagrangian piece for the kinetic term of the gauge boson field involving derivatives of the fields as

$$\mathscr{L}_b = -\frac{1}{2}\mathrm{Tr}(G_{\mu\nu}G^{\mu\nu}). \tag{2.13}$$

Assuming we work in a basis in which the generators are such that

$$\mathrm{Tr}(T^a T^b) = \frac{1}{2}\delta^{ab},$$

the resulting Lagrangian reads

$$\mathscr{L}_b = -\frac{1}{4} G^a_{\mu\nu} G^{\mu\nu,a}. \tag{2.14}$$

Adding the fermion Lagrangian with the gauge bosons kinetic term, we obtain the massless Yang-Mills Lagrangian, $\mathscr{L}^{m=0}_{\mathrm{YM}} = \mathscr{L}_f + \mathscr{L}_b$,

$$\mathscr{L}^{m=0}_{\mathrm{YM}} = -\frac{1}{4} G^a_{\mu\nu} G^{\mu\nu,a} + \bar{\psi} i\gamma^\mu D_\mu \psi. \tag{2.15}$$

Note that, due to the non-commutativity of the generators, the kinetic term has a part that reads

$$ig[G_\mu, G_\nu] = i g_s G^a_\mu G^b_\nu [T^a, T^b] = -g f^{abc} G^a_\mu G^b_\nu T^c.$$

Therefore, when we contract $G_{\mu\nu}G^{\mu\nu}$, there will appear terms containing products of three and four gauge fields, i.e., the gauge bosons interact among themselves, in diagrams with three and four legs, as depicted in Fig. 1. The three-boson interaction has the same

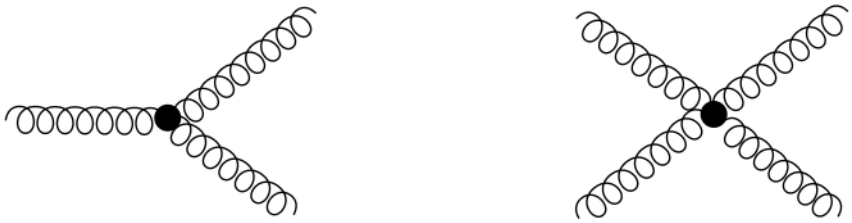

Figure 1 – Feynman diagrams for the three- and four-glouon-vertex which arise from the non-commutativity of the $SU(3)_C$ symmetry group.

Source: By the author.

strength as the one between fermions and gauge particles, given by g (and the group's structure constant). The four-boson vertex has a coupling constant g^2, the square of the original coupling constant. This is the main difference between Abelian and non-Abelian gauge theories — the gauge bosons are charged.[II] As a consequence, since there are more interactions in the Yang-Mills theory than in Abelian theories, the calculation of higher order diagrams becomes more and more complicated (and abundant) as we go farther in perturbation theory. An example of a Yang-Mills theory is QCD, in which the gauge group is the $SU(3)_C$ group.

2.2 The Electroweak sector

We now turn our attention to the construction of the EW sector of the SM Lagrangian. The EW matter content is composed by $SU(2)$ left-handed doublets and $SU(2)$ right-handed singlets[III],

$$L \equiv \begin{pmatrix} \nu_\ell \\ \ell \end{pmatrix}_L, \quad Q \equiv \begin{pmatrix} u \\ d \end{pmatrix}_L, \quad \nu_{\ell R}, \quad \ell_R, \quad u_R, \quad d_R. \tag{2.16}$$

The symmetry group under which we will demand gauge invariance is $SU(2)_L \times U(1)_Y$, where L refers to the left-handiness and Y refers to the hypercharge. The Lagrangian invariant under a global $SU(2)_L \times U(1)_Y$ gauge transformation is defined as

$$\begin{aligned} \mathscr{L}^0_{\text{EW}} = {} & \bar{L} i\gamma^\mu \partial_\mu L + \bar{Q} i\gamma^\mu \partial_\mu Q + \bar{\nu}_{\ell R} i\gamma_\mu \partial_\mu \nu_{\ell R} \\ & + \bar{\ell}_R i\gamma^\mu \partial_\mu \ell_R + \bar{u}_R i\gamma^\mu \partial_\mu u_R + \bar{d}_R i\gamma^\mu \partial_\mu d_R. \end{aligned} \tag{2.17}$$

[II] For QED, the development is exactly identical as the one presented here. However, the gauge group for QED is $U(1)$, i.e. it is an Abelian theory. Therefore, if we assume A_μ to be the gauge field introduced, we note that $[A_\mu, A_\nu] = 0$ and thus the gauge fields do not interact among themselves — they do not possess charge. The rest of the conclusions remain valid for the Abelian case.

[III] For simplicity, we are just considering a single fermion family. However, the theory developed here can be straightforwardly generalized to three families.

Under a $SU(2)_L \times U(1)_Y$ transformation, the lepton fields transform as

$$\begin{cases} L \to L' = e^{iY_L\beta} U_L L, \\ \nu_{\ell R} \to \nu'_{\ell R} = e^{iY_\nu \beta} \nu_{\ell R}, \\ \ell_R \to \ell'_R = e^{iY_\ell \beta} \ell_R, \end{cases} \tag{2.18}$$

with similar transformations for the quark sector. In the above expression, $U_L = e^{iT^a\theta^a}$ is a $SU(2)_L$ element, with T^a the generators of the Lie algebra $su(2)$. We proceed in a similar fashion as in the Abelian and Yang-Mills cases, since now we have a direct product between Abelian and non-Abelian groups, and define the covariant derivatives[IV]

$$\begin{cases} D_\mu L = (\partial_\mu + ig_2 T^a W^a_\mu + ig_1 Y_Q B_\mu) L, \\ D_\mu \nu_{\ell R} = (\partial_\mu + ig_1 Y_u B_\mu) \nu_{\ell R}, \\ D_\mu \ell_R = (\partial_\mu + ig_1 Y_d B_\mu) \ell_R. \end{cases} \tag{2.19}$$

Note that the $U(1)_Y$ interactions are free parameters for each particle (the hypercharge Y, in analogy to the QED charge Q), but the $SU(2)_L$ interaction is fixed (i.e. it is global) because of the commutation relations. The new gauge fields must transform according to its group properties,

$$\begin{cases} W_\mu \to W'_\mu = U_L W_\mu U_L^\dagger + \frac{i}{g_2} (\partial_\mu U_L) U_L^\dagger, \\ B_\mu \to B'_\mu = B_\mu - \frac{1}{g_1} \partial_\mu \beta, \end{cases} \tag{2.20}$$

and the field stregth tensors are similar to the ones derived in the previous section,

$$\begin{cases} B_{\mu\nu} = \partial_\mu B_\nu - \partial_\nu B_\mu, \\ W_{\mu\nu} = \partial_\mu W_\nu - \partial_\nu W_\mu + ig_2 [W_\mu, W_\nu]. \end{cases} \tag{2.21}$$

With these definitions, the new, redefined Lagrangian for the EW sector reads[V]

$$\begin{aligned} \mathscr{L}_{\text{EW}} = {} & \bar{L} i\gamma^\mu D_\mu L + \bar{Q} i\gamma^\mu D_\mu Q + \bar{\nu}_{\ell R} i\gamma^\mu D_\mu \nu_{\ell R} \\ & + \bar{\ell}_R i\gamma^\mu D_\mu \ell_R + \bar{u}_R i\gamma^\mu D_\mu u_R + \bar{d}_R i\gamma^\mu D_\mu d_R - \frac{1}{4} B_{\mu\nu} B^{\mu\nu} - \frac{1}{4} W^a_{\mu\nu} W^{\mu\nu,a} \end{aligned} \tag{2.22}$$

[IV] Note that now the covariant derivative acts differently on left- and right-handed fields

[V] In this Lagrangian it is possible to see why a mass term is forbidden (and therefore why we were not including it in our Lagrangians): The mass term $\mathscr{L}_m$ for, lets say, a lepton, would be $\mathscr{L}_m = -m(\bar{\ell}_R \ell_L + \bar{\ell}_L \ell_R)$, clearly not invariant under $SU(2)_L \times U(1)_Y$ transformations.

and is invariant under local $SU(2)_L \times U(1)_Y$ transformations, as demanded. However, we need to analyze the field structures which appear in the above expression because they are not yet the observed $W^{\pm}$, Z and γ fields. We will start analyzing the field structure interacting with the field L, and a similar conclusion can be reached by replacing L by Q. Assuming the generators of $su(2)$ to be $T^a = \frac{\tau^a}{2}$, with τ^a the Pauli matrices, we have

$$\begin{aligned} D_\mu L = \partial_\mu \mathbb{1} L + i \begin{pmatrix} 0 & \frac{g_2}{2}(W_\mu^1 - iW_\mu^2) \\ \frac{g_2}{2}(W_\mu^1 + iW_\mu^2) & 0 \end{pmatrix} L \\ + i \begin{pmatrix} \frac{g_2}{2} W_\mu^3 + Y_L g_1 B_\mu & 0 \\ 0 & -\frac{g_2}{2} W_\mu^3 + Y_L g_1 B_\mu \end{pmatrix} L. \end{aligned} \tag{2.23}$$

In the above expression, there are (there must be!) two kinds of field interactions, charged ones and neutral ones. Recognizing the only possibility for charged fields (i.e. with a hermitian different from itself) to be the combination $W_\mu^1 \pm iW_\mu^2$, we define the fields

$$W_\mu^{\pm} \equiv \frac{W_\mu^1 \mp iW_\mu^2}{\sqrt{2}}. \tag{2.24}$$

From this, we can already extract the interaction between the charged gauge boson and the fermions, which we will denote by $\mathscr{L}_{Wf\bar{f}}$. From Eqs. (2.22) and (2.23), and including already the contribution from the Q doublet, one concludes that

$$\begin{aligned} \mathscr{L}_{Wf\bar{f}} &= -\frac{g_2}{\sqrt{2}} \bar{L} \gamma^\mu \begin{pmatrix} 0 & W_\mu^+ \\ W_\mu^- & 0 \end{pmatrix} L - \frac{g_2}{\sqrt{2}} \bar{Q} \gamma^\mu \begin{pmatrix} 0 & W_\mu^+ \\ W_\mu^- & 0 \end{pmatrix} Q \\ &= -\frac{g_2}{2\sqrt{2}} W_\mu^+ (\bar{\nu}_\ell \gamma^\mu (1-\gamma^5) \ell + \bar{u} \gamma^\mu (1-\gamma^5) d) + \text{h.c.} \end{aligned} \tag{2.25}$$

The remaining, hermitian fields, must be the real ones, representing the Z_μ and A_μ fields. As we did previously with the charged bosons, we assume they are a combination of the neutral EW gauge bosons and write the mixing as

$$\begin{pmatrix} W_\mu^3 \\ B_\mu \end{pmatrix} = \begin{pmatrix} \cos\theta_W & \sin\theta_W \\ -\sin\theta_W & \cos\theta_W \end{pmatrix} \begin{pmatrix} Z_\mu \\ A_\mu \end{pmatrix}. \tag{2.26}$$

θ_W is called the Weinberg angle. We proceed by substituting W_μ^3 and B_μ in Eq. (2.23), and for the moment we will represent the eigenvalues of $\tau^3/2$ by T_3 and Y is the eigenvalue

of the $U(1)_Y$ matrix. Therefore, the neutral interactions on the $SU(2)_L$ doublet L reads

$$\begin{aligned} -\bar{L}\gamma^\mu &\begin{pmatrix} \frac{g_2}{2}W_\mu^3 + Y_L g_1 B_\mu & 0 \\ 0 & -\frac{g_2}{2}W_\mu^3 + Y_L g_1 B_\mu \end{pmatrix} L \\ &= -\bar{L}\gamma^\mu A_\mu (g_2 \sin\theta_W T_3 + g_1 \cos\theta_W Y_L) L \\ &- \bar{L}\gamma^\mu Z_\mu (g_2 \cos\theta_W T_3 - g_1 \sin\theta_W Y_L) L. \end{aligned} \tag{2.27}$$

Since we want to reproduce the QED interaction,

$$\mathscr{L}_{\gamma f \bar{f}} = -eQ_f A_\mu \bar{\psi}\gamma^\mu \psi,$$

we fix the Weinberg angle by demanding that

$$g_2 \sin\theta_W = g_1 \cos\theta_2 = e \tag{2.28}$$

and define the hypercharge Y — the d.o.f. particular to each particle — in such a way that

$$Y = Q_f - T_3, \tag{2.29}$$

where Q_f is the charge of the particle into analysis. From this definition, we extract the hypercharge of the possible doublets,

$$Y_L = -\frac{1}{2}, \qquad Y_Q = \frac{1}{6}. \tag{2.30}$$

Since all the particles in the three family generations have the same charge according to its location in the fermion table, Tab. 1,[VI] these hypercharge values are true for all generations.

The only gauge boson that interacts with the right-handed fields is the $U(1)_Y$ gauge boson B_μ. Therefore, the interaction reads

$$\begin{aligned} -g_1 Y B_\mu \bar{\nu}_{\ell R}\gamma^\mu \nu_{\ell R} &- g_1 Y B_\mu \bar{e}_R \gamma^\mu e_R \\ &= -g_1 Y (-\sin\theta_W Z_\mu + \cos\theta_W A_\mu)(\bar{\nu}_{\ell R}\gamma^\mu \nu_{\ell R} + \bar{e}_R\gamma^\mu e_R) \\ &= -eY A_\mu (\bar{\nu}_{\ell R}\gamma^\mu \nu_{\ell R} + \bar{e}_R\gamma^\mu e_R) + g_1 Y \sin\theta_W Z_\mu (\bar{\nu}_{\ell R}\gamma^\mu \nu_{\ell R} + \bar{e}_R\gamma^\mu e_R). \end{aligned} \tag{2.31}$$

Thus, the hypercharges of the right-handed fields are simply their Electromagnetic charges,

[VI] The charges in Tab. 1 is organized as follows: the first column, composed by the neutrinos, share the same charge value; the second column, with the massive leptons, share its charge value etc.

which we denoted by Q in the development of QED, i.e.

$$\begin{cases} Y_{e_R} = -1, & Y_{\nu_R} = 0, \\ Y_{u_R} = 2/3, & Y_{d_R} = -1/3. \end{cases} \tag{2.32}$$

An important consequence of what we just developed is that the right-handed neutrino has both vanishing charge and hypercharge, i.e., it has no interaction whatsoever in the theory. This is what is called a *sterile neutrino*[25].

The interaction between the Z-boson and fermions, which we will denote by $\mathscr{L}_{Zf\bar{f}}$, can be written as (here we are just developing the lepton sector; the quark sector is identical)

$$\begin{aligned} \mathscr{L}_{Zf\bar{f}} &= -\bar{L}\gamma^\mu\left(g_2\frac{\tau^3}{2}W_\mu^3 + g_1 Y B_\mu\right)L + g_1 Y_e \bar{e}_R\gamma^\mu B_\mu e_R \\ &= -g_2\cos\theta_W\bar{L}\gamma^\mu\left(\frac{\tau^3}{2}Z_\mu - \frac{g_1\sin\theta_W}{g_2\cos\theta_W}YZ_\mu\right)L + g_2\cos\theta_W Z_\mu\bar{e}_R\gamma^\mu\left(\frac{g_1\sin\theta_W}{g_2\cos\theta_W}YZ_\mu\right)e_R \\ &= -\frac{e\cos\theta_W}{2\sin\theta_W}Z_\mu\sum_f\bar{\psi}_f\gamma^\mu\left(T_3^f(1-\gamma^5) - 2\frac{\sin^2\theta_W}{\cos^2\theta_W}(Q_f - T_3^f)\right)\psi_f, \end{aligned} \tag{2.33}$$

where we defined T_3^f as the eigenvalues of $\frac{\tau^3}{2}$ on the $SU(2)_L$ doublets and the sum is understood over the leptons. Simplifying this expression yields

$$\mathscr{L}_{Zf\bar{f}} = -\frac{e}{2\sin\theta_W\cos\theta_W}Z_\mu\sum_f\bar{\psi}_f\gamma^\mu T_3^f\left(1 - 4\sin^2\theta_W|Q_f| - \gamma^5\right)\psi_f, \tag{2.34}$$

where we note that the positive (or null, in the case of the neutrino) charged particles are always displayed on the upper part of the $SU(2)$ doublets while the negative stands always on the bottom of the doublet, and compensated this by a factor of 2 and the absolute value of the charge of the particle. In this last expression, since the development for the quark sector is identical and so it is for the 3 generations, the sum is over all fermions and this is the general Lagrangian with the interaction between the Z boson and the fermions.

2.3 Spontaneous symmetry breaking and the Higgs mechanism

In this section, we will analyze the mechanism which allows massive particles in the theory, the so-called Higgs mechanism. As we saw until here, particles with nonzero mass are forbidden because mass terms would spoil the gauge symmetry, our cornerstone until now in the generation of interactions.

The Higgs mechanism consists in the introduction of a scalar particle in the theory under a potential with more than one minimum smaller than zero. In this potential, the field acquires a vacuum expectation value (vev), and the fact that there are more than one

vacuum state implies that, when we choose a particular vacuum to quantize the theory, the symmetry of the possible states is broken and we have a *preferred* direction. Expanding the field around this vacuum (which implies that the new perturbation field has now a vanishing vev) allows the generation of masses for the gauge bosons. Furthermore, using the same field, we are able to generate mass for the fermions via Yukawa couplings between the Higgs field and the fermions fields.

2.3.1 Electroweak Spontaneous Symmetry Breaking

As we developed earlier in this chapter, the EW symmetry group is $SU(2)_L \times U(1)_Y$. Since we need to provide mass for three gauge fields, the natural choice is to consider a complex scalar $SU(2)$ doublet (since it has 4 d.o.f.),

$$\phi = \begin{pmatrix} \phi_1 \\ \phi_2 \end{pmatrix}. \tag{2.35}$$

For the generation of boson masses we will only consider the Lagrangian part containing the gauge bosons kinetic terms plus the scalar Lagrangian part. Thus, our Lagrangian reads

$$\mathscr{L} = -\frac{1}{4} W^i_{\mu\nu} W^{\mu\nu,i} - \frac{1}{4} B_{\mu\nu} B^{\mu\nu} + \mathscr{L}_{\mathrm{S}}, \tag{2.36}$$

where $\mathscr{L}_{\mathrm{S}}$ is the Lagrangian of the complex $SU(2)_L$ scalar doublet ϕ,

$$\mathscr{L}_{\mathrm{S}} = (D_\mu \phi)^\dagger D^\mu \phi - V(\phi), \tag{2.37}$$

with

$$V(\phi) = \mu^2 \phi^\dagger \phi + \lambda (\phi^\dagger \phi)^2. \tag{2.38}$$

where μ and λ are free parameters of the theory. This Lagrangian is invariant under local $SU(2)_L \times U(1)_Y$ transformations — i.e. we introduced a new particle and kept the underlying symmetry. We begin by noticing that λ must be positive, or otherwise the potential would not be bounded from below. For $\mu^2 > 0$, we have a unique minimum, $\phi = 0$, and $\mathscr{L}_{\mathrm{S}}$ describes a scalar particle with mass μ, ϕ^4 self-interactions and coupled to the gauge fields W_μ and B_μ. However, if $\mu^2 < 0$, the vacuum is now degenerated, and we have a continuum of minima in the potential, given by

$$0 = \frac{\partial V}{\partial \phi^\dagger} \implies |\phi|^2 = -\frac{\mu^2}{2\lambda} \equiv \frac{v^2}{2}. \tag{2.39}$$

Thus, the vacuum scalar field can be written, e.g., as $\phi = \begin{pmatrix} 0 \\ \frac{v}{\sqrt{2}} e^{i\theta} \end{pmatrix}$ — the continuity of states is encoded in the phase θ. By choosing a particular one — lets say $\theta = 0$ — *the*

symmetry of the vacuum is spontaneously broken (we chose a particular direction), and we have

$$\langle 0|\phi|0\rangle = \langle\phi\rangle_0 = \begin{pmatrix} 0 \\ \frac{v}{\sqrt{2}} \end{pmatrix}, \tag{2.40}$$

with $v = \left(\frac{-\mu^2}{\lambda}\right)^{1/2}$. Now, since ϕ is a $SU(2)$ doublet, the covariant derivative must include also the $SU(2)_L$ gauge fields and thus acts as

$$D_\mu\phi = \left(\partial_\mu + ig_2\frac{\tau^a}{2}W_\mu^a + ig_1Y_\phi B_\mu\right)\phi. \tag{2.41}$$

Now, we expand the scalar field around the minimum, i.e. we rewrite ϕ in terms of four fields, $\theta_{1,2,3}(x)$ and $h(x)$,[VII]

$$\phi(x) \equiv \begin{pmatrix} \frac{1}{\sqrt{2}}(\theta_2(x) + i\theta_1(x)) \\ \frac{1}{\sqrt{2}}(v + h(x)) - \frac{i}{\sqrt{2}}\theta_3(x) \end{pmatrix}, \tag{2.42}$$

which, to first order, can be written as

$$\phi(x) = e^{i\theta^a(x)\tau^a/v}\begin{pmatrix} 0 \\ \frac{1}{\sqrt{2}}(v + h(x)) \end{pmatrix}. \tag{2.43}$$

Due to the gauge freedom, we perform a gauge transformation on ϕ to move it to the unitary gauge,[VIII]

$$\phi(x) \to e^{-i\theta^a\tau^a/v}\phi(x) = \frac{1}{\sqrt{2}}\begin{pmatrix} 0 \\ v + h(x) \end{pmatrix}. \tag{2.44}$$

Expanding the term $(D_\mu\phi)^\dagger D^\mu\phi$ in $\mathscr{L}_\mathrm{S}$ then results in

$$\begin{aligned}(D_\mu\phi)^\dagger D^\mu\phi &= \frac{1}{2}\left(\frac{g_2^2}{4}|W_\mu^1 + iW_\mu^2|^2(v + h(x))^2 + (\partial_\mu h(x))^2 + \frac{1}{4}|g_2W_\mu^3 - 2g_1Y_\phi B_\mu|^2(v + h(x))^2\right) \\ &= \frac{1}{2}\left(\frac{g_2^2}{4}|W_\mu^1 + iW_\mu^2|^2v^2 + (\partial_\mu h(x))^2 + \frac{1}{4}|g_2W_\mu^3 - 2g_1Y_\phi B_\mu|^2v^2\right) + \text{interactions}.\end{aligned} \tag{2.45}$$

[VII] Note that the four fields θ_i and h have vanishing vev.
[VIII] The unitary gauge is defined as the gauge in which only the physical fields appears in the Lagrangian.

Substituting the gauge fields W_μ^i and B_μ by our definitions of the physically observed bosons $W_\mu^\pm$, Z_μ and A_μ, Eqs. (2.24) and (2.26), we have

$$(D_\mu\phi)^\dagger D^\mu\phi = \frac{1}{2}\left(\frac{g_2^2}{2}|W_\mu^-|^2v^2 + (\partial_\mu h(x))^2 + \frac{1}{4}|Z_\mu(g_2\cos\theta_W + 2g_1\sin\theta_W Y_\phi) + A_\mu(g_2\sin\theta_W - 2g_1\cos\theta_W Y_\phi)|^2v^2\right) + \text{interactions}. \tag{2.46}$$

Since we want the photon to be massless, we demand the free parameter Y_ϕ to be such that we remove all bilinear terms in A_μ. Explicitly, we demand

$$0 = g_2\sin\theta_W - 2g_1\cos\theta_W Y_\phi = e(1-2Y_\phi) \implies Y_\phi = \frac{1}{2}. \tag{2.47}$$

Therefore, substituting the hypercharge of the Higgs boson into Eq. (2.46), we have

$$(D_\mu\phi)^\dagger D^\mu\phi = \frac{g_2^2}{4}|W_\mu^-|^2v^2 + (\partial_\mu h(x))^2 + Z_\mu^2\left(\frac{g_2 v}{2\cos\theta_W}\right)^2 + \text{interactions}. \tag{2.48}$$

Collecting the bilinears on the EW gauge fields yields the masses of these bosons,

$$M_W \equiv \frac{g_2 v}{2}, \quad M_Z \equiv \frac{g_2 v}{2\cos\theta_W}, \quad M_A = 0, \tag{2.49}$$

i.e., the EW gauge bosons acquired a massive term in the Lagrangian while the photon remained massless, as demanded.

With this development, we can see that both charged vector bosons have the same mass $M_W = g_2 v/2$, while the neutral EW gauge boson has a mass $M_Z = M_W/\cos\theta_W$.

To conclude our discussion on mass generations, we close this section with the process that enables massive fermions in the theory.

2.3.2 Fermion masses

For the generation of the fermion masses, we need to consider a $SU(2)\times U(1)$ invariant Lagrangian which will couple left- and right-handed fields in such a way that the symmetry is still preserved. For this, we consider the Lagrangian with the Yukawa coupling

$$\mathscr{L}_{\text{Yuk}} = -\lambda_e\overline{L}\phi e_{\text{R}} - \lambda_u\overline{Q}\tilde{\phi}u_{\text{R}} - \lambda_d\overline{Q}\phi d_{\text{R}} + \text{h.c.}, \tag{2.50}$$

where $\tilde{\phi} = i\tau_2\phi^*$ and we are considering just the first family, for simplicity. Note that this Lagrangian is a scalar, $SU(2)_L\times U(1)_Y$ invariant one. We would like to mention that a Yukawa coupling between $\tilde{\phi}$ and the neutrino fields would, in principle, be possible. However, since the right-handed neutrino can not be measured, we could also obtain mass terms with only right-handed neutrinos, i.e. $\sim m\bar{\nu}_{\ell R}\nu_{\ell R}$, since this is also $SU(2)_L\times U(1)_Y$

invariant, allowing more than one way to generate neutrino masses. Neutrino physics is the branch of particle physics that exploits the different mechanisms that could generate neutrino masses and the associated rather rich phenomenology. In the SM, the neutrinos are considered massless and one assumes that the right-handed neutrino does not exist.

Once again, we expand the scalar field as we did previously, i.e.

$$\phi = \frac{1}{\sqrt{2}} \begin{pmatrix} 0 \\ v+h \end{pmatrix},$$

and compute the resulting terms in the Yukawa Lagrangian,

$$\begin{aligned} \mathscr{L}_{\text{Yuk}} &= \frac{1}{\sqrt{2}} \begin{pmatrix} \overline{\nu}_e & \overline{e} \end{pmatrix}_L \begin{pmatrix} 0 \\ v+h \end{pmatrix} e_R + \frac{1}{\sqrt{2}} \begin{pmatrix} \bar{u} & \bar{d} \end{pmatrix}_L \begin{pmatrix} 0 \\ v+h \end{pmatrix} d_R \\ &+ \frac{1}{\sqrt{2}} \begin{pmatrix} \bar{u} & \bar{d} \end{pmatrix}_L \begin{pmatrix} v+h \\ 0 \end{pmatrix} u_R + \text{h.c.} \\ &= -\frac{1}{\sqrt{2}}(v+h)(\lambda_e \bar{e}_L e_R + \lambda_d \bar{d}_L d_R + \lambda_u \bar{u}_L u_R) + \text{h.c.}. \end{aligned} \tag{2.51}$$

Thus, comparing the above terms with the mass term for a fermion in the Dirac Lagrangian,

$$\mathscr{L}_f^{\text{mass}} = -m \bar{f}_L f_R + \text{h.c.}, \tag{2.52}$$

one can identify the masses of the fermions of the first family as

$$m_e \equiv \frac{\lambda_e v}{\sqrt{2}}, \quad m_d \equiv \frac{\lambda_d v}{\sqrt{2}}, \quad m_u \equiv \frac{\lambda_u v}{\sqrt{2}}. \tag{2.53}$$

With this construction we recover the left-right mixing in the mass term while preserving the $SU(2) \times U(1)$ invariance. The process for the remaining families is analogous. It is interesting to note that, from this development, we can already extract the Higgs coupling to fermions, g_{Hff}, resulting from the coupling of the Higgs field in Eq. (2.51). Since the coupling has the same structure, we have

$$\mathscr{L}_{Hf\bar{f}} = -\frac{1}{\sqrt{2}} h(\lambda_f \bar{f}_L f_R) + \text{h.c.} \tag{2.54}$$

and conclude that the vertex of the coupling between the Higgs and the fermions is, through Feynman rules (i.e. change the sign and add an i for interactions), given by

$$g_{Hf\bar{f}} = i\frac{m_f}{v}. \tag{2.55}$$

In words, the Higgs coupling to fermions is proportional to the fermion mass and inversely

proportional to the Higgs vev. This vertex will be important in this work.

To summarize our results, keeping in mind the definitions of this chapter, we finally write down the SM Lagrangian is a compact way as

$$\mathscr{L}_{\rm SM} = \bar{\psi}_i i\gamma^\mu D_\mu \psi_i - \frac{1}{4} W^i_{\mu\nu} W^{\mu\nu,i} - \frac{1}{4} G^a_{\mu\nu} G^{\mu\nu,a} - \frac{1}{4} B_{\mu\nu} B^{\mu\nu} + |D_\mu \phi|^2 - V(\phi) + \mathscr{L}_{\rm Yuk}. \tag{2.56}$$

In the above expression, ψ_i are the fermion fields, and it represents L, Q, e_R etc. The covariant derivative acts differently on each field. For example, for the quark field Q, which transforms under the symmetry $SU(3)_C \times SU(2)_L \times U(1)_Y$, it reads

$$D_\mu Q = (\partial_\mu + i g_s G_\mu + i g_2 W_\mu + i g_1 Y_Q B_\mu) Q, \tag{2.57}$$

where we introduced the gluon field G_μ and the strong coupling g_s (we will explore QCD in more detail in the next chapter), while e.g. for the e_R, which transforms under $U(1)_Y$, it acts as

$$D_\mu e_R = (\partial_\mu + i g_1 B_\mu) e_R. \tag{2.58}$$

This compact Lagrangian of Eq. (2.56) encodes all known fundamental interactions but Gravity, and is one of the biggest successes in modern theoretical physics.

There are two aspects of the SM Lagrangian important for this work that we would like to stress: (i) the Higgs coupling to fermions is proportional to the fermion masses (Eq. (2.55)) and (ii) The Higgs does *not* couple to massless particles. Therefore, in our analysis of the Higgs decay into massless gauge bosons, the leading order diagram is already mediated by fermion loops — more precisely, by triangle loops. In view of the dominance of the top-quark mass over the remaining fermion masses, this quark will play a major role in the Higgs decay to massless particles.

In the next chapter we will talk about Quantum Chromodynamics and its peculiarities, introducing some aspects which will be essential to the conclusion of this work.

3 QCD

Having developed the Yang-Mills theory in the previous section, we now focus in more detail on the sector of the SM involved in the strong interaction, the QCD Lagrangian. The QCD Lagrangian is based on $SU(3)_C$ gauge invariance and is written

$$\mathscr{L}_{\text{QCD}} = \sum_f \bar{q}_f (i\gamma^\mu D_\mu - m_f) q_f - \frac{1}{4} G^a_{\mu\nu} G^{\mu\nu,a}, \tag{3.1}$$

with the covariant derivative given by

$$D_\mu \psi = (\partial_\mu + i g_s T^a G^a_\mu) q \tag{3.2}$$

and

$$G_{\mu\nu} = [D_\mu, D_\nu]. \tag{3.3}$$

There are 8 spin-1 gauge bosons of the strong interaction, G^a_μ, $a = 1, \ldots, 8$, called gluons. The only fermions with colour charge are the quarks; the quark fields are triplets of the fundamental representation, here denoted by q. The $su(3)$ Generators are such that

$$[T^a, T^b] = i f^{abc} T^c, \tag{3.4}$$

where f^{abc} are the structure constants of the $su(3)$ Lie algebra. To understand better the QCD Lagrangian, it is interesting to write explicitly its terms,

$$\begin{aligned} \mathscr{L}_{\text{QCD}} = & -\frac{1}{4}(\partial_\mu G_\nu - \partial_\nu G_\mu)(\partial^\mu G^\nu - \partial^\nu G^\mu) + \sum_f \bar{q}_f (i\gamma^\mu \partial_\mu - m) q_f \\ & - g_s G^a_\mu \sum_f \bar{q}_f \gamma^\mu T^a q_f \\ & - \frac{g_s}{2} f^{abc} (\partial_\mu G^a_\nu - \partial_\nu G^a_\mu) G^{\mu,b} G^{\nu,c} - \frac{g_s^2}{4} f^{abc} f^{ade} G^b_\mu G^c_\nu G^{\mu,d} G^{\nu,e}. \end{aligned} \tag{3.5}$$

The interactions of the theory appear on the second and third lines, while the kinetic terms are displayed on the first line. As we noted in the development of the Yang-Mill theory, the gluons interact among themselves in 3- and 4-fields vertices, while the interaction between quarks and gluons appears in just one type, as in the case of the QED interaction. The Lagrangian in Eq. (3.5) results in the QCD Feynman rules shown in Figs. 2 and 3 [IX].

For explicit calculations performed in the theory, we need to choose a given representa-

[IX] For a proper quantization of the QCD theory, one needs to add a new particle in the theory, known as *ghost*, represented by the dashed line, which do not appear in final states. The development of the ghosts for the Feynman rules is out of the scope of this work.

Propagators:

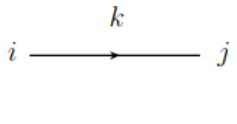

$$i\,\delta_{ij}\frac{(\not{k}+m)}{k^2-m^2+i\epsilon}$$

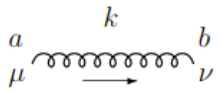

$$\frac{-i\,\delta_{ab}}{k^2+i\epsilon}\left[g_{\mu\nu}-(1-\eta)\frac{k_\mu k_\nu}{k^2}\right]$$

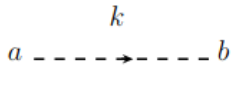

$$\frac{-i\,\delta_{ab}}{k^2+i\epsilon}\,,$$

$$\eta \text{ fixes the gauge: } \eta = \begin{cases} 1, & \text{Feynman gauge} \\ 0, & \text{Landau gauge} \end{cases}$$

Figure 2 – Feynman rules for QCD propagators.

Source: Adapted from FEYNMAN...[27]

tion for the generators of $su(3)$. We will choose the generators such that $T^a = \frac{\lambda^a}{2}$, where λ^a are the eight Gell-Mann matrices,

$$\lambda_1 = \begin{pmatrix} 0 & 1 & 0 \\ 1 & 0 & 0 \\ 0 & 0 & 0 \end{pmatrix}, \quad \lambda_2 = \begin{pmatrix} 0 & -i & 0 \\ i & 0 & 0 \\ 0 & 0 & 0 \end{pmatrix}, \quad \lambda_3 = \begin{pmatrix} 1 & 0 & 0 \\ 0 & -1 & 0 \\ 0 & 0 & 0 \end{pmatrix},$$
$$\lambda_4 = \begin{pmatrix} 0 & 0 & 1 \\ 0 & 0 & 0 \\ 1 & 0 & 0 \end{pmatrix}, \quad \lambda_5 = \begin{pmatrix} 0 & 0 & -i \\ 0 & 0 & 0 \\ i & 0 & 0 \end{pmatrix}, \quad \lambda_6 = \begin{pmatrix} 0 & 0 & 0 \\ 0 & 0 & 1 \\ 0 & 1 & 0 \end{pmatrix}, \tag{3.6}$$
$$\lambda_7 = \begin{pmatrix} 0 & 0 & 0 \\ 0 & 0 & -i \\ 0 & i & 0 \end{pmatrix}, \quad \lambda_8 = \frac{1}{\sqrt{3}} \begin{pmatrix} 1 & 0 & 0 \\ 0 & 1 & 0 \\ 0 & 0 & -2 \end{pmatrix}.$$

Thus, it is easy to check that

$$[\lambda^a, \lambda^b] = 2if^{abc}\lambda^c$$

and

$$\mathrm{Tr}(\lambda^a\lambda^b) = 2\delta^{ab}.$$

Furthermore, we have

$$\left[\frac{\lambda^a}{2}\frac{\lambda^a}{2}\right]_{ij} = \delta_{ij}C_F, \tag{3.7}$$

Vertices:

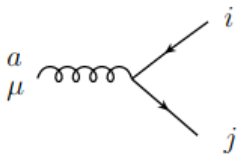

$$ig_s\gamma_\mu T^a_{ji}$$

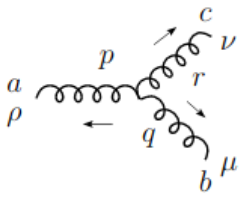

$$-g_s f^{abc}\left[(p-q)_\nu\, g_{\rho\mu}+(q-r)_\rho\, g_{\mu\nu}+(r-p)_\mu\, g_{\nu\rho}\right]$$

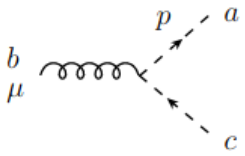

$$g_s\, f^{abc} p_\mu \ (p_\mu \text{ outgoing})$$

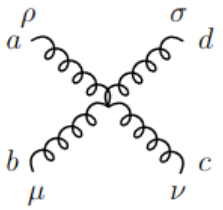

$$\begin{aligned}
&-ig_s^2 f^{abe} f^{cde}\left(g_{\rho\nu}g_{\mu\sigma}-g_{\rho\sigma}g_{\mu\nu}\right)\\
&-ig_s^2 f^{ace} f^{bde}\left(g_{\rho\mu}g_{\nu\sigma}-g_{\rho\sigma}g_{\mu\nu}\right)\\
&-ig_s^2 f^{ade} f^{cbe}\left(g_{\rho\nu}g_{\mu\sigma}-g_{\rho\mu}g_{\sigma\nu}\right)
\end{aligned}$$

Figure 3 – Feynman rules for QCD vertices.

Source: Adapted from FEYNMAN...[27]

where $C_F = \frac{N_C^2-1}{2N_C}$ is the Casimir operator in the fundamental representation. For $N_C = 3$, $C_F = \frac{4}{3}$.

We now have all the tools to calculate QCD processes, and we start with QCD renormalization.

3.1 QCD renormalization

As its name suggests, the strong force has a coupling constant approximately one order of magnitude larger than the QED counterpart. Therefore, in perturbative calculations, QCD corrections will often play a leading role and will generally dominate over EW corrections. In this section we will study renormalization processes in QCD which will lead to the analysis of its coupling constant evolution, resulting in the celebrated *asymptotic freedom*, which, for example, allows perturbative calculations in high energy regimes.

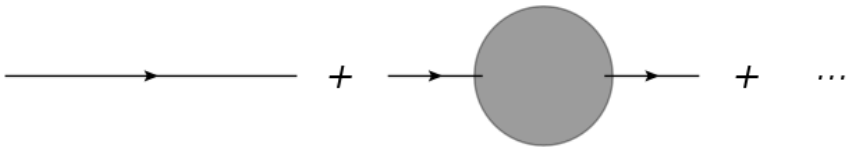

Figure 4 – First 1PI corrections to the quark propagator. The blob represents the sum of all possible 1PI diagrams.

Source: By the author.

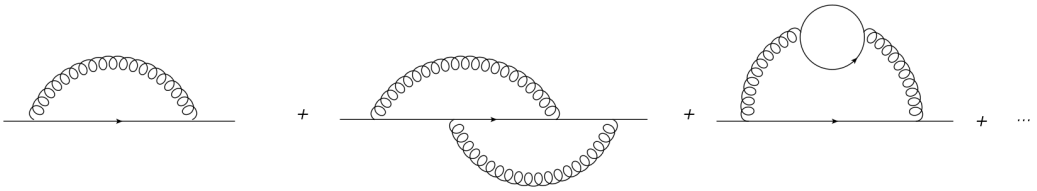

Figure 5 – Some contributions of 1PI diagrams to Σ.

Source: By the author.

The quark two-point function (or propagator) is written, in momentum space, as

$$S_{ij}(p) = -i \int \mathrm{d}^4x e^{ip\cdot x} \langle 0|T q_i(x)\bar{q}_j(0) e^{\int \mathrm{d}^4z \mathscr{L}_I(z)}|0\rangle. \tag{3.8}$$

In the above expression, $\mathscr{L}_I$ is the Lagrangian piece with the QCD interactions and i, j are the colour indices that here we write explicitly. This expression gives the correct full propagator in QCD. However, when we consider the interactions, we need to proceed the calculations in perturbation theory — in this case, in the strong interaction —, correcting the free-quark propagator (i.e. without interactions), $S^{(0)}_{ij}(p)$,

$$S^{(0)}_{ij}(p) = \frac{\not{p} + m}{p^2 - m^2 + i0} \equiv \frac{1}{\not{p} - m + i0}. \tag{3.9}$$

In order to make progress, it is convenient to introduce the *one-particle irreducible* (1PI) diagram concept, defined as any diagram that can not be split in two by removing a single line[28]. Therefore, diagrammatically we can represent *all* corrections to the quark propagator as shown in Fig. 4. The blob in the figure represents the *sum* of all 1PI corrections, with some contributions shown explicitly in Fig. 5. Thus, we can write the contributions of the diagrams in Fig. 4 as

$$S_{ij}(p) = \delta_{ij} S^{(0)}(p) + \delta_{ij} S^{(0)}(p) \Sigma(p) S^{(0)}(p) + \dots. \tag{3.10}$$

We denoted all the 1PI contributions as Σ. Therefore, including more diagrams would result in a series and in the limit of all 1PI contributions, the resulting quantity is the

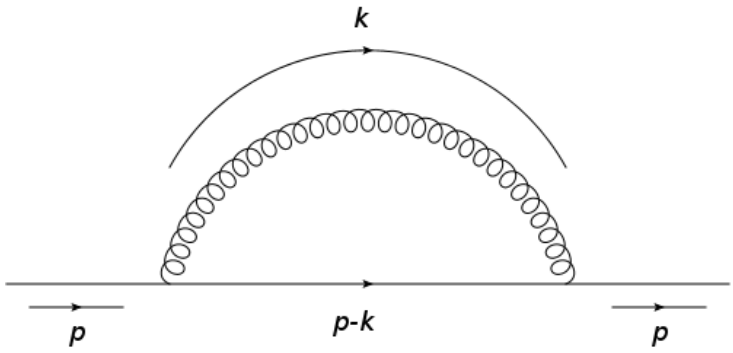

Figure 6 – First QCD correction to the quark propagator.

Source: By the author.

exact propagator,

$$S_{ij}(p) = \sum_{n=0}^{\infty} \delta_{ij} S^{(0)}(p) \left(\Sigma(p) S^{(0)}(p)\right)^n . \tag{3.11}$$

Summing the series — also known as Dyson resummation — results in the resummed quark propagator,

$$S_{ij}(p) = \frac{\delta_{ij}}{\not{p} - m - \Sigma(p) + i0}. \tag{3.12}$$

It is interesting to note that, compared to the free propagator, the full, resummed propagator has its pole shifted from m by $\Sigma(p)$. The solution of this pole,[x]

$$[\not{p} - m - \Sigma(\not{p})]_{\not{p}=m} = 0 \tag{3.13}$$

is the physical mass of the quark.

The first correction to the two-point quark function, $\Sigma^{(1)}$, is shown in Fig. 6. We note that it is the only first-order correction diagram because, in the QCD interaction Lagrangian, the quarks only interacts with gluons. Mathematically, the first correction reads

$$\Sigma^{(1)}(p) = -iC_F g_s^2 \int \frac{d^4k}{(2\pi)^4} \frac{\gamma^\mu(\not{p} - \not{k} + m)\gamma^\nu}{[(p-k)^2 - m^2]k^2} \left(g_{\mu\nu} - (1-a)\frac{k^\mu k^\nu}{k^2}\right). \tag{3.14}$$

Unfortunately, this integral diverges — in fact, it is UV-logarithmic divergent. Thus, we will proceed with the calculation with the so-called dimensional regularization (dimreg), in which we generalize the integration from 4 to D dimensions, with $D = 4 - 2\varepsilon$. At the end of the calculation, the correct dimensionality can be restored taking the limit $\varepsilon \to 0$. With this, we are able to separate the divergent contribution from the finite one, and then we

[x] We changed the argument of the Σ function from p to $\not{p}$ by noting that the only dependence is on $\not{p}$ and $p^2 = \not{p}\not{p}$, which can be summarized as a $\not{p}$ dependence.

can proceed to renormalize the theory. Going from 4 to $D = 4 - 2\varepsilon$ dimensions, we write[XI]

$$\Sigma^{(1)}(p) = -i\mu^{-2\varepsilon} C_F g_s^2 \mu^{2\varepsilon} \int \frac{d^D k}{(2\pi)^D} \frac{\gamma^\mu (\not{p} - \not{k} + m)\gamma^\nu}{[(p-k)^2 - m^2]k^2} \left(g_{\mu\nu} - (1-a)\frac{k^\mu k^\nu}{k^2} \right). \tag{3.15}$$

For the first correction, the gauge parameter a does not play any role[29]. Thus, we will work in the Feynman gauge ($a = 1$). Therefore, we can write the integral as

$$\Sigma^{(1)}(p) = -i\mu^{-2\varepsilon} C_F g_s^2 \mu^{2\varepsilon} \int \frac{d^D k}{(2\pi)^D} \frac{((2-D)(\not{p} - \not{k}) + Dm)}{[(p-k)^2 - m^2]k^2}, \tag{3.16}$$

where we used the anti-commutation relation $\{\gamma^\mu, \gamma^\nu\} = 2g^{\mu\nu}\mathbb{1}$ and $\gamma^\mu\gamma_\mu = D$. Introducing the Feynman parameters,

$$\frac{1}{A^n B^m} = \frac{\Gamma(n+m)}{\Gamma(n)\Gamma(m)} \int_0^1 \mathrm{d}x \frac{x^{n-1}(1-x)^{m-1}}{[Ax + B(1-x)]^{n+m}}, \tag{3.17}$$

we rewrite the denominator as

$$\frac{1}{[(p-k)^2 - m^2]k^2} = \int_0^1 \mathrm{d}x \frac{1}{[(p-k)^2 x - m^2 x + k^2 - k^2 x]^2} = \int_0^1 \mathrm{d}x \frac{1}{[(k-px)^2 - M^2]^2}, \tag{3.18}$$

where in the last equality we completed the square and defined $M^2 \equiv m^2 x - p^2 x(1-x)$. Therefore, changing the order of integration in x and k, our original integral becomes

$$\Sigma^{(1)}(p) = -i\mu^{-2\varepsilon} C_F g_s^2 \mu^{2\varepsilon} D \int_0^1 \mathrm{d}x \int \frac{d^D k}{(2\pi)^D} \frac{(2-D)(\not{p} - \not{k}) + Dm}{[(k-px)^2 - M^2]^2}. \tag{3.19}$$

Now, we shift the integration variable k, $k \to k + px$, in order to simplify the denominator. Thus, the inner integration becomes

$$\begin{aligned} \int \frac{d^D k}{(2\pi)^D} \frac{(2-D)(-\not{p} + \not{k} + \not{p}x) + Dm}{[k^2 - M^2]^2} &= \int \frac{d^D k}{(2\pi)^D} \frac{(2-D)\not{p}(1-x) + Dm}{[k^2 - M^2]^2} \\ &\quad + \int \frac{d^D k}{(2\pi)^D} \frac{(2-D)\not{k}}{[k^2 - M^2]^2}. \end{aligned}$$

In the above expression, the last integral on the r.h.s. is odd, and thus it vanishes since the limits of integration are symmetric around zero. We are left with

$$\Sigma^{(1)}(p) = \not{p}\Sigma_p^{(1)}(p) + m\Sigma_m^{(1)}(p), \tag{3.20}$$

with

$$\Sigma_p^{(1)} = -4\pi i \alpha_s C_F \mu^{2\varepsilon} (2-D) \int_0^1 \mathrm{d}x (1-x) \int \frac{d^D k}{(2\pi)^D} \frac{1}{[k^2 - M^2]^2} \tag{3.21}$$

[XI] The factors μ are added to the expression so that the dimensionality of the resulting quantities do not change.

and

$$\Sigma_m^{(1)} = -4\pi i\alpha_s C_F \mu^{2\varepsilon} D \int_0^1 \mathrm{d}x \int \frac{d^D k}{(2\pi)^D} \frac{1}{[k^2 - M^2]^2}. \tag{3.22}$$

In the last equation, we defined $\alpha_s(\mu) \equiv g_s^2 \mu^{-2\varepsilon}/4\pi$. α_s is what is usually called the QCD coupling. It is important to notice that the coupling that we just defined is a function of the energy scale μ. However, since this energy scale appears in the process of regularization, it can not be a physical quantity and thus observables should not depend on μ.

The inner integral is the simplest one-loop integral — the massive tadpole —, and its result is well known and present in integral tables[30]. It reads[XII]

$$\int \frac{d^D k}{(2\pi)^D} \frac{1}{[k^2 - M^2 + i0]^n} = \frac{i(-1)^n}{(4\pi)^{D/2}} \frac{\Gamma(n - D/2)}{\Gamma(n)} (M^2 - i0)^{D/2-n}. \tag{3.23}$$

Thus, we can solve the k integration,

$$\Sigma_p^{(1)}(p) = \frac{C_F}{4}\frac{\alpha_s}{\pi} \left(\frac{4\pi\mu^2}{m^2}\right)^{\varepsilon} (2\varepsilon - 2) \int_0^1 \mathrm{d}x (x-1) \left(x - \frac{p^2}{m^2} x(1-x)\right)^{-\varepsilon}, \tag{3.24}$$

$$\Sigma_m^{(1)}(p) = \frac{C_F}{4}\frac{\alpha_s}{\pi} \left(\frac{4\pi\mu^2}{m^2}\right)^{\varepsilon} (4 - 2\varepsilon) \int_0^1 \mathrm{d}x \left(x - \frac{p^2}{m^2} x(1-x)\right)^{-\varepsilon}, \tag{3.25}$$

where we factorized $(m^2)^{-\varepsilon}$ outside the integral. For solving the x-integration for $\Sigma_m^{(1)}(p)$, we expand the integrand in ε and concludes that

$$\int_0^1 \mathrm{d}x \left(1 - \varepsilon \ln\left(x - \frac{p^2}{m^2} x(1-x)\right)\right) = 1 - \varepsilon\left(-2 + \frac{m^2 - p^2}{p^2} \ln\left(1 - \frac{p^2}{m^2}\right)\right). \tag{3.26}$$

Expanding $\left(\frac{4\pi\mu^2}{m^2}\right)$ in ε and distributing all multiplications, we arrive at the final result,

$$\Sigma_m^{(1)}(p) = \frac{C_F}{4}\frac{\alpha_s}{\pi}\left(\frac{4}{\hat{\varepsilon}} + 6 - 4\ln\left(\frac{m^2}{\mu^2}\right) - 4\left(1 - \frac{m^2}{p^2}\right)\ln\left(1 - \frac{p^2}{m^2}\right)\right) + \mathscr{O}(\varepsilon). \tag{3.27}$$

In the above expression, we defined

$$\frac{1}{\hat{\varepsilon}} \equiv \frac{1}{\varepsilon} - \gamma_E + \ln(4\pi). \tag{3.28}$$

Proceding in an analogous fashion with $\Sigma_p^{(1)}(p)$, we arrive at the expression

$$\Sigma_p^{(1)}(p) = \frac{C_F}{4}\frac{\alpha_s}{\pi}\left(-\frac{1}{\hat{\varepsilon}} - 1 + \ln\left(\frac{m^2}{\mu^2}\right) + \left(1 - \frac{m^4}{p^4}\right)\ln\left(1 - \frac{p^2}{m^2}\right)\right) + \mathscr{O}(\varepsilon). \tag{3.29}$$

If we try to restore the four dimensions, i.e. take the limit $\varepsilon \to 0$, the factor $\frac{1}{\varepsilon}$ goes to

[XII] For more details about the massive tadpole calculation, cf. e.g. Refs.[28, 30]

infity. However, in the resulting expression, we were able to separate the divergent part from the finite one, i.e. we regularized the calculation. Now we need to *absorb* these infinities such that observables are always finite. For this, we will renormalize the two degrees of freedom present in this calculation, $q(x)$ and m. We begin by writing

$$q_i(x) = Z_{2F}^{1/2} q_i^R(x), \qquad m = Z_m m^R, \tag{3.30}$$

where the quantities on the l.h.s. of the above equations are the bare quantities, i.e. unrenormalized, present in the original Lagrangian. On the r.h.s. the superscript R refers to the renormalized, finite quantities. Thus, the infinities are restricted to the renormalization constants Z_i. We would like to point out that we defined the renormalization of the quark with a power of $1/2$ to compensate the fact that the quark fields appears as bilinears in the Lagrangian.

Rewriting the two-point function with the renormalized quark fields, such that the resulting quantity is finite, we have

$$\begin{aligned} S_{ij}(p) &= -i \int \mathrm{d}^4x e^{ip\cdot x} \langle 0|T q_i^R(x) \bar{q}_j^R(0) e^{\int \mathrm{d}^4z \mathscr{L}_I(z)}|0\rangle \\ &= \frac{1}{Z_{2F}} \left(\frac{\delta_{ij}}{\not{p} - Z_m m^R - \Sigma(p) + i0} \right). \end{aligned} \tag{3.31}$$

Now we assume the renormalization constants can be expanded in perturbation theory,

$$Z_i = 1 + Z_i^{(1)} \frac{\alpha_s}{\pi} + Z_i^{(2)} \left(\frac{\alpha_s}{\pi} \right)^2 + \dots \tag{3.32}$$

Thus, at first order in perturbation theory in α_s, the inverse of the propagator reads[XIII]

$$\begin{aligned} S_{ij}^{-1}(p) &= \left(1 + Z_{2F}^{(1)} a_s\right) \left(\not{p} - (1 + Z_m^{(1)} a_s) m^R - \not{p} \Sigma_p(p) - (1 + Z_m^{(1)} a_s) \Sigma_m(p) \right) \\ &= \not{p} \left(1 + Z_{2F} a_s - \Sigma_p^{(1)}(p) \right) - m^R \left(1 + (Z_{2F}^{(1)} + Z_m^{(1)}) a_s + \Sigma_m^{(1)}(p) \right) \end{aligned} \tag{3.33}$$

In the above equation we defined $a_s \equiv \frac{\alpha_s}{\pi}$. Now, we need to match the renormalization constants Z_i to absorb the infinities from Eqs. (3.27) and (3.29). However, there is more than one way of renormalizing the theory. The Minimal Subtraction scheme, MS, developed independently by Gerard 't Hooft[31] and Steven Weinberg[8], consists in the sole absorption of the pole $\frac{1}{\varepsilon}$ from Σ. In this work we will use the the Modified-Minimal Subtraction scheme, $\overline{\text{MS}}$, in which we subtract the quantity $1/\hat{\varepsilon}$, defined in Eq. (3.28). We would like to stress that these are not the only ways of renormalizing the theory and that physical

[XIII] we will ignore the δ-function in the numerator because we are just interested in the absorption of the infinities

quantities should not depend on such conventions. Therefore, in the $\overline{\text{MS}}$ we have

$$Z_{2F}^{(1)} = -\frac{C_F}{4\hat{\varepsilon}} \tag{3.34}$$

and

$$Z_m^{(1)} = -\frac{3C_F}{4\hat{\varepsilon}}. \tag{3.35}$$

With these modifications, we finally arrive at finite quantities for the quark propagator at the first-order QCD correction level.

Since we studied renormalization at the one loop level, we now turn our attention to the dependence of the strong coupling, α_s, on the energy scale μ.

3.2 The running coupling

The regularization process forces the introduction of a new parameter, which in the case of dimensional regularization is the energy scale μ. However, if we consider an observable $R(q, a_s, m)$, it becomes clear that this physical quantity can not depend on whether we used dimreg or, for renormalization, the MS or $\overline{\text{MS}}$ or any other scheme. Thus, for observable quantities it is mandatory that the dependence on μ is absent. In mathematical language, this is translated to[XIV]

$$\mu^2 \frac{\mathrm{d}R(q, \alpha_s, m)}{\mathrm{d}\mu^2} = \left(\mu^2 \frac{\partial}{\partial \mu^2} + \mu^2 \frac{\mathrm{d}\alpha_s}{\mathrm{d}\mu^2} \frac{\partial}{\partial \alpha_s} + \mu^2 \frac{\mathrm{d}m}{\mathrm{d}\mu^2} \frac{\partial}{\partial m} \right) R(q, \alpha_s, m) = 0. \tag{3.36}$$

Eq. (3.36) is known as the Renormalization Group Equation (RGE). In the parenthesis of the above equation, it is interesting to note the derivatives of the coupling constant and of the mass (the QCD parameters) with respect to the energy scale μ. In fact, these are two important functions, with its own definitions. Therefore, we introduce the β-function, $\beta(a_s)$, defined as

$$\beta(a_s) \equiv \mu^2 \frac{\mathrm{d}a_s}{\mathrm{d}\mu^2} = \sum_{n=0}^{\infty} \beta_n a_s^{n+2}, \tag{3.37}$$

and the mass anomalous dimension, γ, defined as

$$\gamma(a_s) \equiv \frac{\mu^2}{m} \frac{\mathrm{d}m}{\mathrm{d}\mu^2} = \sum_{n=0}^{\infty} \gamma_n a_s^{n+1}. \tag{3.38}$$

We would like to point out that the definitions of the β-function and of the mass anomalous dimension are not unique, and several different conventions can be found in the literature. Here we use the conventions of Ref.[18].

The β-function tells us how the coupling varies with the energy scale μ, while the mass anomalous dimension yields the variation of the mass with μ. As this work is being

[XIV] As we saw in the last section, μ enter in results always squared, μ^2.

written, both are known up to 5-loop accuracy[32,33]. To first order in perturbation theory, Eq. (3.37) reads[XV]

$$\mu^2 \frac{\mathrm{d}\alpha_s}{\mathrm{d}\mu^2} = \beta_0 \alpha_s^2. \tag{3.39}$$

This equation is easily solved by separation of variables, i.e.

$$\int_{a_s(\mu_0)}^{a_s(\mu)} \frac{\mathrm{d}\alpha_s}{\alpha_s^2} = \beta_0 \int_{\mu_0}^{\mu} \frac{\mathrm{d}\mu'^2}{\mu'^2} \implies \alpha_s(\mu) = \frac{\alpha_s(\mu_0)}{1 - 2\beta_0 \alpha_s(\mu_0) \ln\left(\frac{\mu}{\mu_0}\right)}. \tag{3.40}$$

In the resulting expression for $\alpha_s(\mu)$, μ_0 is some arbitrary reference scale. From Eq. (3.40), there is a very important consequence: as we increase the energy μ, $\alpha_s(\mu)$ becomes smaller, going to zero in the limit $\mu \to \infty$. This is what is called asymptotic freedom — in the limit of small distances (i.e. high energy), the quarks are free particles in the strong interaction context. Another interesting aspect is that when

$$\mu \to \Lambda \equiv \mu_0 e^{\frac{1}{2\beta_0 \alpha_s(\mu_0)}}, \tag{3.41}$$

the QCD coupling diverges. Thus, opposed to the high-energy limit where quarks are considered free regarding the strong interaction, when the energy scale is low, i.e. $\mu \sim \Lambda$, the strong interactions dominates over all other interactions.

We can also write $\alpha_s(\mu)$ in terms of the QCD scale Λ. From Eq. (3.41), we have that

$$1 = 2\beta_0 \alpha_s(\mu_0) \ln\left(\frac{\Lambda}{\mu_0}\right).$$

and, therefore, Eq. (3.40) can be rewritten as

$$\alpha_s(\mu) = \frac{1}{2\beta_0 \ln\left(\frac{\Lambda}{\mu}\right)}. \tag{3.42}$$

The Λ scale possesses an interesting property. Note that

$$\frac{\mathrm{d}\Lambda}{\mathrm{d}\mu_0} = e^{\frac{1}{2\beta_0 \alpha_s(\mu_0)}} \left(1 - \frac{\mu_0}{2\beta_0 \alpha_s^2(\mu_0)} \frac{\mathrm{d}\alpha_s(\mu_0)}{\mathrm{d}\mu_0}\right) = 0. \tag{3.43}$$

Therefore, Λ does *not* depend on the arbitrary reference scale μ_0: it is an intrinsic scale from the theory. However, it should be noted that Λ is renormalization-scheme dependent — for example, in the $\overline{\mathrm{MS}}$ scheme, $\Lambda \approx 200\mathrm{MeV}$. Λ can be interpreted as an indication of the energy scale where perturbation theory is not useful anymore, and we should resort to non-perturbative calculations, e.g. lattice QCD.

In Fig. 7 we can see various extractions of the strong coupling α_s in different experiments

[XV] The first five coefficients of the β-function are displayed in App. 7

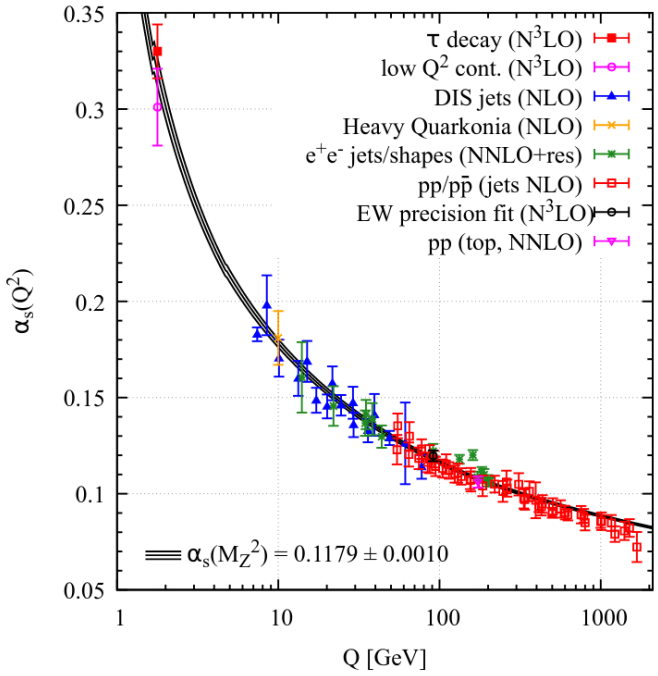

Figure 7 – α_s measurements in various experiments varying with the energy scale compared with the theoretical prediction of tha α_s evolution. NNLO+res represents the NNLO matched to a resummed calculation.

Source: Adapted from ZYLA *et al.*[26]

and in different energy scales compared with the theoretical prediction of the α_s evolution, displayed in the continuous line. The world average for the α_s at the M_Z^2 scale is $\alpha_s(M_Z^2) = 0.1179 \pm 0.0010$[26]. It is possible to see that the extractions, regardless of the process analyzed, match the theoretical evolution with the energy scale μ to a high accuracy, thus reinforcing the validity of QCD perturbative calculations. It should be noted that the values of the extractions displayed in Fig. 7 in each process are the mean of various independent extractions by different authors.

3.3 Large-n_f and large-β_0 limits

Our strategy to estimate QCD higher-order terms in the decay of the Higgs boson into photons relies on the so-called large-β_0 limit. This limit can reproduce the full-QCD amplitude with accuracy in several processes and in almost every process it is very useful for obtaining qualitative and semi-quantitative information about the series behaviour in large orders[21–23]; therefore, it is an interesting framework to try to estimate QCD results in higher-order calculations which are extremely complicated to be performed in the complete theory: for example, the time span between the 4-loop calculation of the QCD β-function[34] and the 5-loop calculation[32] was 19 years.

To proceed to the large-β_0 limit, first we need to calculate the leading-n_f terms of

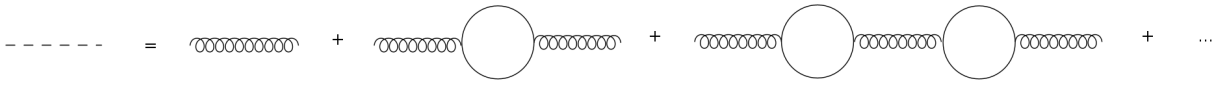

Figure 8 – Corrections to the gluon propagator due to light-quark loops, yielding the leading-n_f terms. Each bubble loop counts as $n_f\alpha_s$.

Source: By the author.

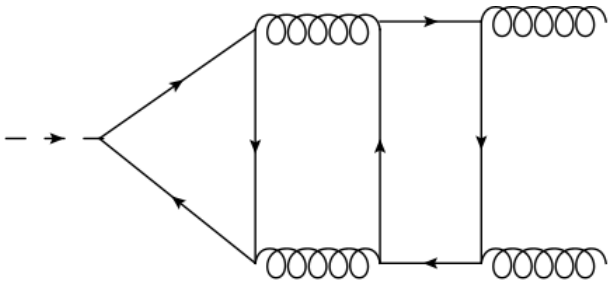

Figure 9 – Singlet diagram which also contributes to the leading-n_f term in the decay $H \to gg$ at NNLO which are not due to light-quark bubble corrections to the gluon propagator.

Source: By the author.

the process at hand, i.e. the terms in which n_f appears with the highest power;[XVI] the argument to justify the solely calculation of the leading-n_f terms is that, in the full result, $n_f\alpha_s \sim \mathcal{O}(1)$, and therefore the leading-n_f term in the sense of this power counting dominates over the remaining terms. Thus, calculating only the leading-n_f terms corresponds to an effective theory in which we take the limit where the number of flavours in the theory goes to infinity, $n_f \to \infty$, while keeping the product $n_f\alpha_s \sim \mathcal{O}(1)$ constant; accordingly, in this power-counting scheme, $\alpha_s \sim 1/n_f$.

For the decay $H \to \gamma\gamma$, the leading-n_f terms can be obtained from corrections to the gluon propagator, that appears in the NLO diagrams, due to light-quark bubble loops, shown in Fig. 8 — the successive additions of these loop corrections contribute with $n_f\alpha_s$ terms in perturbation theory. (We note that when there are external gluon legs — for example, in the decay $H \to gg$ —, there are other types of diagrams which contribute to the leading-n_f terms; as an example, at the NNLO level of $H \to gg$, light-fermion box diagrams also contribute to the leading-n_f term, as shown in the diagram of Fig. 9.)

Thus, the introduction of these loop corrections (Fig. 8) to the gluon propagator in the process $H \to \gamma\gamma$ at NLO generates the leading-n_f terms. However, for working in this limit and proceed to the large-β_0 limit, it is useful to work in the so-called *Borel space*. We will now briefly introduce the concept of divergent series and the Borel transform, and after that we return to the discussion of the large-β_0 limit which will be instrumental in the introduction of the key concept of *renormalons*.

[XVI] n_f denotes the number of active flavours in the theory; it is important to not mistake this by the large-N_c limit: N_c is the number of colours of the QCD gauge group SU(N_c).

3.3.1 Divergent series and the Borel transform

The discussion presented in the section is based mainly in Ref.[18].

Let us assume we have an observable R which admits a power expansion in the strong coupling α_s,

$$R \sim \sum_n r_n \alpha_s^n. \tag{3.44}$$

It has been known for a long time, through an argument by Dyson in 1952, that these series expansions in QED are divergent even after charge and mass renormalization[35]. For quantum field theories such as QED and QCD, it is assumed that the series expansion for observables are *asymptotic* — when we truncate the series at a certain order, it agrees to a great accuracy with experiments and therefore it seems to be approaching the true result. By asymptotic we mean that there exist numbers K_N such that

$$|R(\alpha_s) - \sum_{n=0}^{N} r_n \alpha_s^n| < K_{N+1} \alpha_s^{N+1} \tag{3.45}$$

for all α_s in a region $\mathscr{C}$ of the complex α_s-plane and the truncation error at order N is uniformly bounded to be of order α_s^{N+1} . In other words, at intermediate orders the series approaches the exact result for the observables; after an optimum order in the series expansion — generally when the difference between following terms is minimum —, the terms start to diverge from the exact result.

Now we arrive at the question about the series summation. For factorially divergent series,[XVII] the best method to arrive at a *definition*[XVIII] of a sum is through the *Borel summation*. First, we need to introduce the *Borel transform*, which heuristically speaking tames the divergent behaviour of the series by dividing each term of the series by $n!$. Formally, the definition of the Borel transform of an asymptotic divergent series R, $B[R]$, reads

$$R \sim \sum_{n=0}^{\infty} r_n \alpha_s^{n+1} \implies B[R](t) = \sum_{n=0}^{\infty} r_n \frac{t^n}{n!}. \tag{3.46}$$

Notice that this transformation results in a one-to-one correspondence between the Borel series and the original series, i.e., if we have the expansion in t we also have the coefficients of the expansion in the original parameter, in our case α_s.

Then, if the resulting series is sufficiently well behaved in the positive real axis, we can sum the series, in the Borel sense, through the Borel integral $\tilde{R}$, which is basically a Laplace transform,

$$\tilde{R} = \int_0^{\infty} dt e^{-t/\alpha_s} B[R](t). \tag{3.47}$$

[XVII] When we substitute the original gluon propagator by the resummed gluon propagator (Fig. 8), at two-loops, the resulting expression will be factorially divergent terms for the series in low- and high-energy limits, as we will see below.

[XVIII] It is not trivial to *define* the sum of a divergent series. For more about this, cf.[18].

Notice that, if there are singularities along the positive real axis, the contour must be distorted — such as the displacement of t, $t \to t \pm i\delta$. This leads to ambiguities in the Borel sum which are related to exponentially small terms that need to be added to the original series. These exponential terms are non-perturbative, i.e. it indicates the existence of non-perturbative contributions.

To better explain this, we will present an example: Consider that, for a given observable R, the coefficients of the series expansion Eq. (3.44) read

$$r_n = Ka^n\Gamma(n+1+b), \tag{3.48}$$

which is the typical behaviour of series in Quantum Field Theories. We will consider $a > 0$.[XIX] For simplicity, we will also consider $b > 0$. The Borel transform of the series, using the formula

$$\frac{1}{(1-x)^s} = \sum_{k=0}^{\infty} \binom{s+k-1}{k} x^k, \tag{3.49}$$

is

$$B[R](t) = \frac{K\Gamma(1+b)}{(1-at)^{(1+b)}}. \tag{3.50}$$

Thus, we see that the Borel integral is not well defined because the resulting Borel transform has a pole in $1/a$ of degree $1+b$. Using the formula for residues of higher-order poles,

$$\mathrm{Res}(B[R](t), 1) = \frac{1}{b!} \lim_{z\to 1} \frac{d^b}{dz^b}((z-1)^{b+1} f(z)), \tag{3.51}$$

where we substituted $z \equiv at$, it is easy to conclude that

$$\mathrm{Im}(\tilde{R}(\alpha)) = \mp \frac{\pi K}{a} e^{-1/(a\alpha_s)} (a\alpha_s)^{-b}. \tag{3.52}$$

In the above expression, the signs represent the contour on the upper and lower complex plane, respectively. We can check that, since we are dealing with small terms $(a\alpha_s)$, the resulting expression is exponentially small and non-perturbative, since a series expansion of $e^{-1/(a\alpha_s)}$ is impracticable.

Thus, this non-perturbative behaviour is related to the running coupling, shown in Fig. 7. While at short-distances the perturbative approach is correct, at large-distances it does not work — α_s is not a small perturbative parameter anymore. It is possible to separate the short- and long-distance parts, where the short-distance is characterized by a large scale Q, while the large-distance is characterized by a small scale Λ, with $\Lambda \sim 1$ GeV. However, the Operator Product Expansion (OPE), which factorizes the short- and

[XIX] This will become clearer soon: as we will see, non-sign-alternating series are related to infrared, non-perturbative divergences.

long-distances behaviours, is exact up to power corrections[18],

$$R(Q,\Lambda) = C(Q,\mu) \otimes \langle \mathscr{O} \rangle(\mu,\Lambda) + \text{power corrections} \left(\frac{\Lambda}{Q}\right)^p. \tag{3.53}$$

The relation between both expressions comes from the logarithmic expression for α_s — substituting Eq. (3.42), where we used the scale $\mu_0 \equiv Q$, in Eq. (3.52) yields

$$\begin{aligned} \text{Im}(\tilde{R}(\alpha_s)) &= \mp \frac{\pi K}{a} e^{-\frac{2\beta_0}{a}\ln(\Lambda/Q)} (-2a\beta_0 \ln(\Lambda/Q))^{-b} \\ &= \mp \frac{\pi K}{a} \left(\frac{\Lambda}{Q}\right)^{-2\beta_0/a} (-2a\beta_0 \ln(\Lambda/Q))^{-b}. \end{aligned} \tag{3.54}$$

In the above expression we note that the ambiguity possess a behaviour analogous to the power corrections in Eq. (3.53). Thus the terms present in the OPE can, in principle, cancel the ambiguity present in $\tilde{R}$. In fact this cancellation should occur, since observables can not have ambiguities, although in practice this remains a conjecture.

Therefore, this example shows that the ambiguity in the Borel integral is related to exponentially small terms due to IR divergences; the inclusion of OPE power corrections which needs to be inserted due to the non-perturbative character of QCD at low-energies then should cancel the ambiguity and result in a unambiguous observable.

Borel transform of the resummed gluon propagator

Since the leading-n_f terms in $H \to \gamma\gamma$ are due to the corrections to the gluon propagator shown in Fig. 8 (which we usually call *resummed gluon propagator*) at the NLO level, it is useful to introduce the resummed gluon propagator in Borel space.

Consider the gluon propagator, $G_{\mu\nu}$, with the corrections given by light quarks bubbles,

$$G_{\mu\nu} = \frac{-i}{k^2}\left(g_{\mu\nu} - \frac{k_\mu k_\nu}{k^2}\right)\frac{1}{1+\Pi_0(k^2)} + (-i)\xi\frac{k_\mu k_\nu}{k^4}. \tag{3.55}$$

The term $1+\Pi_0(k^2)$ in the denominator of the above expression encodes the effect of the corrections due to quark loops. Each renormalized fermion loop is given by

$$-\beta_{0,f}\alpha_s[\ln(-k^2/\mu^2) + C], \tag{3.56}$$

where

$$\beta_{0,f} = \frac{n_f}{6\pi} \tag{3.57}$$

is the fermionic contribution to the first term of the QCD β-function. The constant C depends on the renormalization scheme. For the $\overline{\text{MS}}$ scheme, $C = -5/3$; in the MS scheme, $C = -5/3 + \gamma_E - \ln 4\pi$.

Using the definition in Eq. (3.46), the resummed gluon propagator in Borel space reads[18]

$$B[\alpha_s G_{\mu\nu}](u) = \frac{(-i)}{k^2}\left(g_{\mu\nu} - \frac{k_\mu k_\nu}{k^2}\right)\left(-\frac{\mu^2}{k^2}e^{-C}\right)^u + (-i)\xi\frac{k_\mu k_\nu}{k^4}, \tag{3.58}$$

where

$$u = -\beta_{0,f}t. \tag{3.59}$$

Notice that, in the definition of the transformation (Eq. (3.58)), we multiplied the gluon propagator by α_s; thus, the lowest order term in the u expansion corresponds already to the first QCD correction. Furthermore, in Eq. (3.58), besides the factor $(-\mu^2 e^{-C})^u$, the first term of the propagator is basically the original gluon propagator in Landau gauge, with a modification in the power of the denominator momentum, $k^2 \to (k^2)^{1+u}$. Substituting this propagator in the first QCD correction due to a gluon exchange yields the leading-n_f terms, i.e., the large-n_f limit.

3.4 Large-β_0 limit

After calculating the leading-n_f terms for the process at hand, we finally are ready to proceed to the so-called large-β_0 limit, which consists in modifying the term n_f in the resulting expression by

$$n_f \to 6\pi\beta_0, \tag{3.60}$$

where β_0 is the first coefficient of the full β-function. Note that this seems to contradict our definition of $\beta_{0,f}$, Eq. (3.57), since now we are substituting $\beta_{0,f}$ by β_0. This procedure is known as *naive non-abelianization*[XX] — by substituting the fermionic contribution of the first term of the β-function by the full first term of the β-function, we are in some sense including a set of non-Abelian diagrams of QCD in our result. Therefore, the naive non-abelianization incorporates the non-Abelian character of QCD into our calculation, in particular asymptotic freedom, which is behind the behaviour shown in Fig. 7. The substitution of Eq. (3.60) is crucial given the fact that $\beta_{0,f}$ and β_0 have opposite signs, which leads to fundamental differences between non-Abelian and Abelian field theories[36] and has an important consequence in the sign alternation of the series coefficients, as we will see in the next section.

3.5 Renormalons

The divergent behaviour of the series in α_s leads to singularities on the real axis in Borel space. Thus, the study of these singularities is of big importance, because they contain information about the behaviour of the original series at short- and long-distances.

[XX] Both naive non-abelianization and the large-β_0 limit refers to the same procedure. We cited the former to show the idea behind this procedure.

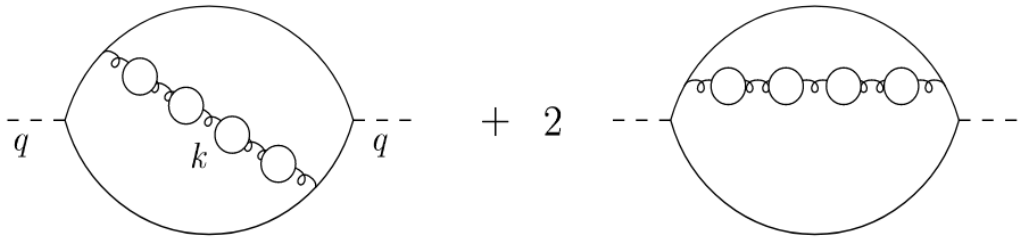

Figure 10 – Diagrams of the gluons corrections for the computation of the Adler function. Note that each bubble diagram in the gluon propagator leads to a leading-n_f term in the series expansion.

Source: Adapted from SHIFMAN.[36]

Renormalon is the name given to the singularities that may appear in the u-variable real axis in calculations in Borel space, due to the low- and high-energy behaviour of the original series. The renormalon closest to the origin is called the *leading renormalon*. Consider, for example, the Borel transform of a function with two poles, $x = x_1$ and $x = x_2$, with $|x_1| > |x_2|$. Generically, the contributions of these poles to the series can be written

$$B[R](u) = \frac{A}{(u - x_1)^\gamma} + \frac{B}{(u - x_2)^\gamma}. \tag{3.61}$$

Expanding the above expression, we have

$$B[R](u) = \sum_{n=0}^{\infty} \left[\frac{(\gamma + n - 1)!\,(-1)^\gamma}{(\gamma - 1)!\,n!} \left(\frac{A}{(x_1)^{\gamma+n}} + \frac{B}{(x_2)^{\gamma+n}} \right) u^n \right] \tag{3.62}$$

which, in view of the correspondence with the original series, can be written

$$R(\alpha_s) = \sum_{n=0}^{\infty} \left[\frac{(\gamma + n - 1)!\,(-1)^\gamma (-\beta_{0,f})^n}{(\gamma - 1)!} \left(\frac{A}{(x_1)^{\gamma+n}} + \frac{B}{(x_2)^{\gamma+n}} \right) \alpha_s^n \right] \tag{3.63}$$

In the above expression, one can see the factorial divergent behaviour of the original series. Furthermore, the closest the pole is to the origin, the more dominant it is: it sets the pace of the divergence in the denominator, since $1/x_1 < 1/x_2$.

Additionally, the location of the dominant renormalon is an indicator of the series sign alternation. The positive singularities are called infrared (IR) renormalons, because they originate from IR regions in the higher-order diagrams, while the negative singularities are called ultraviolet (UV) renormalons, since they originate from UV regions in the bubble corrections. If the leading renormalon is an IR one, the series coefficients have a fixed

sign; otherwise, the series coefficients have alternating sign — this can be checked in the development of Eq. (3.63). The leading renormalon tell us what kind of divergence dominates in large-β_0 calculations.

To better explain why we call these singularities IR and UV renormalons, we will present a canonical example, based on Ref.[36]. Consider the correlation function depicted in Fig. 10, $\Pi_{\mu\nu}$, where the external legs (i.e. the dashed lines) are from massless quarks:

$$\Pi_{\mu\nu}(q) = i\int d^4x e^{-iq\cdot x}\langle T\{j_\mu(x)j_\nu(0)\}\rangle = \Big(q_\mu q_\nu - q^2 g_{\mu\nu}\Big)\Pi(Q^2), \tag{3.64}$$

where $j_\mu = \bar{\psi}\gamma_\mu\psi$ and $Q^2 = -q^2$. The number of flavours is n_f. (This correlation function is related to vacuum polarization contributions to the photon propagator, for example.) It is clear that Q^2 sets the scale of the problem, since it is the only available scalar scale. We will work with the (reduced) Adler function, D_A, defined as

$$D_A(Q^2) = -4\pi^2 Q^2 \frac{d\Pi(Q^2)}{dQ^2} \tag{3.65}$$

and is normalized to 1 at LO.

Now, we consider the collection of all possible bubble corrections in Fig. 10. There is a decoupling between the loops internal to the gluon propagator and the outer loop; therefore, when we consider all corrections, the net result is a two-loop diagram with a modified gluon propagator (as depicted in Fig. 8). The exact result for the above expression can be found in Ref.[37]. However, for our purposes, the simplified expression

$$D_A = (\text{const}) \times Q^2 \int dk^2 \, \frac{k^2\alpha_s(k^2)}{(k^2+Q^2)^3}, \tag{3.66}$$

where (const) is a numerical constant which will not be important for our analysis, coincides with the exact result in the limits $k^2 \gg Q^2$ and $k^2 \ll Q^2$ (up to some details which do not influence our study). In this simplified expression, the integration on the original two-loop integral over one loop-momentum and over the angular dependence of the remaining loop-momentum, which we denoted k, were already performed.

Now, we will analyze both the IR and UV regime (compared to the scale Q^2) of the Adler function. In the IR regime, where $k^2 \ll Q^2$, the Adler function expansion, up to a constant, reads[36]

$$D_A \sim \frac{\alpha_s^Q}{Q^4}\sum_{n=0}^{\infty}\Big(-\beta_{0,f}\alpha_s^Q\Big)^n \int dk^2 k^2 \left[\ln\left(\frac{Q^2}{k^2}\right)\right]^2, \tag{3.67}$$

where we defined $\alpha_s^Q \equiv \alpha_s(Q^2)$. The logarithm comes from the α_s running, as e.g. in

Eq. (3.42). Now, if we perform the change of variables

$$y = 2\ln\left(\frac{Q^2}{k^2}\right),$$

we end up with the resulting expression

$$D_A(Q^2) \sim -\frac{\alpha_s^Q}{2}\sum_{n=0}^{\infty}\left(-\frac{\beta_{0,f}\alpha_s^Q}{2}\right)^n \int dy\, e^{-y}y^n. \tag{3.68}$$

The integral in the above expression is simply $\Gamma(n+1)$,

$$\int dy\, e^{-y}y^n \equiv \Gamma(n+1) = n!\,. \tag{3.69}$$

Therefore, for k^2 in the IR region, we have

$$D_A(Q^2) \sim -\frac{\alpha_s^Q}{2}\sum_{n=0}^{\infty}\left(-\frac{\beta_{0,f}\alpha_s^Q}{2}\right)^n n!\,, \qquad k^2 \ll Q^2. \tag{3.70}$$

As we noted before, the IR regime results in a factorially divergent series. Thus, when we perform the Borel transform of this expression, the division by $n!$ leads to a geometric progression formula, which introduces a singularity when summed, i.e.,

$$B[D_A(Q^2)](t) \sim \sum_{n=0}^{\infty}\left(-\frac{\beta_{0,f}t}{2}\right)^n = \sum_{n=0}^{\infty}\left(\frac{u}{2}\right)^n, \tag{3.71}$$

which can be summed to

$$B[D_A(Q^2)](t) \sim \frac{1}{1-\frac{u}{2}}. \tag{3.72}$$

where we substituted $u = -\beta_{0,f}t$ in the last equality sign of Eq. (3.71). Thus, we conclude that the contribution of the IR region in Eq. (3.66) leads to positive singularities in the real axis. Note also that, in Eq. (3.71), the series in u have a fixed sign. This can be seem in the original series in α_s, Eq. (3.71) — although this seems to be a alternating sign series, when we perform the large-β_0 limit, i.e. change $\beta_{0,f}$ by β_0, due to the fact that $\beta_{0,f}$ and β_0 have different signs ($\beta_{0,f}$ is positive while β_0 is negative), the original series have fixed sign in the large-β_0 limit.

On the other hand, in the UV regime, where $k^2 \gg Q^2$, the Adler function, up to a constant, reads[36]

$$D_A(Q^2) \sim Q^2\alpha_s^Q\sum_{n=0}^{\infty}\left(\beta_{0,f}\alpha_s^Q\right)^n \int dk^2\frac{1}{k^2}\left[\ln\left(\frac{k^2}{Q^2}\right)\right]^n. \tag{3.73}$$

Performing the change of variable $y = \ln\left(\frac{k^2}{Q^2}\right)$, we have the following expression:

$$D_A(Q^2) \sim \alpha_s^Q \sum_{n=0}^{\infty} \left(\beta_{0,f}\alpha_s^Q\right)^n \int dy\, e^{-y} y^n = \alpha_s^Q \sum_{n=0}^{\infty} \left(\beta_{0,f}\alpha_s^Q\right)^n n!\,. \tag{3.74}$$

As we noted earlier, once again, the high-energy limit leads to a factorially divergent behaviour of the series expansion. Therefore, the Borel transform of this expression would lead to

$$B[D_A(Q^2)](t) \sim \sum_{n=0}^{\infty} \left(\beta_{0,f} t\right)^n = \sum_{n=0}^{\infty} (-u)^n = \frac{1}{1+u}. \tag{3.75}$$

Here there are two things to note: first, the singularity in this regime has an opposite sign compared to the IR singularity — the UV singularities are on the negative real axis. Once again we see that, in the original series expansion, Eq. (3.73), performing the large-β_0 limit yields an alternating sign series. Second, the IR pole is located at $u = 2$, while the UV pole is located at $u = -1$, i.e., the UV renormalon is closest to the origin than the IR one. In our example, we see that, for (very) high-orders, the UV divergences dominates over the IR ones. Therefore, in higher-orders we have alternating sign.

In full QCD, the singularities are no longer poles. In fact, using renormalization group methods, it is possible to show a correspondence between the large-β_0 poles in u and *branch cuts* in full QCD at the same location, i.e. the renormalons in the naive non-Abelianization are translated to branch cuts in QCD.

Having studied the construction of the Standard Model and investigated the basic properties of QCD at high orders — which will be important for our perturbative calculations —, we conclude the SM theoretical framework with the Higgs sector, where we will introduce the basics about the Higgs particle to proceed with our main calculation.

4 THE HIGGS SECTOR

The Brout-Englert-Higgs boson, or simply Higgs boson, was the name given to the scalar particle proposed in 1964[10,11] in order to enable massive terms for the Electroweak gauge bosons in the SM Lagrangian while keeping the underlying symmetry intact.

Discovered in 2012 by the independent LHC collaborations ATLAS and CMS with an averaged mass $M_H = 125.09 \pm 0.24$ GeV[14,15], it was the missing piece in the SM Lagrangian. After its discovery, in the intermediate mass range between the EW bosons and the top quark masses, the calculation of precise perturbative corrections became necessary in order to match the increasing experimental accuracy and test the SM validity or its domain of validity.

An important Higgs observable to check whether there are deviations from the SM are the so-called *signal strengths*, the ratio between the cross section of production and decay of the Higgs measured (by the LHC) and the theoretical predictions obtained within Standard Model. Mathematically, for a given decay channel X, it is defined as

$$\mu_X = \frac{\sigma(pp \to H \to X)^{\text{exp}}}{\sigma(pp \to H \to X)^{\text{SM}}}. \tag{4.1}$$

This is an interesting quantity because if the Higgs behaves as the SM one, μ_X should be compatible with one for all decay channels X, while deviations from this value indicate the possibility of physics Beyond the Standard Model (BSM).

The combined measurements of the CMS and ATLAS Run-1 results in an averaged signal strength are given by[14]

$$\bar{\mu}_{\text{Run1}} = 1.09 \pm 0.11, \tag{4.2}$$

in agreement with the SM. For the Run-II, the global signal strength result is[16]

$$\bar{\mu}_{\text{Run2}} = 1.06 \pm 0.07, \tag{4.3}$$

once again showing no significant deviations from the SM, but presenting already an important error reduction, stressing the role of precise calculations. Other properties, such as parity measurements, reinforce the agreement with the SM proposed particle[38] — the measured boson presents properties compatible with a scalar particle, not a pseudo-scalar one. Therefore, so far the Higgs boson announced in 2012, which awarded the 2013 Nobel prize in physics to Higgs and Englert[39,40], seems to possess the properties predicted more than 50 years before its discovery.

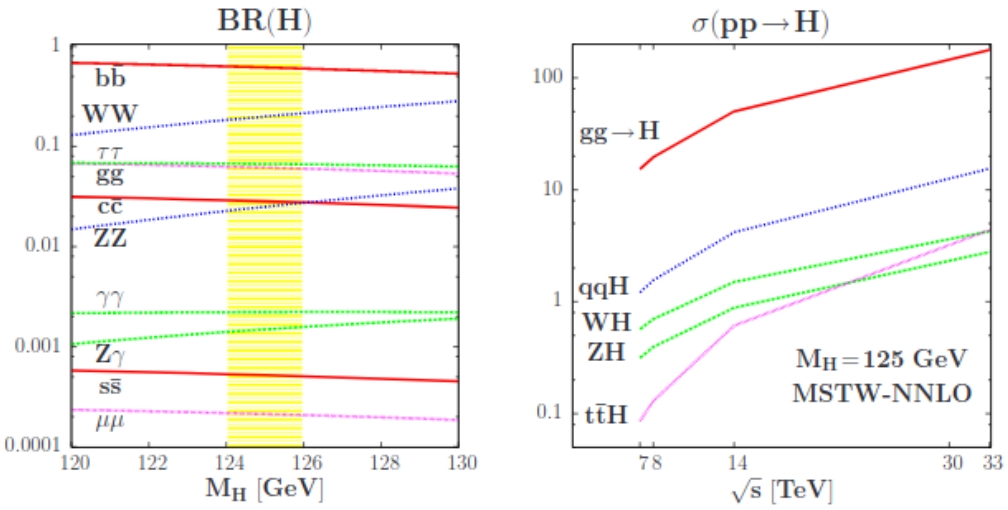

Figure 11 – Left: branching ratios for a Higgs boson with SM properties in the mass range $120 - 130$ GeV. Right: cross-section for the Higgs production in a proton collider as a function of the c.m. energy.

Source: Adapted from DJOUADI.[42]

4.1 The Higgs boson at the LHC

The LHC is a hadron collider located in Geneva near the border between France and Switzerland. Currently, it is the largest and most powerful particle accelerator in the world[41]. Its debut year was 2008, with the Run-1 starting in 2009. After the first run, with a center of mass (c.m.) energy of $\sqrt{s} = 7$ and 8 TeV, in 2013 the Long Shutdown 1 (LS1) was implemented to perform upgrades in the accelerator (improve c.m. energy and luminosity). The Run-2 started in 2015 with a c.m. energy of $\sqrt{s} = 13$ TeV (although the original plan was to reach 14 TeV). At the time of writing, LHC is under its Long Shutdown 2 (LS2) for further improvements in the luminosity of the hadron collider.

The Higgs boson production at the LHC, both in the Run-I c.m. energy $\sqrt{s} = 7$ and $\sqrt{s} = 8$ GeV and at the current c.m energy $\sqrt{s} = 13$ TeV, occurs mainly through gluon fusion, whose leading order diagram is shown in Fig. 12. On the right-hand panel of Fig. 11 we can see that it is approximately 10 times larger than the second-to-dominant production mode at LHC, quark fusion, as can be seen comparing the red and blue lines.

The main decay channel for a Higgs boson with mass $M_H = 125.10$ GeV[26] is into a $b\bar{b}$ pair, followed by the decay into a pair of charged electroweak bosons, W^+W^- (one of them off-mass shell). The left-hand panel of Fig. 11 shows the decay widths of the Higgs boson at the LHC. As one can see, the Higgs decay into photons, with which we are concerned in this work, is not among the dominant decays. However, it was the first channel where the Higgs particle was detected.[14,15] This is so because this channel is a clean one, i.e. it has not a strong background noise. On the other hand, the dominant decay channel,

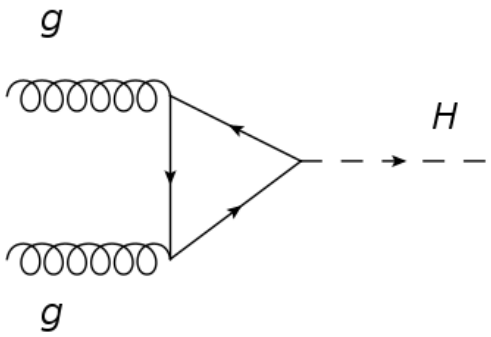

Figure 12 – LO diagram of the gluon fusion, the main Higgs production at the LHC.

Source: By the author.

into a $b\bar{b}$ pair, has a significant background contamination — because it involves jets and hadronization, the creation of hadrons — and is thus of much more complex detection in the environment of a hadronic collider. For this reason, the decay $H \to b\bar{b}$ was observed (with 5σ confidence level) only in 2018 with the combination of the data from Run 1 and Run 2[43].

4.2 The Leading Order decay into photons

As we saw in Ch. 2, the Higgs coupling to fermions, $g_{Hf\bar{f}}$, is given by

$$g_{Hf\bar{f}} = i\frac{m_f}{v}, \tag{4.4}$$

i.e., it is proportional to the fermion mass, m_f, and inversely proportional to the Higgs v.e.v., v. Furthermore, the Higgs boson does not interact with massless SM constituents. Thus, the LO Higgs decay into photons must be mediated by loops of massive particles — more precisely, by triangle loops of massive fermions and of massive charged gauge bosons, as shown in Fig. 13. The decay width of the process $H \to \gamma\gamma$ can be written as

$$\Gamma(H \to \gamma\gamma) = \frac{M_H^3}{64\pi} \mid A_W(\tau_W) + \sum_f A_f(\tau_f) \mid^2, \tag{4.5}$$

where the first amplitude, A_W, is due to the purely bosonic diagram, with the LO shown on the left-hand panel of Fig. 13, while A_f is due to the decay mediated by fermion loops, with the LO shown on the right-hand panel of Fig. 13 — both these amplitudes are series expansions in the theory couplings. In the above expression, $\tau_f = \frac{M_H^2}{4m_f^2}$ and $\tau_W = \frac{M_H^2}{4M_W^2}$. Numerically, the relevant τ-values for our work read $\tau_t \approx 0.13$ and $\tau_W \approx 0.6$.

We are interested in the top contribution — more specifically in the limit where $m_t \to \infty$ because the first correction in the expansion τ_t is of approximately 10%, i.e., the infinitely heavy top quark is a good approximation. Thus, we will now calculate the leading order expression for the Higgs decay into photons in detail in this heavy-quark

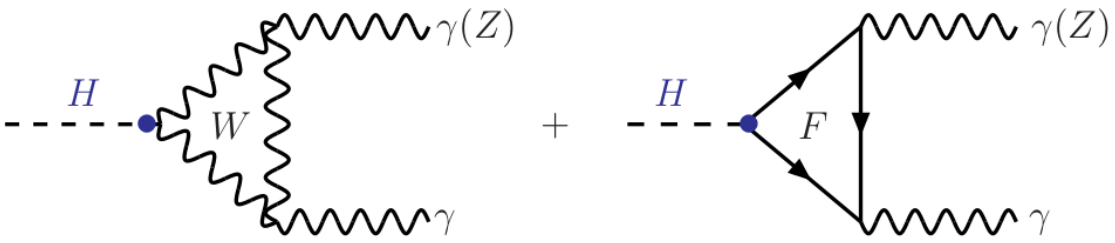

Figure 13 – The two types of Feynman diagrams present in the LO decay of the Higgs boson into photons. The left diagram represents the purely bosonic amplitude, A_W, while the right diagram represents the amplitude due to and fermion-loop induced decay.

Source: Adapted from DJOUADI.[42]

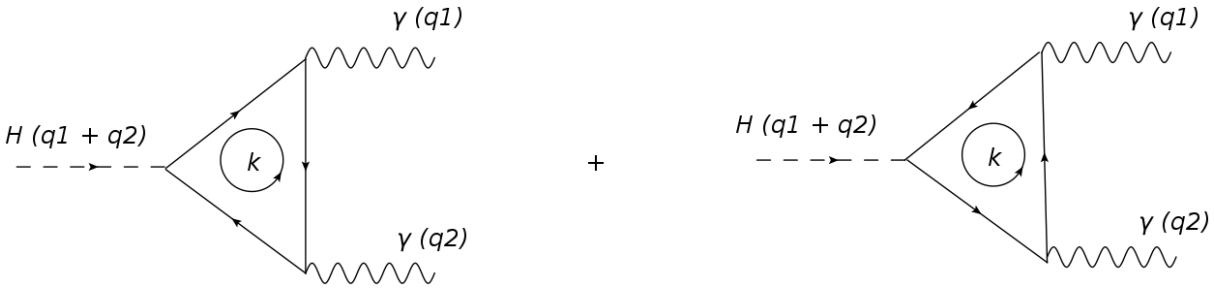

Figure 14 – Feynman diagrams for the LO decay of the Higgs boson into a pair of photons.

Source: By the author.

limit to start our quantitative analysis; then, we will proceed in later chapters to the QCD corrections.

Since the final state particles are identical, we have two diagrams for the LO process $H(q_1+q_2)\to\gamma(q_1)+\gamma(q_2)$, shown in Fig. 14. Note that the interchange of the final-state photons is equivalent to changing the direction of top momentum in the loop while keeping the loop-momentum flow unchanged. Using the Feynman rules, the transition amplitude is given by

$$\begin{aligned} i\mathscr{M} &= e^2 Q_t^2 N_c \left(\frac{m_f}{v}\right) \varepsilon^{\mu}_{\lambda_1}(q_1)\varepsilon^{\nu}_{\lambda_2}(q_2) \\ &\times \left(\int \frac{d^D k}{(2\pi)^D} \frac{\mathrm{Tr}[(\not{k}+\not{q}_2+m_t)\gamma_\nu(\not{k}+m_t)\gamma_\mu(\not{k}-\not{q}_1+m_t)]}{[(k+q_2)^2-m_t^2][k^2-m_t^2][(k-q_1)^2-m_t^2]} \right. \\ &\left. + \int \frac{d^D k}{(2\pi)^D} \frac{\mathrm{Tr}[(\not{q}_1-\not{k}+m_t)\gamma_\mu(-\not{k}+m_t)\gamma_\nu(-\not{k}-\not{q}_2+m_t)]}{[(k+q_2)^2-m_t^2][k^2-m_t^2][(k-q_1)^2-m_t^2]} \right), \end{aligned} \tag{4.6}$$

where e is the positron electromagnetic charge (so that $Q_e=-1$), Q_t is the top-quark charge and N_c is the number of colours of the QCD gauge group $SU(N_c)$. $\lambda_{1,2}$ are the two possible photon polarizations and a minus sign was included in view of the fermion loop.

Solving the trace we have

$$
\begin{aligned}
i\mathscr{M} &= e^2 Q_t^2 N_c \frac{8m_t^2}{v} \varepsilon^{\mu}_{\lambda_1}(q_1)\varepsilon^{\nu}_{\lambda_2}(q_2) \\
&\times \int \frac{d^D k}{(2\pi)^D} \frac{g_{\mu\nu}(m_t^2 - k^2 - q_1\cdot q_2) + 4k_\mu k_\nu + q_{1\nu}q_{2\mu}}{[(k+q_2)^2 - m_t^2][k^2 - m_t^2][(k-q_1)^2 - m_t^2]},
\end{aligned}
\tag{4.7}
$$

where we used the Ward's identity[28], $q_1 \cdot \varepsilon^{\mathrm{A}}_{\lambda_1}(q_1) = q_2 \cdot \varepsilon^{\mathrm{A}}_{\lambda_2}(q_2) = 0$. Now we use the Feynman parameters, the fact that the final state photons are on-shell — i.e. $q_1^2 = q_2^2 = 0$ — and exchange the order of integration such that

$$
\begin{aligned}
i\mathscr{M} &= e^2 Q_t^2 N_c \frac{8m_f^2}{v} \varepsilon^{\mu}_{\lambda_1}(q_1)\varepsilon^{\nu}_{\lambda_2}(q_2) \\
&\times \int_0^1 dx \int_0^{1-x} dy \int \frac{d^D k}{(2\pi)^D} \frac{g_{\mu\nu}(m_t^2 - k^2 - q_1\cdot q_2) + 4k_\mu k_\nu + q_{1\nu}q_{2\mu}}{[(k - yq_1 + xq_2)^2 + 2xyq_1\cdot q_2 - m_t^2]^3}.
\end{aligned}
\tag{4.8}
$$

As is always the case for 1-loop diagrams where we introduce Feynman parameters, we shift the integration momentum, $k \to k + yq_1 - xq_2$. We note that linear terms in the numerator vanish because the integrand in these cases is odd. The tensor integral can be reduced to scalar ones through Passarino-Veltman reduction[44] (or simply tensor reduction). In our case we need to write

$$
\int \frac{d^D k}{(2\pi)^D} \frac{k_\mu k_\nu}{[k^2 - M]^3} = g_{\mu\nu} C_2. \tag{4.9}
$$

Note that, on the r.h.s. of the above expression, $g_{\mu\nu}$ is the only rank-two tensorial structure available in the kernel of the integration, that is, it is the only d.o.f. allowed since there are no q's in the integrand. Now, contracting both sides with $g^{\mu\nu}$ yields

$$
C_2 = \frac{1}{D} \int \frac{d^D k}{(2\pi)^D} \frac{k^2}{[k^2 - M]^3}. \tag{4.10}
$$

Substituting the rank-two tensorial factor (Eq. 4.9), we end up with the scalar integral

$$
\begin{aligned}
i\mathscr{M} &= e^2 Q_t^2 N_c \frac{8m_t^2}{v} \varepsilon^{\mu}_{\lambda_1}(q_1)\varepsilon^{\nu}_{\lambda_2}(q_2) \\
&2 \times \int_0^1 dx \int_0^{1-x} dy \\
&\times \int \frac{d^D k}{(2\pi)^D} \frac{g_{\mu\nu}(m_t^2 + k^2(\frac{4}{D} - 1) - q_1\cdot q_2(2xy-1)) + q_{1\nu}q_{2\mu}(1-4xy)}{[k^2 + 2xyq_1\cdot q_2 - m_t^2]^3}.
\end{aligned}
\tag{4.11}
$$

The resulting inner integrals are rather simple and tabulated, e.g. in Ref.[30]. The results needed are

$$
\int \frac{d^D k}{(2\pi)^D} \frac{1}{(k^2 - A)^\lambda} = \frac{i\pi^{D/2}}{(2\pi)^D} (-1)^\lambda \frac{\Gamma(\lambda - D/2)}{\Gamma(\lambda) A^{\lambda - D/2}} \tag{4.12}
$$

and

$$\int \frac{d^D k}{(2\pi)^D} \frac{k^2}{(k^2 - A)^\lambda} = \frac{i\pi^{D/2}}{(2\pi)^D} (-1)^\lambda \frac{\Gamma(\lambda - D/2)}{\Gamma(\lambda) A^{\lambda - 1 - D/2}} \frac{(-D/2)}{\lambda - 1 - D/2}. \tag{4.13}$$

Thus, the transition amplitude is left as a two-dimensional integral on the Feynman parameters x and y,

$$\begin{aligned} i\mathscr{M} = &-\frac{ie^2 Q_t^2 N_c}{(4\pi)^{2-\epsilon}} \frac{8m_f^2}{v} \Gamma(1+\epsilon) \varepsilon^\mu_{\lambda_1}(q_1) \varepsilon^\nu_{\lambda_2}(q_2) \\ &2 \times \int_0^1 dx \int_0^{1-x} dy \, \frac{g_{\mu\nu} q_1 \cdot q_2 (4xy - 1) + q_{1\nu} q_{2\mu} (1 - 4xy)}{(m_t^2 - 2q_1 \cdot q_2 xy)^{1+\epsilon}}, \end{aligned} \tag{4.14}$$

where we replaced $D = 4 - 2\epsilon$. Using the kinematic identity $q_1 \cdot q_2 = \frac{m_H^2}{2}$ and substituting $e^2 \to 4\pi\alpha \left(\frac{\mu^2 e^{\gamma_E}}{4\pi} \right)^\epsilon$, where α is the fine structure constant, whose value is[45] $\alpha(Q^2 = 0) = 1/137.035999084(21)$, we have the expression

$$\begin{aligned} i\mathscr{M} = &-i \frac{\alpha}{\pi} \frac{2m_t^2}{v} (\mu^2 e^{\gamma_E})^\epsilon \Gamma(1+\epsilon) \varepsilon^\mu_{\lambda_1}(q_1) \varepsilon^\nu_{\lambda_2}(q_2) \\ &\times \int_0^1 dx \int_0^{1-x} dy \, \frac{(g_{\mu\nu} \frac{m_H^2}{2} - q_{1,\nu} q_{2,\mu})(4xy - 1)}{(m_t^2 - m_H^2 xy)^{1+\epsilon}} + \mathscr{O}(\epsilon). \end{aligned} \tag{4.15}$$

Now, notice that the quantity $\tau_t \equiv \frac{M_H^2}{4m_t^2}$ can be introduced in the denominator of the integral, and we can write

$$\begin{aligned} &\int_0^1 dx \int_0^{1-x} dy \, \frac{(g_{\mu\nu} \frac{m_H^2}{2} - q_{1,\nu} q_{2,\mu})(4xy - 1)}{(m_t^2 - m_H^2 xy)^{1+\epsilon}} \\ &\quad = \frac{(g_{\mu\nu} \frac{m_H^2}{2} - q_{1,\nu} q_{2,\mu})}{\left(m_t^2\right)^{1+\epsilon}} \int_0^1 dx \int_0^{1-x} dy \, \frac{4xy - 1}{(1 - 4xy\tau_t)^{1+\epsilon}}. \end{aligned} \tag{4.16}$$

Thus, expanding the expression in the infinitesimal parameter $\epsilon \sim 0$ yields

$$i\mathscr{M} = -\frac{i2\alpha}{\pi v} I(\tau_t) \varepsilon^\mu_{\lambda_1}(q_1) \varepsilon^\nu_{\lambda_2}(q_2) \left(g_{\mu\nu} \frac{m_H^2}{2} - q_{1,\nu} q_{2,\mu} \right) + \mathscr{O}(\epsilon), \tag{4.17}$$

where we defined $I(\tau_t)$ as the integral

$$\begin{aligned} I(\tau_t) &= \int_0^1 dx \int_0^{1-x} dy \, \frac{4xy - 1}{1 - 4xy\tau_t} \\ &= \int_0^1 dx \int_0^{1-x} dy \, (4xy - 1) \left(1 + 4xy\tau_t + 16x^2 y^2 \tau_t^2 + \mathscr{O}(\tau_t^3) \right) \\ &= -\frac{1}{3} - \frac{7}{90}\tau_t - \frac{2}{63}\tau_t^2 + \mathscr{O}(\tau_t^3), \end{aligned} \tag{4.18}$$

where we expanded in τ_t in the second equality sign. Solving the leading term (i.e. τ_t^0)

explicitly and ignoring the τ_t corrections, we arrive at the final result,

$$i\mathscr{M} = N_c \frac{2i\alpha Q_t^2}{3\pi v} \varepsilon^{\mu}_{\lambda_1}(q_1)\varepsilon^{\nu}_{\lambda_2}(q_2)\left(g_{\mu\nu}\frac{m_H^2}{2} - q_{1,\nu}q_{2,\mu}\right) + \mathscr{O}(\epsilon, \tau_t). \tag{4.19}$$

Now, we will analyze the tensorial structure left in the expression. Since we are interested in the amplitude squared, and we need to average over the final-state photon polarizations, we have[XXI]

$$\begin{aligned}
&\frac{1}{4}\sum_{\lambda_1,\lambda_2} \varepsilon^{\mu}_{\lambda_1}(q_1)\varepsilon^{\lambda}_{\lambda_1}(q_1)\varepsilon^{\nu}_{\lambda_2}(q_2)\varepsilon^{\rho}_{\lambda_2}(q_2)\left(g_{\mu\nu}\frac{m_H^2}{2} - q_{1,\nu}q_{2,\mu}\right)\left(g_{\lambda\rho}\frac{m_H^2}{2} - q_{1,\rho}q_{2,\lambda}\right) \\
&\quad = \frac{1}{4}g^{\mu\lambda}g^{\nu\rho}\left(g_{\mu\nu}\frac{m_H^2}{2} - q_{1,\nu}q_{2,\mu}\right)\left(g_{\lambda\rho}\frac{m_H^2}{2} - q_{1,\rho}q_{2,\lambda}\right) \\
&\quad = \frac{M_H^4}{8}.
\end{aligned} \tag{4.20}$$

Therefore, we can write

$$|\mathscr{M}|^2 = \frac{M_H^4}{8}\left|\frac{2\alpha Q_t^2 N_c}{3\pi v}\right|^2 + \mathscr{O}(\epsilon, \tau_t). \tag{4.21}$$

Now we use the phase space expression for two-body decays[26],

$$d\Gamma = \frac{1}{32\pi^2}|\mathscr{M}|^2\frac{|\mathbf{p}_1|}{M_H^2}d\Omega, \tag{4.22}$$

where $\mathbf{p}_1$ is the 3-momentum of one of the final particles in the center of mass frame and $d\Omega$ is the element of solid angle. Notice that the transition amplitude has no angular dependence and thus the integral in Ω is easily summed to 4π. Casting the final decay width expression in the desired form,

$$\Gamma(H \to \gamma\gamma) = \frac{M_H^3}{64\pi}|A_W(\tau_W) + A_t(\tau_t)|^2, \tag{4.23}$$

we conclude, from our development, that the LO term for the top contribution to the decay is given by

$$A_t = \frac{2\alpha Q_t^2 N_c}{3\pi v}, \tag{4.24}$$

in agreement with Ref.[46]. For completeness, the amplitude due to the purely bosonic diagrams, A_W, which will not be calculated in this work, is given by[24]

$$A_W(\tau_W) = \frac{\alpha}{2\pi v}A_1(\tau_W), \tag{4.25}$$

[XXI] A factor of $1/2$ is included as a normalization factor for the 2 polarizations, while $\sum_\lambda \varepsilon^{\mu}_{\lambda}\varepsilon^{\nu}_{\lambda} = g^{\mu\nu}$.

where the function $A_1(\tau_W)$ is defined as

$$A_1(\tau_W) = -[2\tau_W^2 + 3\tau_W + 3(2\tau_W - 1)f(\tau_W)]\tau_W^{-2} \tag{4.26}$$

with

$$f(\tau_W) = \arcsin^2(\sqrt{\tau_W}). \tag{4.27}$$

As a side comment, although necessary because of some recent discussions, we explain the use of dimensional regularization in this calculation. It was argued recently, in Ref[47], that since the LO decay is already at the one-loop level and in view of the impossibility of addition of counterterms to absorb divergences, the result must be finite, and the calculation in dimreg is not necessary and leads to the wrong result. However, it turns out that, although the final result is indeed finite, the introduction of dimensional regularization is necessary because the calculation presents UV divergences separately which only cancel after their sum[48]. A simple example present in Ref.[48] shows this feature in a neat way. Consider the integral

$$F = \int_0^1 dx\, x^\epsilon (1-x)^\epsilon \left(x + \frac{1}{x} - \frac{1}{1-x} \right) \tag{4.28}$$

with $\epsilon > 0$. This integral yields a finite result,

$$F = \frac{\Gamma(1+\epsilon)\Gamma(2+\epsilon)}{\Gamma(3+2\epsilon)} = \frac{1}{2} + \mathcal{O}(\epsilon). \tag{4.29}$$

However, the integral

$$\int_0^1 dx \left(x + \frac{1}{x} - \frac{1}{1-x} \right) \tag{4.30}$$

is ill-defined — the integral does not converge (the divergences do not cancel). Therefore, we can not exclude the regulators $x^\epsilon(1-x)^\epsilon$ *before* the integration, i.e., we need to introduce dimensional regularization in order to have a well-defined integrand where the divergences *cancel* and the final result converges. Thus, we proceeded with the calculation in conventional dimreg which yielded the correct result in literature.

Returning to our calculation, we would like to note that this framework expanding in powers of $M_H^2/4m_t^2$ constitute an Effective Field Theory. In this effective theory, when we consider only the first term in the expansion (i.e. $m_t \to \infty$), the net effect is the transformation of the internal structure of the loop into a local interaction of the Higgs with photons, Fig. 15. Therefore, in this framework, we can write a Lagrangian interaction piece between the Higgs boson and photons,

$$\mathscr{L}_{\text{eff}} = -\frac{1}{4} H C_{H\gamma\gamma} F_{\mu\nu} F^{\mu\nu}, \tag{4.31}$$

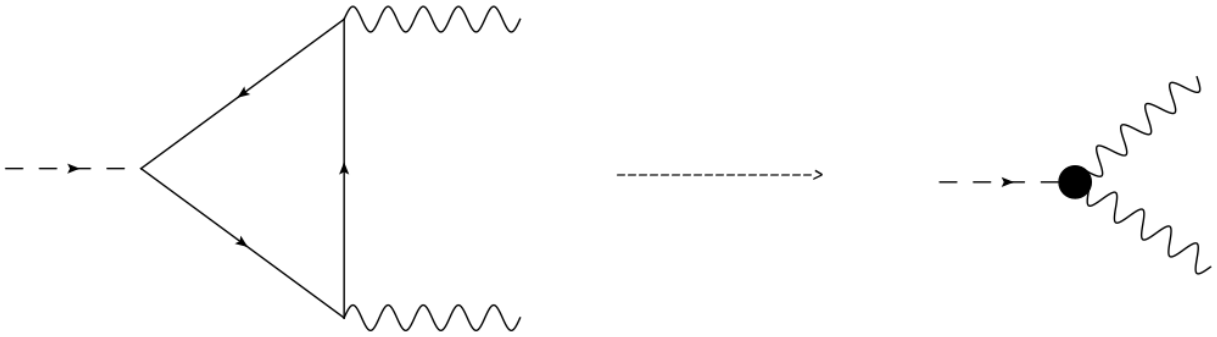

Figure 15 – Effective coupling of the Higgs boson with photons in the EFT with an infinitely heavy top quark. In this EFT, the internal structure (i.e. the triangle loop and its corrections) is ignored and only its net effect is considered.

Source: By the author.

We can write, for later convenience, the *effective coupling* $C_{H\gamma\gamma}$ as

$$C_{H\gamma\gamma} = \frac{2\alpha Q_t^2 N_c}{3\pi v} \sum_{n=0}^{\infty} C_{H\gamma\gamma}^{(n)} \left(\frac{\alpha_s}{\pi}\right)^n \tag{4.32}$$

With this interaction Lagrangian, the Feynman rules for the diagram in the right-hand panel of Fig. 15 reads

$$\begin{aligned} i\mathscr{M} &= \langle \gamma_\mu(q_1)\gamma_\nu(q_2)|T\{i\int d^4x \mathscr{L}_{\text{eff}}\}|H(q_1+q_2)\rangle \\ &= iC_{H\gamma\gamma}\varepsilon^\mu_{\lambda_1}(q_1)\varepsilon^\nu_{\lambda_2}(q_2)\left(g_{\mu\nu}\frac{m_H^2}{2} - q_{1,\nu}q_{2,\mu}\right). \end{aligned} \tag{4.33}$$

Considering the LO results, with only $n = 0$ in the summation, we recover the result of Eq. (4.19) with $C_{H\gamma\gamma}^{(0)} = 1$. We note that the addition of QCD corrections are encoded in the coefficients $C_{H\gamma\gamma}^{(n)}$, with $n > 0$, and in view of the factor outside the summation, these corrections are compared to unity. Thus, both approaches are equivalent (the one in full QCD expanding in powers of the inverse of the top quark mass and the EFT), i.e. we are constructing an EFT where we integrate out of the theory the top quark; in other words, the top quark is not a d.o.f. anymore in the EFT we just developed.

Having exhausted the LO scenario, we focus on the QCD corrections. The first QCD correction is related to the exchange of a virtual gluon between the virtual quarks in the triangle loop. Since the EW bosons do not interact strongly, they will not participate in the purely QCD corrections. Thus, only A_t will enter in our perturbative calculations.

These corrections involve several diagrams, and thus its calculation is lengthy and complex (for example, the NLO correction is already a 2-loop calculation) and is better performed with the help of computer programs. In the next chapter we will introduce the programs used in our calculations of the QCD corrections for the decay of the Higgs into photons.

5 INTRODUCTION TO MATAD

In the introductory chapters of this work we laid the theoretical basis for the calculation of the decay $H \to \gamma\gamma$. However, as we noted in the end of last chapter, the calculation at higher orders is lengthy and involves several diagrams. For the calculations presented in this work, the diagrams were generated using the program QGRAF[49]; the calculation of those diagrams were performed by the program MATAD[50]. MATAD is a program package for the computation of MAssive TADpoles written in FORM[51] by Matthias Steinhauser. It is aimed at the calculation of one-, two- and three-loop diagrams. By definition, "a tadpole is a part of a diagram which can be disconnected from all external legs if you cut just one line."[52] In our context, the tadpole structure is obtained when we expand the resulting loop-integrals in powers of q_i^2/m_t^2; with this expansion, the resulting integrals are topologically similar to tadpoles integrals — this is the procedure used by MATAD: after the program applies the projector, there is the expansion in inverse powers of the heavy parameter and then the mapping between with 1-, 2- or 3-loop tadpole integrals.

In this chapter we will introduce MATAD in a detailed manner using, as an example, the calculation of the Higgs decay into photons at the LO level, which was already investigated in detail in Sec. 4 and, therefore, can be compared and better understood.

The codes used in this work are available at the link https://github.com/g-neves/hgg-large-beta0. The folder `c_hgamgamlo/hgamgamlo` contains the problem $H \to \gamma\gamma$ at LO, while the folder `c_hgagalargeb0/hgagalargeb0` contains the calculation of the leading-n_f terms of the same decay at the NLO level. The auxiliary file `gnlargeB0tad2l` is on the main folder. In the remainder of this chapter we discuss the technical details of our implementation of this calculation.[XXII]

5.1 Introdution to MATAD

The `/matad` folder possesses the `/calc` file, which basically contains the whole program, and the `startform` file, which calls FORM to execute the program. The `/calc` folder is divided into several folders — `/common`, `/formswap`, `/generic`, `/matad` and `/problems` — which stores the program's built-in procedures, files and the problems to be calculated. The problem folder (where we specify the problem at hand) possesses the following files:[XXIII]

- `declare.#problem`
- `MISC (optional)`
- `#diagrams.dia`

[XXII] This pedagogical section can be skipped and represents no loss for the remaining of the text.
[XXIII] We use the symbol # to refer to a generic name, which is an input by the user.

- `GLOBAL`
- `#com.frm`

The `declare.#problem` file defines the variables used in the problem (functions, symbols etc) other than the built-in variables; it is important to be consistent with the problem's folder name and the declare file: both need to possess the same name.

The `MISC` file is optional; it is the file with the command lines to run the program to solve the problem at hand. The example problem files built-in the program contain examples of the content of the `MISC` file with command lines for the calculation of single diagrams and the sum of all diagrams after the QCD structure is computed.

The file `#diagrams.dia` is reserved for the implementation of the Feynman diagrams. It should be noted that the file name is free, but one needs to be consistent when calling the program with the command line present on the `MISC` file.

The `GLOBAL` file executes user specified actions during the stages of calculation, which are divided into `TREAT` folders in `FORM`. As an example, it is in this file where the user needs to implement the projector for the amplitude so that the program deals only with scalar quantities.

After the calculation of the diagrams separately, the calculation of the colour factors and the sum of all diagrams, the file `#com.frm` is called in order to perform the last simplifications to present the final result.

Although there are some good references in the internet (cf. e.g. Ref.[53]), `MATAD` can be difficult to grasp. Therefore, we will explain in detail the LO calculation of the decay $H \to \gamma\gamma$ for pedagogical purposes.

The detailed explanation of the implementation of this calculation in `MATAD` is meant to serve as additional documentation about the program. Basic knowledge of `FORM` is assumed.

5.2 $H \to \gamma\gamma$ at LO on `MATAD`

To explain in detail the workings of the program, we will calculate the transition amplitude for the decay of the Higgs boson into a pair of photons with the help of `MATAD`. Since we already calculated this decay in detail in Sec. 4, Eq. (4.19), we can see how the program works.

In the decay $H(q_1 + q_2) \to \gamma(\mu, q_1) + \gamma(\nu, q_2)$, the most general structure for the transition amplitude, which we denote by $\mathscr{M}^{\mu\nu}$, is

$$\mathscr{M}^{\mu\nu} = q_1 \cdot q_2 g^{\mu\nu} A + q_1^\nu q_2^\mu B + q_1^\mu q_2^\nu C, \tag{5.1}$$

with A, B and C scalar quantities. It can be shown, due to Ward's Identity[28], that $A = -B$. For real transversal massless particles (which is the case of the photon), the structure C

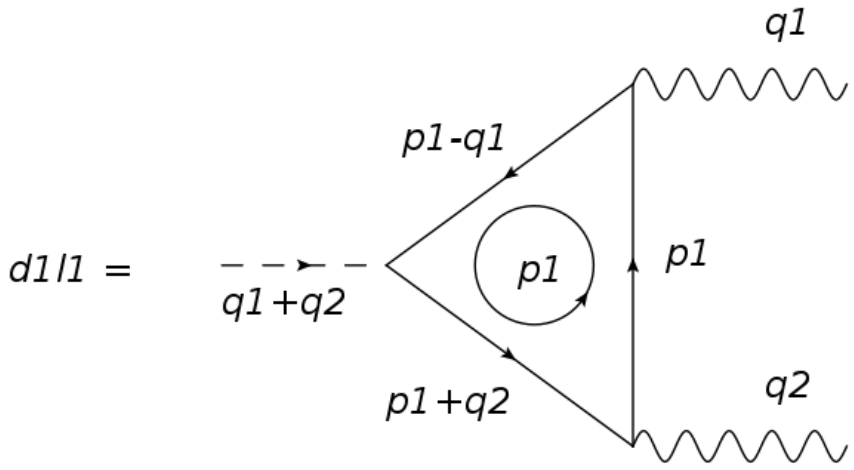

Figure 16 – d1l1 diagram present in the `dia` file.

Source: By the author.

does not contribute. Contracting Eq. (5.1) with the three Lorentz structures present in it and solving the resulting equations for A, B and C yields the projectors $P_i^{\mu\nu}$, with i the projected structure,

$$\begin{cases} P_A^{\mu\nu} = \frac{1}{(D-2)(q_1\cdot q_2)^2}(q_1\cdot q_2 g^{\mu\nu} - q_1^\mu q_2^\nu - q_1^\nu q_2^\mu), \\ P_B^{\mu\nu} = \frac{1}{(D-2)(q_1\cdot q_2)^2}(-q_1\cdot q_2 g^{\mu\nu} + (D-1)q_1^\mu q_2^\nu + q_1^\nu q_2^\mu), \\ P_C^{\mu\nu} = \frac{1}{(D-2)(q_1\cdot q_2)^2}(-q_1\cdot q_2 g^{\mu\nu} + q_1^\mu q_2^\nu - (D-1)q_1^\nu q_2^\mu), \end{cases} \tag{5.2}$$

where D is the dimensionality of the space-time in which we are working.

We will start this section explaining the `d1l.dia` file, which stands for diagrams at 1-loop.

5.2.1 `d1l.dia`

We will explain in detail the construction of the first diagram, shown in Fig. 16, which we call `d1l1`. The diagrams will be expanded in powers of q_i/m_t by `MATAD`, where q_i stands for the external momenta. This is exactly the same procedure we performed in Eq. (4.18). For example, $(q_1+q_2)^2/m_t^2 = M_H^2/2m_t^2 = 2\tau_t$. Since we are interested in the leading term in the τ_t series, we will only collect the first term in this expansion.

We start by noticing that the 1-loop diagrams color structures are trivial — therefore, the color diagrams are simply composed by delta functions. `MATAD` uses standard `FORM` notation, which will not be explained in detail, but can be found on the good tutorial material in the link https://www.nikhef.nl/~form/maindir/courses/courses.html. We note that the `j#` indices denote *internal* fermion lines (external lines are denoted by the index `i#`), and we just need to be consistent with the proper indices. For the `d1l1` diagram, the color structure reads

```
*--#[ fqcd1l1 :

    1
    *d_(j1,j6)
    *d_(j6,j5)
    *d_(j5,j4)
    *d_(j4,j3)
    *d_(j3,j2)
    *d_(j2,j1)
    ;

*--#] fqcd1l1 :
```

The Lorentz structure (i.e., the diagram without the colour structure) is written in the `d1l1` folder,

```
*--#[ d1l1 :

    (-1)
    *FT1(
        L,16,+p11,pM1,M1,pM1,exp,-q1,pQ1,16,L
    )
    *FT1(mu1)
    *FT1(
        L,19,+p11,pM1,M1,pM1,19,L
    )
    *FT1(mu2)
    *FT1(
        L,13,+p11,pM1,M1,pM1,exp,+q2,pQ2,13,L
    )
    ;

    #define INT1 "tad1l"
    #define MASS1 "M1"
    #define DALA1 "0"

*--#] d1l1 :
```

In the code above, `FT1` is the built-in function which represents the spinor lines. For example, `FT1( L,16,+p11,pM1,M1,pM1,exp,-q1,pQ1,16,L)` $\equiv (m_t - (\not{p}_1 - \not{q}_1))^{-1}$. The `#define INT1 "tad1l"` refers to which topology we are dealing with. In this case, we

are dealing with 1-loop tadpoles,[XXIV] and thus this is the command to call to solve the resulting integrals.

`#define MASS1 "M1"` refers to the heavy scale of our problem, which we denoted as M1 — M1 is the top mass.

`#define DALA1 "0"` sets no external momenta factorization.

To finish this file, we end up with the folder for the expansion:

```
*--#[ expd1l1 :

    multiply, eM1^1*pM1^4;
    #call denoexp{M1}
    #include matad.info # time

*--#] expd1l1 :.
```

First, we multiply the whole diagram by `eM1` since it is a 1-loop diagram and $\texttt{eM1} \equiv \left(\frac{\mu^2}{M1^2}\right)^{\epsilon}$ — in `MATAD` one needs to introduce some factors by hand, and this is the first case; the multiplication by `pM1` is to include more terms in the heavy-scale expansion, since `pM1` is a power-counting variable for M1. The second line calls the procedure that expands the expression in inverse powers of the heavy scale; the last line just displays some information about the calculation.

5.2.2 MISC

The `MISC` file contains only two command lines. The first command line,

```
../startform3 -S form.set -d CLASS=c\_hgamgamlo -d PROBLEM=hgamgamlo -d
LOOPS=1 -d DIAFILE=d1l.dia -d RESDIR=results -d DIAGRAM=d1l1 generic/maindia.frm
```

calls individual diagrams. It is important to note that this command line must be called in the `calc` folder. The `CLASS` and `PROBLEM` attributes refer to the first two problem folders. The `LOOPS` variable is set to 1, because we are at LO; `DIAFILE` needs to be set to the `.dia` file in the inner problem's folder. `RESDIR` sets the directory where the results will be saved; the variable `DIAGRAM` is the one where you set the individual diagrams. In our case (2 diagrams), we will have to run this whole command line two times, changing this variable to `DIAGRAM=d1l2` in the second time to calculate the remaining diagram. The last command sets the form file for the proper calculation of the diagrams (`generic/maindia.frm` is a built-in file).

The second line of the `MISC` file is

[XXIV] Since we are expanding in powers of the external momenta over m_t, the resulting diagrams are tadpoles.

```
../startform3 -S form.set -d CLASS=c\_hgamgamlo -d PROBLEM=hgamgamlo -d
LOOPS=1 -d DIAFILE=d1l.dia -d RESDIR=results -d START=1
-d END=2 generic/comdia.frm
```

It is very similar to the first line and calculates the color structure and sum the results. Since we have only 2 diagrams in this decay, the `START` variable is set to 1 and the `END` variable set to 2. `generic/comdia.frm` is the built-in `FORM` file that executes these actions.

5.2.3 `GLOBAL` file

The first folder,

```
*--#[ GLOBAL :

#define LOWLIMM1 "-2"
#define GAUGE "0"
#define NUMEXTMOM "2"

*--#] GLOBAL :
```

sets the order of expansion of $Q1/M1$ (We would set `LOWLIMM1` to -6 if we did not multiply the whole expression by `pM1^4` in the `dia` file with the same result). `GAUGE` defines the gauge in which we are working (in our case, the sum of all diagrams is gauge invariant, which can be verified modifying the `GAUGE` parameter in this code to an arbitrary gauge `"Xi"`); `NUMEXTMOM` is set to 2 since we have two external momenta, p_1 and p_2, for the two external photons.

In folder `TREAT1`,

```
*--#[ TREAT1 :

multiply, ( deno(2,-2)*(q1.q2)^-2) )*( [A] * ( d_(mu1, mu2)*(q1.q2)
    - q1(mu2)*q2(mu1) - q1(mu1)*q2(mu2) ) + [B] * ( -(q1.q2)*d_(mu1,mu2)
    + q1(mu2)*q2(mu1) + (3 - 2*ep)*q1(mu1)*q2(mu2) ) );
.sort

*--#] TREAT1 :
```

we multiply the amplitude by its structure projectors, Eq. (5.2). In `MATAD`, `deno(a,b)` $\equiv 1/(a+b\epsilon)$. Thus, we already substituted $D = 4-2\epsilon$ in our projector and ignored the C structure, which does not appear.

In the `TREAT4` folder we just set some kinematical identities. Note that the external momenta are in uppercase because in this step the Wick rotation was already implemented.

5.2.4 `com.frm` file

To finish this documentation section, we describe the `com.frm` file, which we renamed as `comhgamgamlo.frm`. At line 2 there is the command line to call this file. In this file, first we defined the used variables. After this, we loaded the result from the second `MISC` line command and defined a local variable (`res1l`) to store the results:

```
load results/hgamgamlo1l1to2.res;

l res1l = hgamgamlo1l1to2;

.sort
```

To finish the calculation, we set some useful kinematical identities, corrected a minus sign[XXV] and multiplied correction factors which `MATAD` does not account for: for example, factors of 4π, particle couplings etc. To finish, we separate the final expression in useful brackets and print the result. In our case, the final result for the LO decay, which we called `res1l`, reads

```
res1l =

      + eM1*[b]*[al/pi]*nc*vev^-1 * (
         + 2/3
         )

      + eM1*[a]*[al/pi]*nc*vev^-1 * (
         - 2/3
         )

      + ep^2*eM1*[b]*[al/pi]*nc*vev^-1 * (
         + 1/3*z2
         )

      + ep^2*eM1*[a]*[al/pi]*nc*vev^-1 * (
         - 1/3*z2
         );
```

in our notation, `[al/pi]` $\equiv \alpha/\pi$. `[a]`, `[b]` are the projector structures and `z2` represents ζ_2. Setting $\epsilon = 0$ yields the correct final result.

These procedures are the usual step-by-step for `MATAD` calculations; each problem — and its particular structures — needs to be analyzed individually, for example, for the

[XXV] This minus sign issue is always present in `MATAD` and needs to be corrected by hand.

proper implementation of the projector or the tensor reduction. Furthermore, one needs to be alert for the necessity of the inclusion of counter-terms on the final expression. However, the main workings of `MATAD` were shown in this pedagogical example.

In the next chapter, we will analyze the results for the leading-n_f terms of the QCD corrections in the decay $H \to \gamma\gamma$ as well as the modifications to `MATAD` needed to obtain these results.

6 RESULTS

In this section we will present our results; we will start by introducing the modifications performed to MATAD in order to include the Borel variable u in our calculations.

6.1 $H \to \gamma\gamma$ in the large-β_0 limit

To begin our calculation of the leading-n_f terms of the decay $H \to \gamma\gamma$, we need to generate the NLO diagrams. The diagrams were generated by the program QGRAF, resulting in 12 diagrams for the NLO decay. Basically, there are two kinds of diagrams: the ones in which there is an exchange of gluons between different quark propagators and the ones of the self-energy type. Adding to these the same diagrams with the reverse order for the top momentum, we arrive at the twelve diagrams. The main sample of these diagrams is shown in Fig. 17.

The next step consists in the substitution of the original gluon propagators in Fig. 17 by the transformed resummed gluon propagator, Eq. (3.58); this substitution is depicted in Fig. 18, where the dashed lines represent the resummed gluon propagator. The result of the sum of all diagrams with this modification can be expanded in a series in the Borel variable u which, in view of the correspondence between the original and the transformed series, yields the leading-n_f terms to all orders of the original series.

This calculation requires modifications to the MATAD code, in order to deal with the inclusion of the Borel variable u present in the resummed gluon propagator. We describe these modifications in detail in the next section.

6.1.1 Modifications to MATAD

The MATAD program is aimed at calculating processes in QCD. Therefore, since we introduced a new variable u for working in Borel space, we need to proceed with modifications to the original MATAD package.

There are two main modifications we perform. The first one is related to the modification to the gluon propagator, Eq. (3.58); this modification is essentially the generalization of the power of k^2 in the denominator of the gluon propagator to any real value, and not just integers as MATAD expects. The second one is to the resulting integrals performed by the program which are not ready to include the modified gluon propagator and the Borel variable u.

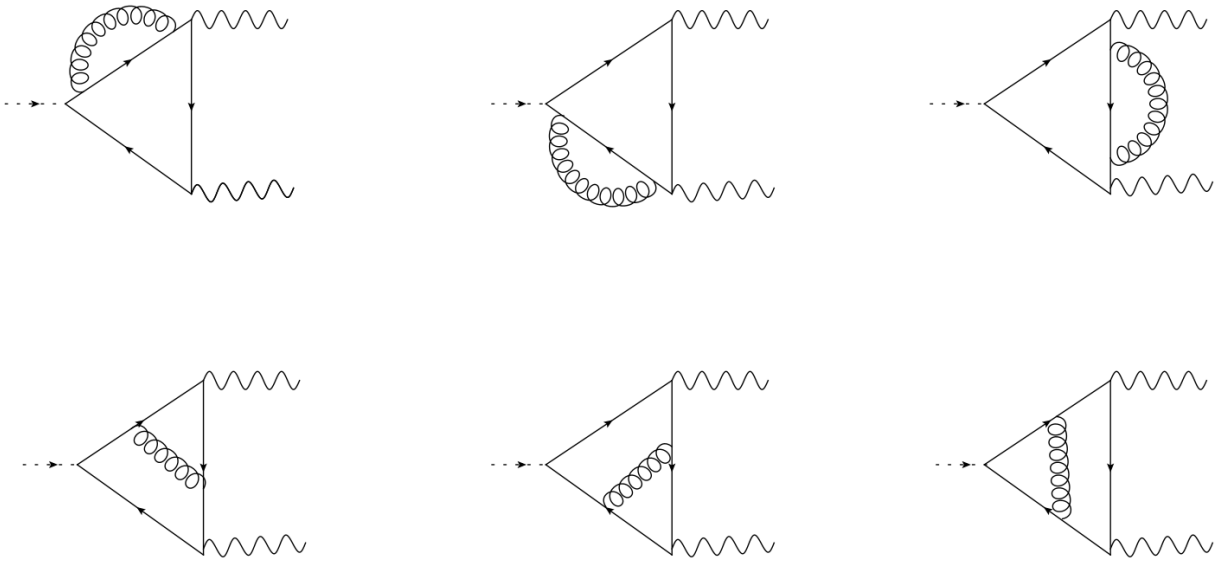

Figure 17 – Feynman diagrams for the decay of the Higgs boson into a pair of photons at the NLO level. There are 12 diagrams for this calculation; each diagram in the figure results in two diagrams by interchanging the virtual fermion momentum while keeping the loop-momentum unchanged, as we did for the LO calculation in Ch.4. This change correspond to the interchanging of the identical final state photons.

Source: By the author.

Modification to the gluon propagator

The first modification is to the gluon propagator to account for Eq. (3.58). This modification is performed in the file `GLOBAL`. We arranged the diagrams in the `#problem.dia` file so that the gluon propagators always carried momentum p_3, without any external momenta. With this, the modification is rather simple, and we only need to multiply the original propagator by the new function `Denu`, which accounts for the factors of u in the modified propagator, which in standard `FORM` notation amounts to

```
id Dg(?x) = Dg(?x)*Denu(u);
```

In the folder `TREAT4` we perform, manually, a Passarino-Veltman reduction[44]. Basically, `MATAD` does not deal with numerators with the dot product $q_i \cdot p_j$, where q_i denotes an external momentum while p_j denotes an internal momentum — the numerators can not mix external and internal momenta dot products. The `totensor` command separates these dot products and leaves, for the moment, just the internal Lorentz structure. In our example, $q_i \cdot p_j \to q_{i,\mu} p^{j,\mu}$. Then we perform the Passarino-Veltman reduction for the internal vectors p_j^μ and applied the resulting reduction to the external momentum q_i^μ which are left behind.

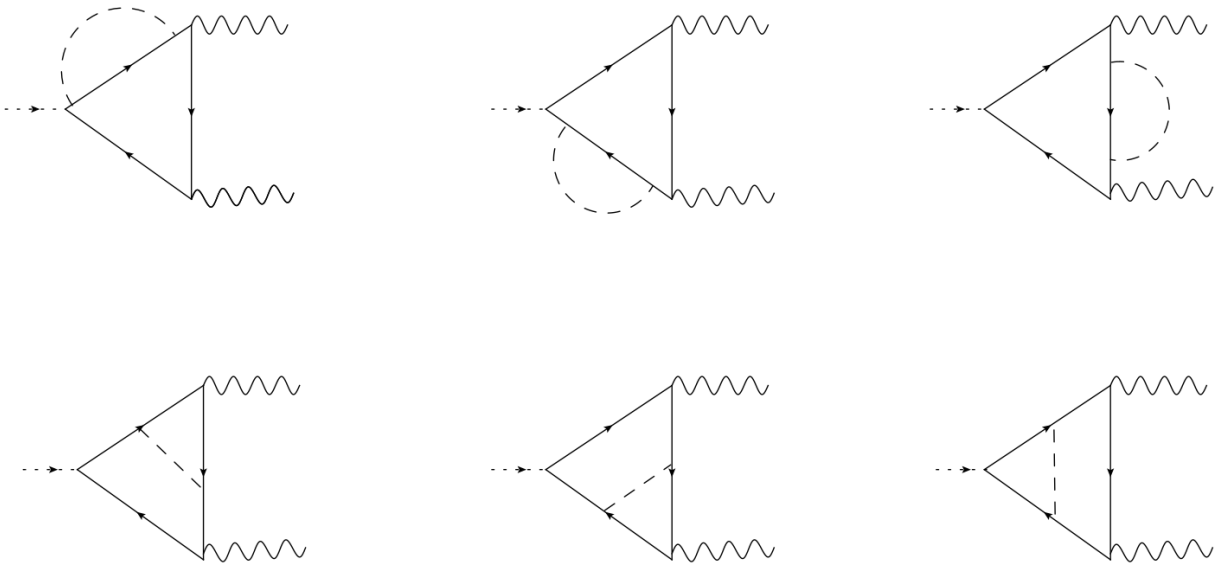

Figure 18 – Sample of diagrams for the calculation of the leading-n_f terms for the decay $H \to \gamma\gamma$. The dashed line represents the resummed gluon propagator, Fig. 8.

Source: By the author.

6.1.2 `tad2l` modification

To calculate the resulting integrals, we need to change the file `matad/inc/tad2l`, which deals with 2-loop tadpoles. Our modified file is called `gnlargeB0tad2l`. It starts writing the dot products of the loop variables in terms of its propagators, e.g.

$$p_i^2 = S(p_i)^{-1} - m_i^2,$$

where $S(p_i)$ is the propagator of the virtual particle with (internal-only) 4-momentum p_i. In the program's language and using standard `FORM` commands, it reads

```
id p2.p2 = s2m^-1 - M^2;
id p2.p3 = (s1m^-1 - s2m^-1 - p3.p3)/2;
.sort
```

We would like to note that the mass appears with a negative sign because at this stage of the calculation, in `MATAD`, the Wick rotation was already performed. The p_1 loop-momentum need not be dealt with since we defined $p_1 = p_2 - p_3$.[XXVI]

The convolution of all possible functions of u is the next modification, to unify the u variable into single functions,

```
repeat;
```

[XXVI] The direction of momentum flow for 2-loop diagrams is specified in the program's documentation.

```
id, once Denu2(u1?)*Denu2(u2?) = Denu2(u1 + u2);
id, once gnpref(u1?)*gnpref(u2?) = gnpref(u1 + u2);
endrepeat;
```

We describe this modification for completeness since, for the problem at hand, this modification is not important since there are single gluon propagators in the NLO calculation and thus only one u variable for each diagram. For processes such as $H \to gg$ this is not the case as more than one gluon propagator appears, and thus this modification becomes essential.

The next step is to unify the scalar integrals into a single function with the relevant coefficients for the tabulated integrals[30],

```
id s1m^a1?*s2m^a2?/p3.p3^a3? = f(a1,a2,a3);
```

After this, we simply exclude the scaleless integrals which integrate to zero in dimensional regularization,

```
id f(a1?,a2?neg0_,a3?) = 0;
id f(a1?neg0_,a2?,a3?) = 0;
.sort
```

Finally we perform the scalar loop integrals, which are the master integrals for our problem and from Ref.[30] read

$$\begin{aligned}\int\int \frac{d^Dk d^D\ell}{(-k^2+m^2)^{a_1}(-\ell^2+m^2)^{a_2}[-(k+\ell)^2]^{a_3}} \\ = (i\pi^{D/2})^2 \frac{\Gamma(a_1+a_3+\varepsilon-2)\Gamma(a_2+a_3+\varepsilon-2)\Gamma(2-\varepsilon-a_3)}{\Gamma(a_1)\Gamma(a_2)\Gamma(2-\varepsilon)} \\ \times \frac{\Gamma(a_1+a_2+a_3+2\varepsilon-4)}{\Gamma(a_1+a_2+2a_3+2\varepsilon-4)} (m^{-2})^{a_1+a_2+a_3+2\varepsilon-4}.\end{aligned} \tag{6.1}$$

The u variable is attached to the massless propagator, i.e., in our case it appears together with the a_3 variable. We implement this with the following `id` statement:

```
id f(a1?,a2?,a3?)*Denu(u?) = eMu(u) * M^(2*(4 - a1-a2-a3))
    * Gam(a1+a3-2,1,u)*Gam(a2+a3-2,1,u)*Gam(2-a3,-1,-u)
    * iGam(a1,0,0)*iGam(a2,0,0)*iGam(2,-1,0)
    * Gam(a1+a2+a3-4,2,u)*iGam(a1+a2+2*a3-4,2,2*u);
.sort
```

On the r.h.s. of the equality sign, `eMu` is a function containing the factor $(-\mu^2 e^{-C}/k^2)^u$ in

the modified gluon propagator in Eq. (3.58), that is

$$\texttt{eMu(u)} \equiv \left(-\frac{\mu^2}{k^2} e^{-C} \right)^u .$$

The functions `Gam` and `iGam` (`iGam` $\equiv 1/$`Gam`) are modified Γ-functions to deal with the u dependence. Basically the first entry of the `Gam` (and `iGam`) is reserved for integer values, the second to the coefficients in front of the variable ϵ and the last entry to the coefficients in front of the variable u. As an example, the function $1/\Gamma(1+3\epsilon+2u)$ reads `iGam(1,3,2)`.

After the modifications are implemented, we follow the usual procedure and calculate the twelve diagrams, the colour structure, sum the result and correct the factors which are not included by `MATAD`. With these modifications, the final result should contain three functions: `eMu, Gam` and `iGam`. It is then a matter of simplification of the resulting Γ-functions, which we implement using a series of `FORM` substitutions, to arrive at the final result in a readable form. It should be noted that, in our calculation, we are only considering terms in the limit $m_t \to \infty$, i.e. we are not considering mass corrections.

With the modifications explained, we are ready to present our higher order results for the decay $H \to \gamma\gamma$ in the large-n_f limit and in the large-β_0 limit.

We will write the decay width for $H \to \gamma\gamma$ as

$$\Gamma(H \to \gamma\gamma) = \frac{M_H^2}{64\pi} \mid A_W(\tau_W) + A_t(\tau_t) \mid^2 \tag{6.2}$$

with

$$A_t = \hat{A}_t \left(\sum_{n=0}^{\infty} A_t^{(n)} \left(\frac{\alpha_s}{\pi} \right)^n \right), \tag{6.3}$$

where $\hat{A}_t = N_c \frac{2Q_t^2 \alpha}{3\pi v}$ is the LO top contribution to the amplitude — thus, $A_t^{(0)} = 1$[XXVII] at LO in τ_t. For completeness, the first $\tau_t = M_H^2/4m_t^2$ corrections to $A_t^{(0)}$ can be extracted from Eq. (4.18) and read

$$A_t^{(0)} = 1 + \frac{7}{30}\tau_t + \frac{2}{21}\tau_t^2 + \frac{26}{525}\tau_t^3 + \frac{512}{17325}\tau_t^4 + \frac{1216}{63063}\tau_t^5 + \mathcal{O}(\tau_t^6). \tag{6.4}$$

Our amplitude for the top contribution to the decay of the Higgs into photons in the large-β_0 limit will be denoted by

$$A_{t,\text{large-}\beta_0} \equiv \hat{A}_t \sum_{n=1}^{\infty} A_t^{(n)} a_s^n, \tag{6.5}$$

with $a_s \equiv \alpha_s/\pi$. With the procedure outlined above, we obtain the following result (in

[XXVII] Note the close connection of this notation with the effective coupling from the last section, $C_{H\gamma\gamma}$.

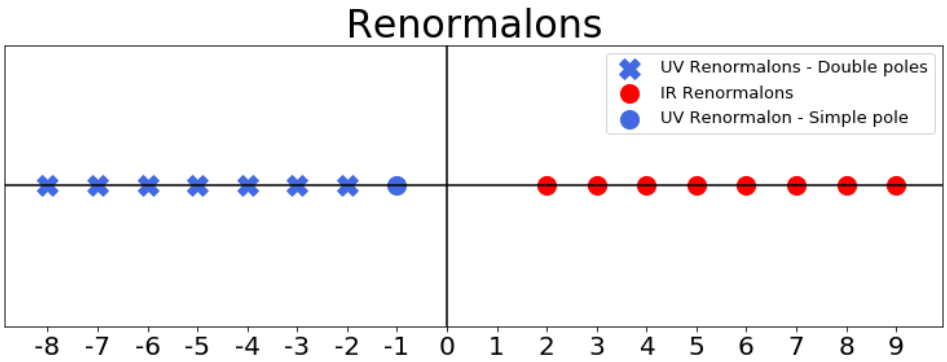

Figure 19 – Renormalons present in the Borel transform of the large-β_0 result. The UV renormalons (except at $u = -1$) are double poles, while the IR renormalons are simple poles.

Source: By the author.

closed form) for the Borel transform, $B[A_{t,\text{large-}\beta_0}]$, which is the main result of this work:

$$B[A_{t,\text{large-}\beta_0}] = \left(\frac{Q_t^2\alpha}{v}\right)\left(\frac{C_A^2-1}{4\pi^2}\right)\frac{e^{5u/3}(\frac{\mu^2}{m_t^2})^u(u^2-1)\Gamma(1-u)\Gamma(1+u)^3}{(1+2u)\Gamma(1+2u)}. \tag{6.6}$$

Fig. 19 shows the position of the renormalons present in Eq. (6.6). Except for the pole at $u = -1$, the UV renormalons are double poles. On the other hand, all IR are simple poles. Furthermore, the pole closest to the origin, which should dominate the behaviour of the series at higher orders, is the one at $u = -1$. It should be noted that there is no renormalon at $u = 1$. This is not a coincidence and is related to the fact that, when performing the OPE, the lowest dimension operator for the non-perturbative contribution has dimension 4 — it is not possible to write a gauge-invariant dimension-2 operator. As can be seem when we developed Eq. (3.67) through Eq. (3.72), the dimension-4 operator yields a renormalon at $u = 2$. Generalizing this argument, a dimension-$2p$ operator generates a renormalon at $u = p$; thus, dimension-2 operators are related to renormalons at $u = 1$. Therefore, it could not exist any renormalon at $u = 1$ since we can not write a dimension-2 operator in the OPE.[XXVIII]

The residue of the first pole on the negative real axis reads

$$\text{Res}(B,-1) = -\left(\frac{Q_t^2\alpha}{v}\right)\frac{C_A^2-1}{\pi^2}\frac{e^{-5/3}m_t^2}{\mu^2}, \tag{6.7}$$

while the residue of the first pole on the positive axis is

$$\text{Res}(B,2) = \left(\frac{Q_t^2\alpha}{v}\right)\frac{(C_A^2-1)}{20\pi^2}\frac{e^{10/3}\mu^4}{m_t^4}. \tag{6.8}$$

[XXVIII] Remember that the IR renormalons are related to non-perturbative effects.

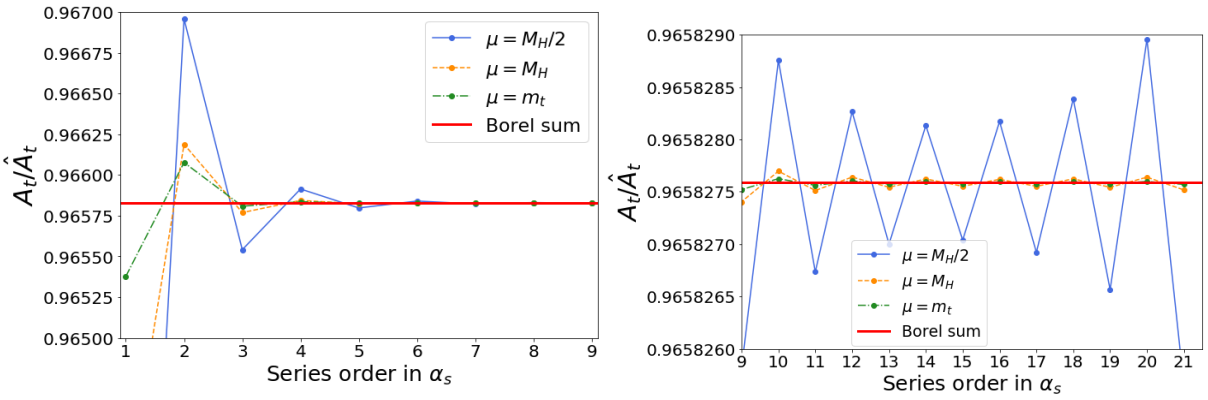

(a) Series approach to the Borel sum at different energy scales

(b) Divergent behaviour of the series

Figure 20 – Series according to order in perturbation theory

Source: By the author.

Table 2 – Contribution of the renormalons on the first coefficients of the QCD expansion of the top loop amplitude for the decay $H \to \gamma\gamma$. We are analyzing the amplitudes at the scale $\mu = m_t = 172.76$ GeV.

Pole	$A_t^{(1)}$	$A_t^{(2)}$	$A_t^{(3)}$	$A_t^{(4)}$	$A_t^{(5)}$	$A_t^{(6)}$	$A_t^{(7)}$	$A_t^{(8)}$
$u = -2$	-29%	-86%	-20%	-23%	-10%	-8%	-4%	-2%
$u = -1$	76%	226%	72%	125%	84%	106%	94%	101%
$u = 2$	280%	-420%	66%	-58%	20%	-12%	5%	-3%
$u = 3$	-848%	848%	-89%	52%	-12%	5%	-1%	1%

Source: By the author.

From the results of Eq. (6.7) and (6.8), we can see that the dependence on the scale μ varies according to whether you are considering UV or IR renormalons. For UV renormalons, there is an inverse dependence with μ^2 while the IR renormalons are proportional to powers of μ^2. This behaviour can be seen in Fig. 20, where for small values of μ the series sign alternation — which is a manifestation of UV renormalons — is enhanced, while for higher values of μ this alternation ceases, as can be seen in Fig. 21. For scales $\mu \gtrsim 200$ GeV, the series has a fixed sign behaviour, approaching the Borel sum from above.

Figs. 20 and 21 also show the renormalization scale in which the large-β_0 limit can be better examined — at $\mu \sim 200$ GeV, the series approach to the Borel sum is very good already at the first 3 orders. Therefore, for the analysis of the series in large-β_0, this scale range must yield good quantitative results.

The contribution of the poles to the first coefficients at $\mu = m_t$ can be read off from Tab. 2. One can see that the the UV renormalon closest to the origin ($u = -1$) dominates in higher-order corrections, as we had anticipated in Sec. 3. At lower-orders, this does not happen as the IR renormalons also contribute considerably to the coefficients.

We can expand in full analytical form the result of Eq. (6.6) in u and, through the

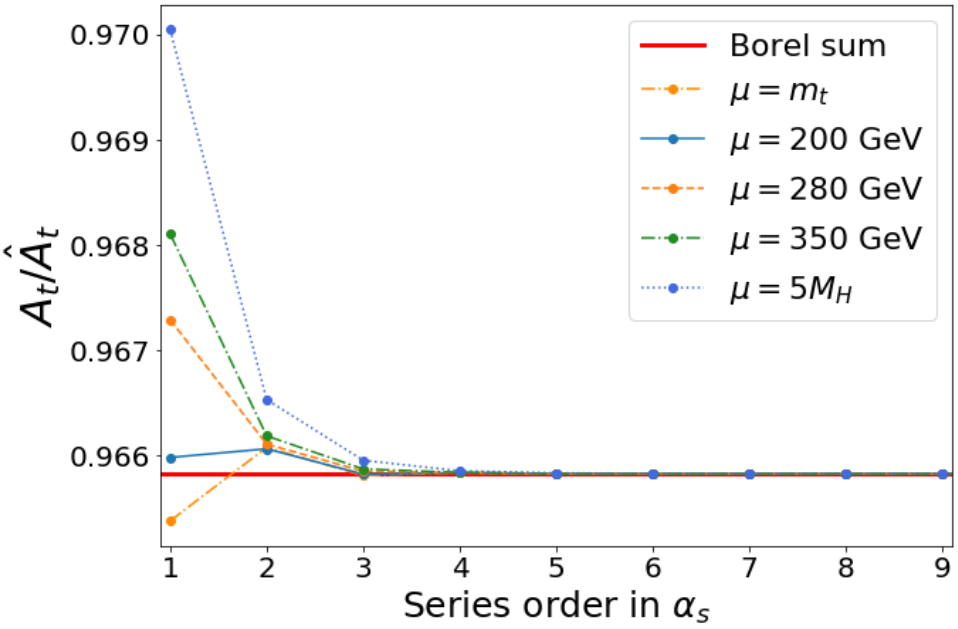

Figure 21 – Cessation of the sign alternation with increasing renormalization scale μ.

Source: By the author.

correspondence between the original series and the Borel transform, Eq. (3.46), obtain the leading-n_f terms for the QCD corrections at each order in perturbation theory exactly. At the three-loop order our result reads

$$A^{(2)}_{t,n_f} = -C_F T_F n_f \left(\frac{1}{12} - \frac{\ell_\mu}{4}\right), \tag{6.9}$$

where $\ell_\mu \equiv \ln\left(\frac{\mu^2}{m_t^2}\right)$, in agreement with Refs.[46,54]. Our results for $C_t^{(3)}$ and $C_t^{(4)}$ are, respectively,

$$A^{(3)}_{t,n_f^2} = -C_F T_F^2 n_f^2 \left(\frac{19}{108} - \frac{\ell_\mu}{18} + \frac{\ell_\mu^2}{12}\right) \tag{6.10}$$

and

$$A^{(4)}_{t,n_f^3} = -C_F T_F^3 n_f^3 \left(\frac{487}{972} - \frac{\zeta_3}{3} - \frac{19}{108}\ell_\mu + \frac{\ell_\mu^2}{36} - \frac{\ell_\mu^3}{36}\right), \tag{6.11}$$

where ζ_i is the Riemann Zeta Function evaluated at i. Once again both results are in agreement with Ref.[46].

A new result of this work is the leading n_f-terms to all orders in perturbation theory, i.e. $A^{(n)}_{t,n_f^{n-1}}$ for any n. As an example, the N^{5}LO coefficient, $A^{(5)}_{t,n_f^4}$, reads

$$A^{(5)}_{t,n_f^4} = -C_F T_F^4 n_f^4 \left(\frac{9613}{8748} - \frac{\pi^4}{135} - \frac{4\zeta_3}{27} + \ell_\mu\left(\frac{4\zeta_3}{9} - \frac{487}{729}\right) + \frac{19}{162}\ell_\mu^2 - \frac{\ell_\mu^3}{81} + \frac{\ell_\mu^4}{108}\right), \tag{6.12}$$

while the N^{6}LO coefficient, $A^{(6)}_{t,n_f^5}$ is

$$A^{(6)}_{t,n_f^5} = -C_F T_F^5 n_f^5 \left[\frac{307765}{78732} - \frac{\pi^4}{243} - \frac{190}{243}\zeta_3 - \frac{20}{9}\zeta_5 + \ell_\mu\left(-\frac{48065}{26244} + \frac{\pi^4}{81} + \frac{20}{81}\zeta_3\right) + \ell_\mu^2\left(\frac{2435}{4374} - \frac{10}{27}\zeta_3\right) - \frac{95}{1458}\ell_\mu^3 + \frac{5}{972}\ell_\mu^4 - \frac{1}{324}\ell_\mu^5\right]. \tag{6.13}$$

The higher-order coefficients can be easily generated from Eq. (6.6) by substituting u by $-\beta_{0,f}t$ and performing the correspondence between the original series and the series in Borel space, Eq. (3.46).

It is also interesting to analyze the series approach to the 'real' value by computing the Borel integral of the analytical result, $\tilde{A}_{t,m_t\to\infty}$, as well as the series coefficients. For our calculation, we will use $m_t = 172.76$ GeV. Since the ambiguity arising from the IR poles is extremely small compared to the real part of $\tilde{A}_{t,m_t\to\infty}$ (it is 12 orders of magnitude smaller than the real part), we will not consider it in our calculations. This small value for the ambiguity is a manifestation of the sub-leading character of non-perturbative effects — we are considering a scale where α_s is clearly perturbative, and thus the non-perturbative effects are negligible compared to uncertainties due to α_s, scale variation or the series truncation. Our result for the Borel sum of Eq. (6.6) reads

$$\tilde{A}_{t,m_t\to\infty} = -0.0341724\hat{A}_t, \tag{6.14}$$

In Fig. 20a we displayed the series behaviour for various energy scales according to the order in perturbation theory. It is possible to notice that the series approach to the Borel sum is fast — there is good 'convergence'[XXIX] around N5LO —, and the approach to the Borel sum is faster when one increases μ. Fig. 20b was included to show the divergent behaviour of the series: for energies $\mu \sim M_H/2$, the series starts to diverge around $\mathcal{O}(\alpha_s^{15})$ — this is essentially the behaviour of an asymptotic series: they first approach the true result of the series and then diverge, in this case with alternating sign since the renormalon located at $u = -1$ is the leading renormalon. Fig. 22 shows the decay width of the Higgs decay into photons in the large-β_0 limit varying the coupling renormalization scale μ for a fixed top mass $m_t = 172.76$ GeV. One can notice that it is related to Fig. 20 — at N4LO the series approach to the Borel sum is very good. At N5LO, the approach to the value of the Borel sum is present in practically all energy range $50 < \mu < 350$ GeV., i.e. at N5LO, in large-β_0, the perturbative expansion gives an excellent and stable approximation to the true value of the observable.

Before comparing the results in QCD and large-β_0, there is an important comment

[XXIX] We are using the word *convergence* here to express the approach of the asymptotic series to the result of the Borel sum. It can be noted in Fig. 20b that the series diverge and, therefore, could not converge in the strict sense of the word.

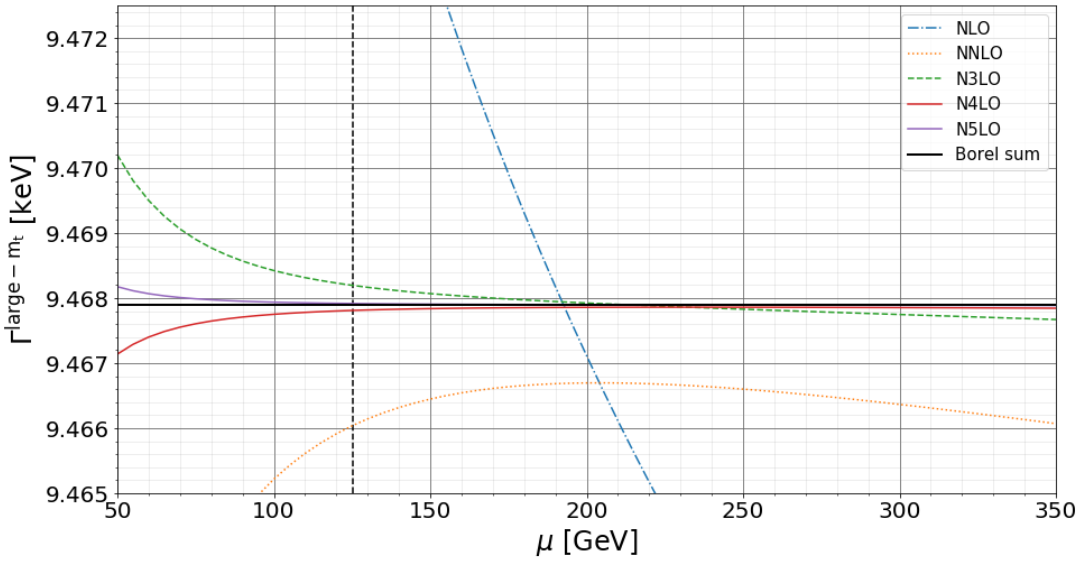

Figure 22 – $\Gamma(H \to \gamma\gamma)$ for a fixed $m_t = 172.76$ GeV.

Source: By the author.

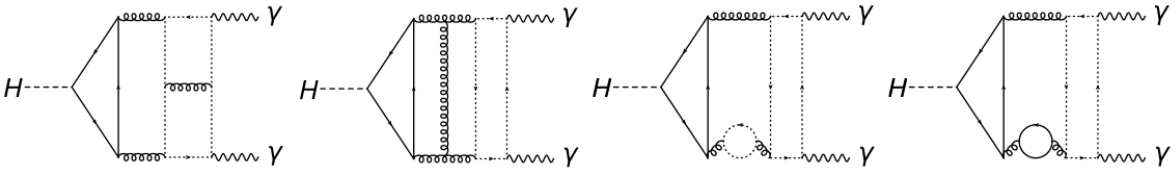

Figure 23 – Some examples of singlet diagrams: the final state photons are not coupled to the fermions which are coupled to the Higgs boson. In this work, we do not consider those diagrams in our calculations because they are sub-leading in $1/n_f$.

Source: By the author.

about the energy scale μ and the types of diagrams involved in this decay. There are two types of diagrams involved in QCD higer-order corrections of $H \to \gamma\gamma$, singlet and non-singlet diagrams. Non-singlet diagrams are the ones in which the final state photons couple to the same fermions coupled to the Higgs-boson while singlet diagrams are defined as the ones in which the final state photons do not couple to the same fermions coupled to the Higgs-boson. Some examples of singlet diagrams are displayed in Fig. 23. Furthermore, observables should, in principle, not depend on μ; however, since we are truncating the series, there is a residual dependence. Thus, the contribution of the singlet and non-singlet diagrams to the decay width varies with μ. This dependence needs to be adjusted in order for us to obtain good quantitative results in large-β_0, since in this work we are not calculating singlet diagrams. For our results, it is interesting to compare the results in energy scales where the singlet contributions do not dominate over the non-singlet ones.

In Ref.[46], it is shown that with the scale choice $\mu = \overline{m}_t(\overline{m}_t)$, at the 3-loop level the singlet diagrams are approximately of the same magnitude as the non-singlet diagrams, while at $\mu = m_H$ the singlet contribution is approximately three times larger than the non-singlet contribution. It is argued that one might expect the same to happen at 4- and 5-loop orders. Thus, if the large-β_0 limit represents well quantitatively the non-singlet diagrams in full QCD, at higher values of μ, the difference between the result in QCD and in large-β_0 should decrease.

Thus, we will compare our results at the scale $\mu = \overline{m}_t(\overline{m}_t)$ with Eq. (18) of Ref.[46]. Our result, after the naive non-abelianization, reads ($a_s \equiv \alpha_s/\pi$)

$$A_{t,\text{large-}\beta_0} = \frac{2Q_t^2 N_c \alpha}{3\pi v}(1 - a_s + 0.583a_s^2 - 6.465a_s^3 + 25.443a_s^4 - 201.823a_s^5 + \mathscr{O}(a_s^6)). \tag{6.15}$$

In our conventions, from Eq. (18) of Ref.[46], we find for the result in QCD in the large-m_t limit

$$\begin{aligned} A_t = \frac{2Q_t^2 N_c \alpha}{3\pi v}\Bigg(1 - a_s - a_s^2(1.292 + (0.889 - 1.440i)_{\text{si}}) \\ + a_s^3(5.937 + (0.992 + c_3)_{\text{si}}) - a_s^4(23.220 + c_4) + \mathscr{O}(a_s^5)\Bigg). \end{aligned} \tag{6.16}$$

c_3 and c_4 are constants which have yet to be calculated. One can notice in the above expression that the singlet contribution (which is indicated by the sub-index 'si') to the 3-loop result has an imaginary part, which can be traced through Eq. (22) of Ref.[46] to arise from a logarithm with negative argument. Another way of visualizing the appearance of the imaginary part is that some diagrams in Fig. 23 can be cut into allowed processes (i.e. the propagators can be on-shell), such as $H \to gg$, for example; this is not the case for the top triangle-loop, since $M_H < 2m_t$. Thus, through the Optical Theorem, the singlet diagrams necessarily have an imaginary part. The imaginary part is yet unknown for order α_s^3 and higher.

Although the magnitude of the non-singlet coefficients in large-β_0 at N3LO and N4LO are remarkably close to the exact result in QCD, there is a difference in sign.

In Figs. 24 and 25 we incorporated the amplitudes in both QCD and large-β_0 into the decay width, Eq. (6.2). In these plots, we are introducing the contribution of A_W into $\Gamma(H \to \gamma\gamma)$ and ignoring singlet contributions. For the running mass of the top-quark in the large-β_0 limit we used the expression relating γ_m and the β-function of Ref.[17],

$$\gamma_m = -\frac{\beta}{3\beta_0}\frac{N(-\beta, 0)}{B(2+\beta, 2+\beta)\Gamma(3+\beta)\Gamma(1-\beta)}, \tag{6.17}$$

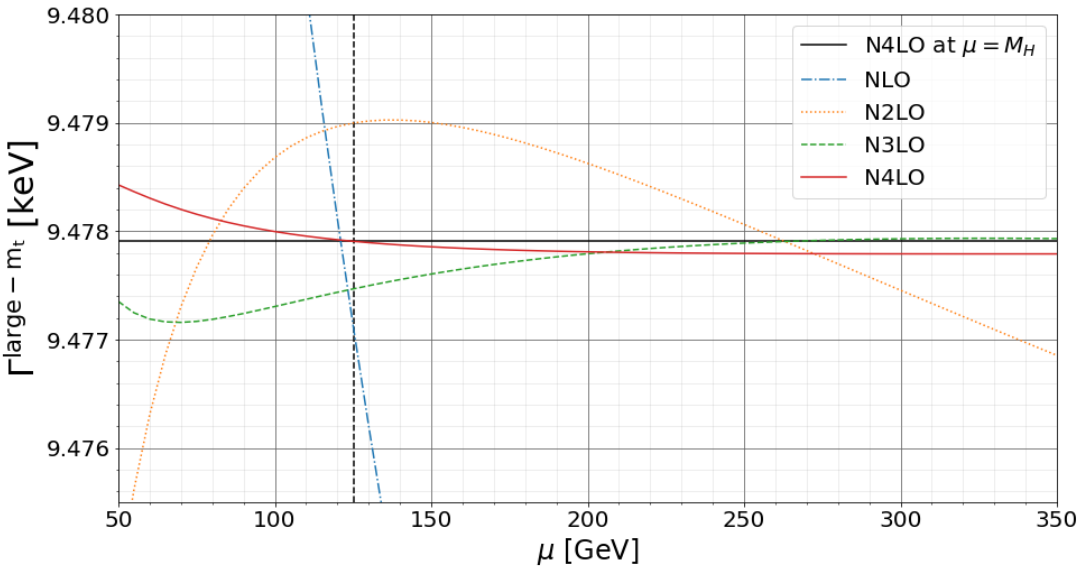

Figure 24 – $\Gamma(H \to \gamma\gamma)$ in QCD without singlet and mass corrections.

Source: By the author.

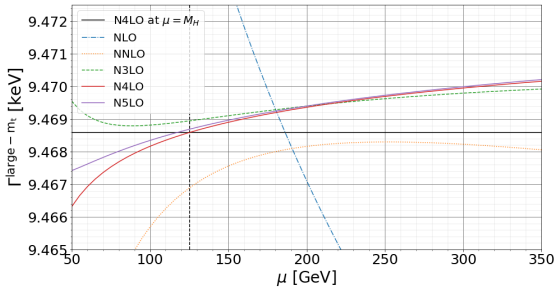

(a) $\Gamma(H \to \gamma\gamma)$ in the large-β_0 limit.

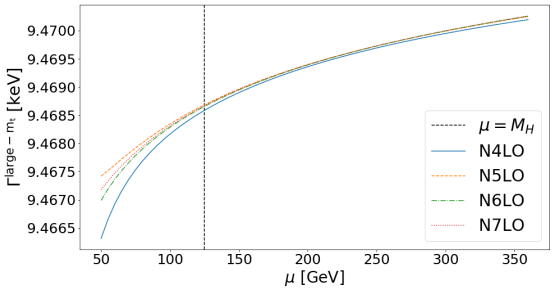

(b) $\Gamma(H \to \gamma\gamma)$ in the large-β_0 limit at higher-orders.

Figure 25 – $\Gamma(H \to \gamma\gamma)$ in large-β_0 at first orders and higher-orders without singlet and mass corrections.

Source: By the author.

where

$$N(-\varepsilon, u) = -C_F(3 - 2\varepsilon)(u - \varepsilon). \tag{6.18}$$

β is the β-function in the large-β_0 limit, given by $\beta = -\beta_0\alpha_s$ according to the definitions of Ref.[17]. $B(x, y)$ is the (mathematical) Beta function, defined as

$$B(x, y) = \int_0^1 t^{x-1}(1 - t)^{y-1}dt. \tag{6.19}$$

Comparing the results for $\Gamma(H \to \gamma\gamma)$ in QCD, Fig. 24, and in large-β_0, Fig. 25, we can see that there is an instability of the large-β_0 result with the energy scale μ for higher-orders.

This instability is expected and due to the fact that we are considering the γ_m-function only up to $1/\beta_0$; however, when calculating the running mass, the exponentiation of the γ_m-function generates terms of higher orders in $1/\beta_0$ which are not compensated in the coefficients which we calculated strictly in the large-β_0 limit.

One can notice, from Figs. 24 and 25a, that

$$(\Gamma(H \to \gamma\gamma)_{\text{QCD, large-}m_t} - \Gamma(H \to \gamma\gamma)_{\text{large-}\beta_0,\text{large-}m_t}) \sim 0.01\text{keV}, \tag{6.20}$$

i.e. they are remarkably close. However, these calculations do not take into account mass corrections in τ_t as well as singlet contributions; in the following, we will include them. For the numerical evaluation, our input parameters were $\alpha = 1/137.035999074$, $\alpha_s(M_Z) = 0.1179$ (which was evolved to the Higgs-boson mass scale $\mu = M_H = 125.10$ GeV, $\alpha_s(M_H) = 0.1130$) and $M_W = 80.379$ GeV. The τ_t corrections, up to τ_t^5 at LO and NLO, were obtained in Ref.[55] and the known singlet contributions in Ref.[46]. Our result with the mass and singlet corrections in QCD reads

$$\begin{aligned}\Gamma(H \to \gamma\gamma) =&[9.120_{\text{1-loop}} + 0.156_{\text{2-loop}} + 0.008_{\text{3-loop}} \\ &- 0.002_{\text{4-loop}} + 0.0004_{\text{5-loop}}]\ \text{keV} = 9.2824\ \text{keV}\end{aligned} \tag{6.21}$$

Our result in large-β_0, with singlets and mass corrections, reads

$$\begin{aligned}\Gamma(H \to \gamma\gamma)_{\text{large-}\beta_0} =&[9.119_{\text{1-loop}} + 0.155_{\text{2-loop}} - 0.004_{\text{3-loop}} \\ &+ 0.002_{\text{4-loop}} - 0.0004_{\text{5-loop}} \\ &+ 0.0001_{\text{6-loop}}]\ \text{keV} = 9.2717\ \text{keV}.\end{aligned} \tag{6.22}$$

The difference between the known corrections in full QCD and the large-β_0 limit corrections is approximately 0.1%. We note that, although the order of the corrections agree, there is a difference in sign starting at the 3-loop level, which was already noted when comparing the series. We will also compare our results in a similar fashion as in Eqs. (6.21) and (6.22) at the renormalization scale $\mu = 200$ GeV, which was argued to be approximately the best scale for the analysis of the series approach to the true value of the observable. At $\mu = 200$ GeV, we have in QCD, with all available corrections,

$$\begin{aligned}\Gamma(H \to \gamma\gamma) =&[9.105_{\text{1-loop}} + 0.144_{\text{2-loop}} + 0.017_{\text{3-loop}} \\ &- 0.001_{\text{4-loop}} + 0.0002_{\text{5-loop}}]\ \text{keV} = 9.2652\ \text{keV}\end{aligned} \tag{6.23}$$

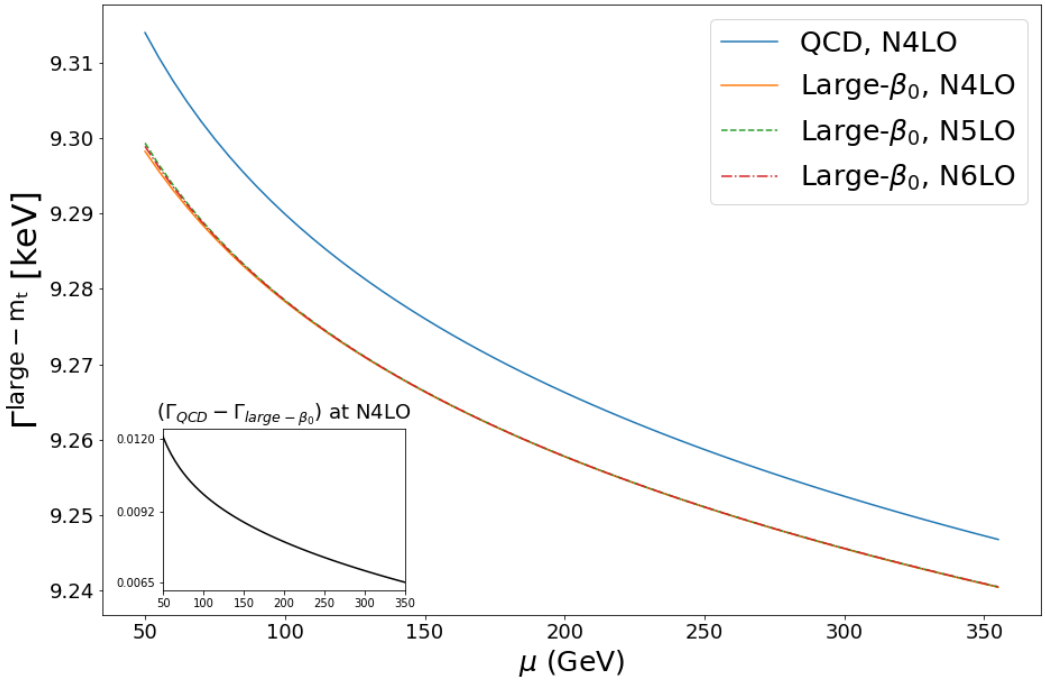

Figure 26 – Comparison of the decay width at N4LO in QCD and large-β_0 along with the relative difference between both scenarios.

Source: By the author.

In large-β_0, with all available corrections, our result at $\mu = 200$ GeV reads

$$\begin{aligned}\Gamma(H \to \gamma\gamma)_{\text{large-}\beta_0} =& [9.106_{\text{1-loop}} + 0.145_{\text{2-loop}} + 0.006_{\text{3-loop}} \\ &+ 0.001_{\text{4-loop}} - 0.0003_{\text{5-loop}} \\ &+ 0.0004_{\text{6-loop}}]\ \text{keV} = 9.2581\ \text{keV}.\end{aligned} \tag{6.24}$$

At this renormalization scale, the difference between QCD and large-β_0 amounts to 0.08%. However, the 3-loop correction in QCD doubles compared to the result at $\mu = M_H$; this suggests an interference between singlet and non-singlet diagrams at $\mu = 200$ GeV. Fig. 26 shows the decay width with all known QCD corrections at N4LO and in the large-β_0 limit at N4LO, N5LO and N6LO. The first interesting thing to note is that, starting at N4LO, the behaviour of $\Gamma(H \to \gamma\gamma)$ stabilizes with each increasing order in perturbation theory — a fact that is reinforced in Fig. 25b — at $\mu = M_H$, the series already almost match. This is very different from the behaviours of Fig. 25a, where there is a very different curve shape from order to order. Furthermore, the behaviour of the curves in QCD and large-β_0 are quite similar, with the difference between both results shrinking as the energy scale becomes larger, as can be seen in the inner plot of Fig. 26 and the results at $\mu = M_H$ and $\mu = 200$ GeV. This is in agreement with the argument in Ref.[46]: for higher values

of μ, the importance of singlet diagrams decreases while the non-singlet ones increases, and thus the diagrams which were not included in our calculations become less important — the large-β_0 limit seems to be a good approach to study this process in higher-orders. However, it should be noted that the instability of the higher-order results with respect to μ in the large-β_0 limit can also contribute to this reduction in the difference between this limit and the QCD results.

In view of the above results, we argue that this behaviour will continue to N5LO and beyond in QCD and that, although both scenarios diverge quantitatively, there is an agreement qualitatively. Therefore, one might expect that the QCD corrections might stabilize with each increasing order in perturbation theory starting at N4LO and that the magnitude of the QCD corrections must match the ones in the large-β_0 limit.

The large-β_0 6- and 7-loop corrections, at $\mu = M_H$, are 0.1 eV and -0.03 eV, respectively. Once again, in view of the correspondence in the magnitude of the corrections in both QCD and large-β_0, we can expect a similar behaviour for higher-orders. Since the order-by-order corrections when comparing QCD and large-β_0 results are astoundingly close at $\mu = M_H$, we will proceed with our predictions in this renormalization scale.[xxx] Thus, we expect

$$| \Gamma(H \to \gamma\gamma)_{\text{QCD, 6-loop}} - \Gamma(H \to \gamma\gamma)_{\text{QCD, 5-loop}} | = 2 \times 10^{-4} \text{keV}, \tag{6.25}$$

where we multiplied the large-β_0 result by 2 to be conservative. Therefore, the perturbative error when truncating the series at N4LO in QCD is of the order of 0.2 eV, i.e. 0.002%.

From the qualitative side, we expect that the series has good stability with respect to the order in perturbation theory starting at the N4LO — starting at the 5-loop level this differences shrinks considerably in the large-β_0 scenario. Although the N4LO curves in QCD and in the large-β_0 limit possess different characteristics, the agreement in the magnitude of the corrections for each order in perturbation theory suggests that this will also hold in QCD — the next corrections will not differ considerably from the N4LO curve.

To compare our result of Eq. (6.25) with other sources of uncertainties, we compute $\Gamma(H \to \gamma\gamma)$ using the uncertainty of the strong running coupling, $\alpha_s(M_Z^2) = 0.1179 \pm 0.0010$[26]. When using the lower uncertainty to calculate the decay width, we find that the 2-loop contribution is 0.154 (againts 0.156), i.e. the difference between the 2-loop contribution using $\alpha_s(M_Z^2) = 0.1179$ and $\alpha_s(M_Z^2) = 0.1169$ is of the order of 2 eV — 10 times larger than our prediction for the 6-loop correction in QCD. Another source of uncertainty is the top-mass; as we discussed previously, m_t in the argument of the logarithm ℓ_μ makes the decay width highly sensitive to variations in this mass parameter (note, for example, the instability of the result in large-β_0 at higher-orders). Therefore,

[xxx] The computation of the QCD result at $\mu = 200$ GeV showed an interference between the singlet and non-singlet diagrams which increased the 3-loop correction by one magnitude order; surprisingly, at $\mu = M_H$ the results order by order were much more compatible and thus we believe it is sensible to analyze and estimate results at $\mu = M_H$.

the uncertainty related to the top mass should surpass the uncertainty due to the 6-loop correction.

Thus, as of today, the limiting factors to the precise calculation of $\Gamma(H \to \gamma\gamma)$ are not related to the QCD higher-order calculations but to other sources of uncertainty in parameters used for the computation of the observable, as for example in the running coupling α_s

With the results and arguments presented, we can draw some conclusions:

- It seems advantageous to perform the calculations in larger scales, $\mu > M_H$; in this energy range, the 'convergence' in large-β_0 is enhanced and the singlet contributions decrease — this is very important since the singlet diagrams are hard to compute and are known completely only up to α_s^2.

- At higher-orders $\mu \sim 200$ GeV, the non-singlet diagrams should dominate over the singlet ones. Furthermore our result shows that it is reasonable to expect the QCD corrections to be of the same magnitude as the ones in large-β_0. This would generate a 6-loop correction, in QCD and at $\mu = M_H$, of 0.2 eV (or 0.002%).

- The perturbative error, when compared to other sources of uncertainty, is sub-leading by one order of magnitude. Thus, at time of writing, it is more important to invest in the reduction of the uncertainties of α_s and m_t than to calculate unknown perturbative corrections to $H \to \gamma\gamma$.

7 CONCLUSIONS

In this work, we studied the Higgs boson decay into two photons in higher-orders in QCD within the large-β_0 limit. We started presenting the basic theoretical framework for understanding the construction of the SM and to settle the foundations for our calculations. We presented, in detail, the LO decay in the $m_t \to \infty$ effective theory, in which we expand the original calculation in powers of $\tau_t \equiv M_H^2/4m_t^2$. We proceeded introducing `MATAD`, the program we used for the calculation in the large-β_0 limit. Our result for the Borel transform of the top contribution to the amplitude $A_{t,\text{large-}\beta_0}$, $B[A_{t,\text{large-}\beta_0}]$, in closed form, reads

$$B[A_{t,\text{large-}\beta_0}] = \left(\frac{Q_t^2\alpha}{v}\right)\left(\frac{C_A^2-1}{4\pi^2}\right)\frac{e^{5u/3}(\frac{\mu^2}{m_t^2})^u(u^2-1)\Gamma(1-u)\Gamma(1+u)^3}{(1+2u)\Gamma(1+2u)}. \tag{7.1}$$

With this procedure, we were able to reproduce the known leading-n_f terms up to N4LO and to obtain the leading-n_f terms to all orders in perturbation theory. A new result of this work is the N5LO leading-n_f term, which is the first previously unknown leading-n_f contribution,

$$A_{t,n_f^4}^{(5)} = -C_F T_F^4 n_f^4\left(\frac{9613}{8748} - \frac{\pi^4}{135} - \frac{4\zeta_3}{27} + \ell_\mu\left(\frac{4\zeta_3}{9} - \frac{487}{729}\right) + \frac{19}{162}\ell_\mu^2 - \frac{\ell_\mu^3}{81} + \frac{\ell_\mu^4}{108}\right). \tag{7.2}$$

Our analysis of the series approach to the Borel sum of $H \to \gamma\gamma$ at higher-orders showed that the renormalization scale $\mu \sim 200$ GeV seemed to be a good choice to study the problem through the large-β_0 limit because it approaches the value of the Borel integral faster.

When comparing our result for A_t in large-β_0 with the QCD result without any singlet or mass corrections, at $\mu = \overline{m}_t(\overline{m}_t)$, we noted that, although the magnitude of our corrections are remarkably close to the exact result, there is an inversion in the sign of the perturbative corrections; this comparison serves as a qualitative analysis of the large-β_0 limit at higher-orders for the process into question. Thus, at energies $\mu \sim 200$ GeV, the full non-singlet (order-by-order) amplitudes in QCD do not differ considerably, in absolute value, from the large-β_0 limit and the higher-order corrections can be estimated with this procedure.

As the next step, we incorporated the amplitude due to the $W^\pm$ loop, A_W, and calculated $\Gamma(H \to \gamma\gamma)$ in the large-β_0 limit. When plotting the result, we noted an unstable behaviour with respect to the renormalization scale μ of the series at higher-orders, a fact that can be related to the incorporation of higher orders powers of $1/\beta_0$ when calculating the running mass in the large-β_0 limit. Thus, this behaviour is expected

in large-β_0 results.

Nevertheless, we proceeded with the inclusions of the available known corrections — singlet diagrams at the three-loop level and τ_t corrections at LO and NLO up tp τ_t^5. Our results showed that the difference $\Gamma(H \to \gamma\gamma)_{\rm QCD} - \Gamma(H \to \gamma\gamma)_{\rm large-\beta_0}$ shrinks as the energy goes higher. This behaviour is due to the decrease in the contribution of the singlet diagrams; however, the instability of the large-β_0 limit with respect to μ also contributes to this reduction.

For a numerical evaluation, we compared the results in full QCD and large-β_0 in both $\mu = M_H$ and $\mu = 200$ GeV. The difference between both scenarios were of the order of 0.1%, i.e. the large-β_0 approach seems to be a good method to analyze the Higgs decay into photons at higher-orders. An interesting conclusion of this comparison is that, when comparing the order by order perturbative corrections, the analysis in large-β_0 at $\mu = M_H$ presents results almost identical to the QCD known corrections in magnitude. Thus, we argued that, for quantitative predictions — and following the same renormalization scale as in Ref.[46] —, it is better to use $\mu = M_H$.

With this quantitative information, we argued that, since the magnitude of the large-β_0 corrections do match the magnitude of the non-singlet QCD contributions astoundingly well to all known orders in perturbation theory, this behaviour must continue to higher (yet unknown) orders. Thus, we were able to estimate the next QCD correction (the 6-loop correction) to be of the order of 0.2 eV. Therefore, the truncation error with the current knowledge of the QCD corrections amounts to 0.002% of the observable $\Gamma(H \to \gamma\gamma)$. In QCD, the decay width including the singlet corrections at the 3-loop level and the mass corrections up to τ_t^5 at LO and NLO, reads

$$\begin{aligned}\Gamma(H \to \gamma\gamma) =& [9.120_{\text{1-loop}} + 0.156_{\text{2-loop}} + 0.008_{\text{3-loop}} \\ & - 0.002_{\text{4-loop}} + 0.0004_{\text{5-loop}} \\ & \pm 0.0002_{\text{6-loop}}]\ \text{keV} = (9.2824 \pm 0.0002)\ \text{keV},\end{aligned} \tag{7.3}$$

where in the last contribution we give our estimate of the perturbative uncertainty from the truncation of the series. However, the uncertainties due to the running coupling α_s amounts to 2 eV, one order of magnitude larger than the QCD corrections. Therefore, we argue that, for the computation of $\Gamma(H \to \gamma\gamma)$, to the date of this work, it is better to decrease the uncertainty in the parameters used in the calculation — such as α_s and m_t — than to calculate higher-order terms in perturbation theory.

REFERENCES

1 DIRAC, P. A. M. Quantum theory of emission and absorption of radiation. *Proceedings of the Royal Society London A*, v. 114, n.767, p. 243, 1927.

2 FERMI, E. Quantum theory of radiation. *Reviews of Modern Physics*, v. 4, n. 1, p. 87–132, 1932.

3 FEYNMAN, R. P. Space - time approach to quantum electrodynamics. *Physical Review*, v. 76, n. 6, p. 769–789, 1949.

4 SCHWINGER, J. S. Quantum electrodynamics. I a covariant formulation. *Physical Review*, v. 74, n. 10, p. 1439, 1948.

5 TOMONAGA, S. On a relativistically invariant formulation of the quantum theory of wave fields. *Progress of Theoretical Physics*, v. 1, n. 2, p. 27–42, 1946.

6 YANG C.-N.; MILLS, R. L.. Conservation of isotopic spin and isotopic Gauge invariance. *Physical Review*, v. 96, n. 1, p. 191–195, 1954.

7 GLASHOW S. L.. Partial symmetries of weak interactions. *Nuclear Physics*, v. 22, n. 4, p. 579–588, 1961.

8 WEINBERG, S. New approach to the renormalization group. *Physical Review D*, v. 8, n. 10, p. 3497–3509, 1973.

9 SALAM, A. Weak and electromagnetic interactions. *Conference Proceedings C*, p. 367–377, 1968. DOI: 10.1142/9789812795915_0034

10 ENGLERT, F.; BROUT, R. Broken symmetry and the mass of Gauge vector mesons. *Physical Review Letters*, v. 13, n. 9, p. 321–323, 1964

11 HIGGS, P. W. Broken symmetries and the masses of Gauge bosons. *Physical Review Letters*, v. 13, n. 16, p. 508–509, 1964.

12 FRITZSCH, H.; GELL-MANN, M.; LEUTWYLER, H. Advantages of the color octet gluon picture. *Physics Letters B*, v. 47, n. 4, p. 365–368, 1973.

13 GELL-MANN, M. A schematic model of baryons and mesons. *Physics Letters*, v. 8, n. 3, p. 214–215, 1964.

14 AAD, G. *et al.* Observation of a new particle in the search for the standard model Higgs boson with the ATLAS detector at the LHC. *Physics Letters B*, v. 716, n. 1, p. 1–29, 2012.

15 CHATRCHYAN, S. *et al.* Observation of a new boson at a mass of 125 GeV with the CMS experiment at the LHC. *Physics Letters B*, v. 716, n. 1, p. 30–61, 2012.

16 ATLAS Collaboration. A combination of measurements of Higgs boson production and decay using up to 139 fb^{-}1 of proton–proton collision data at $\sqrt{s} = 13$ TeV collected with the ATLAS experiment. 2020. Available from: https://inspirehep.net/files/417e073545cf6491ab9b909925bf51f4. Accessible at: 30 Oct. 2020.

17 GROZIN, A. G. Renormalons: technical introduction. 2003. Available from: https://arxiv.org/pdf/hep-ph/0311050.pdf. Accessible at: 23 Jan. 2020.

18 BENEKE, M. Renormalons. *Physics Reports*, v. 317, n. 1, p. 1–142, 1999.

19 GROZIN, A. G. Summing next-to-next-to-leading logarithms in $b \to c$ transitions at zero recoil. 2005. Available from: https://arxiv.org/pdf/hep-ph/0509328.pdf. Accessible at: 23 Jan. 2020.

20 CAMPANARIO, F.; LUKE, M.; ZUBERI, S. High order perturbative corrections to the determination of $|V(ub)|$ from the $P^{(+)}$ spectrum in $B \to X_u \ell \bar{\nu}_\ell$. *Physical Review D*, v. 79, n. 9, p. 094007, 2009.

21 BENEKE, M.; MARQUARD, P. NASON, P.; STEINHAUSER, M. On the ultimate uncertainty of the top quark pole mass. *Physics Letters B*, v. 775, p. 63–70, 2017. DOI: 10.1016/j.physletb.2017.10.054.

22 RAVASIO, S. F.; NASON, P.; OLEARI, C. All-orders behaviour and renormalons in top-mass observables. *Journal of High Energy Physics*, v. 01, p. 203, 2019. DOI: 10.1007/JHEP01(2019)203.

23 BOITO, D.; OLIANI, F. Renormalons in integrated spectral function moments and extractions. *Physical Review D*, v. 101, n. 7, p. 074003, 2020

24 DJOUADI, A. The anatomy of electro-weak symmetry breaking. I: the Higgs boson in the standard model. *Physics Reports*, v. 457, n. 1-4, p. 1–216, 2008.

25 PICH, A. The standard model of electroweak interactions. 2012. Available from: https://arxiv.org/pdf/1201.0537.pdf. Accessible at: 23 Jan. 2020.

26 ZYLA, P.A. *et al.* Review of particle physics. *Progress of Theoretical and Experimental Physics*, v. 2020, n. 8, p. 083C01, 2020.

27 FEYNMAN rules for QCD. 2019. Available from: https://www.itp.kit.edu/~baj/TTP2/feynman-rules.pdf. Accessible at: 19-Nov. 2020.

28 PESKIN, M. E.; SCHROEDER, D. V. An introduction to quantum field theory. Reading: Addison-Wesley, 1995.

29 JAMIN, M. QCD and renormalisation group methods. Available from: https://www.maria-laach.tp.nt.uni-siegen.de/downloads/files/2006/Jamin-2006.pdf. Accessible at: 19 Nov. 2020

30 SMIRNOV, V. A. Analytic tools for Feynman integrals. New York: Springer, 2012. (Springer tracts in modern physics, v.250)

31 HOOFT, G. 'T. Dimensional regularization and the renormalization group. *Nuclear Physics B*, v. 61, p. 455–468, 1973. DOI: 10.1016/0550-3213(73)90376-3.

32 CHETYRKIN, K.; BAIKOV, P.; KÜHN, J. The β-function of quantum chromodynamics and the effective Higgs-gluon-gluon coupling in five-loop order. 2016. Available from: https://inspirehep.net/files/346190b181a34c5c0d2c06ec52119071. Accessible at: 19 Nov. 2020.

33 LUTHE, T.; MAIER, A.; MARQUARD, P.; SCHRÖDER, Y. Five-loop quark mass and field anomalous dimensions for a general gauge group. *Journal of High Energy Physics*, v. 01, p. 081, 2017. DOI: 10.1007/JHEP01(2017)081

34 VAN RITBERGEN, T.; VERMASEREN, J.A.M.; LARIN, S.A. The four loop β-function in quantum chromodynamics. *Physics Letters B*, v. 400, p. 379–384, 1997. DOI: 10.1016/S0370-2693(97)00370-5

35 DYSON, F.J. Divergence of perturbation theory in quantum electrodynamics. *Physical Review* v. 85, p. 631–632, 1952. DOI: 10.1103/PhysRev.85.631

36 SHIFMAN, M. New and old about renormalons: in memoriam Kolya Uraltsev. *International Journal of Modern Physics A*, v. 30, n. 10, p. 1543001, 2015.

37 NEUBERT, M. Scale setting in QCD and the momentum flow in Feynman diagrams. *Physical Review D*, v. 51, p. 5924–5941, 1995. DOI: 10.1103/PhysRevD.51.5924

38 AAD, G. *et al.* Study of the spin and parity of the Higgs boson in diboson decays with the ATLAS detector. *European Physical Journal C*, v. 75, n. 10, p. 476, 2015. DOI: 10.1140/epjc/s10052-015-3685-1

39 HIGGS, P. W. Nobel Lecture: Evading the Goldstone theorem. *Reviews of Modern Physics*, v. 86, n. 3, p. 851, 2014. DOI: 10.1103/RevModPhys.86.851

40 ENGLERT, F. Nobel lecture: The BEH mechanism and its scalar boson. *Reviews of Modern Physics*, v. 86, n. 3, p. 843, 2014. DOI: 10.1103/RevModPhys.86.843

41 CERN, The Large Hadron Collider. Available from: https://home.cern/science/accelerators/large-hadron-collider. Accessible at: 18 Nov. 2020.

42 DJOUADI, A. Implications of the Higgs discovery for the MSSM. *European Physical Journal C*, v. 74, p. 2704, 2014. DOI: 10.1140/epjc/s10052-013-2704-3.

43 AABOUD, M. *et al.* Observation of $H \to b\bar{b}$ decays and VH production with the ATLAS detector. *Physics Letters B,* v. 786, p. 59–86, 2018. DOI: 10.1016/j.physletb.2018.09.013

44 PASSARINO, G.; VELTMAN, M. J. G. One Loop Corrections for e^+e^- Annihilation Into $\mu^+\mu^-$ in the Weinberg Model. *Nuclear Physics B*, v. 160, p. 151–207, 1979. DOI: 10.1016/0550-3213(79)90234-7

45 PARTICLE Data Group. Physical Constants (a major revision). 2019. Available from: https://pdg.lbl.gov/2020/reviews/rpp2020-rev-phys-constants.pdf. Accessible at: 18 Nov. 2020

46 STURM, C. Higher order QCD results for the fermionic contributions of the Higgs-boson decay into two photons and the decoupling function for the $\overline{\text{MS}}$ renormalized fine-structure constant. *European Physics Journal C*, v. 74, n. 8, p. 2978, 2014. DOI: 10.1140/epjc/s10052-014-2978-0

47 GASTMANS, R.; WU, S. L.; WU, T. T. Higgs Decay $H \to \gamma\gamma$ through a W Loop: difficulty with dimensional regularization. Available from: https://arxiv.org/pdf/1108.5322.pdf. Accessible at: 26 Aug. 2020.

48 WEINZIERL, S. Review on loop integrals which need regularization but yield finite results. *Modern Physics Letters A*, v. 29, n. 15, p. 1430015, 2014. DOI: 10.1142/S0217732314300158

49 NOGUEIRA, P. Automatic Feynman graph generation. *Journal of Computational Physics*, v. 105, p. 279–289, 1993. DOI: 10.1006/jcph.1993.1074

50 STEINHAUSER, M. MATAD: A Program package for the computation of MAssive TADpoles. *Computer Physics Communications*, v. 134, p. 335–364, 2001. DOI: 10.1016/S0010-4655(00)00204-6

51 VERMASEREN, J. A. M. New features of FORM. Available from: https://arxiv.org/pdf/math-ph/0010025.pdf. Accessible at: 19 Oct. 2020.

52 EVANS, T. 'Diagramology' — Types of Feynman Diagrams. Accessible at: https://www.imperial.ac.uk/media/imperial-college/

research-centres-and-groups/theoretical-physics/msc/current/qft/handouts/qftdiagramtypes.pdf. Accessed on: 11 Dec. 2020.

53 STEINHAUSER, M. Loop integrals, integration-by-parts and MATAD. Available from: https://www.ttp.kit.edu/~ms/capp09.pdf. Accessible at: 30 Nov. 2020.

54 MAIERHÖFER, P.; MARQUARD, P. Complete three-loop QCD corrections to the decay $H \rightarrow \gamma\gamma$. *Physics Letters B*, v. 721, p. 131–135, 2013. DOI: 10.1016/j.physletb.2013.02.040

55 STEINHAUSER, M. Corrections of $\mathcal{O}(\alpha_s^2)$ to the decay of an intermediate mass Higgs boson into two photons. *Ringberg Workshop: The Higgs Puzzle - What can We Learn from LEP2, LHC, NLC, and FMC?*. Available from: https://arxiv.org/pdf/hep-ph/9612395v1.pdf. 18 Dec. 1996.

56 BJORKEN, J. D.; DRELL, S. D. Relativistic quantum fields. *New York: McGraw-Hill*. 1965

Appendix A Notation and conventions

In this work, we use natural units,

$$c = \hbar = 1. \tag{Appendix A.1}$$

We refer to Lorentz indices as Greek letters ($\mu, \nu = 0, 1, 2, 3$); for other indices, we use Roman letters (i, j etc). Furthermore, we assume Einstein's summation, in which when two indices appears repeated in an expression, their sum is implied.

We use the metric

$$g^{\mu\nu} = (1, -1, -1, -1). \tag{Appendix A.2}$$

The derivative ∂_μ is defined as

$$\partial_\mu = (\partial_t, \boldsymbol{\nabla}). \tag{Appendix A.3}$$

The Pauli matrices read

$$\sigma_1 = \begin{pmatrix} 0 & 1 \\ 1 & 0 \end{pmatrix}, \quad \sigma_2 = \begin{pmatrix} 0 & -i \\ i & 0 \end{pmatrix}, \quad \sigma_3 = \begin{pmatrix} 1 & 0 \\ 0 & -1 \end{pmatrix}. \tag{Appendix A.4}$$

We will use the Bjorken and Drell convention[56] for the γ matrices,

$$\gamma^0 = \begin{pmatrix} 1 & 0 \\ 0 & -1 \end{pmatrix}, \quad \gamma^i = \begin{pmatrix} 0 & \sigma^i \\ -\sigma^i & 0 \end{pmatrix}, \tag{Appendix A.5}$$

where 1 (0) represents the identity (null) 2×2 matrix and σ^i are the Pauli matrices. Furthermore, we define γ^5 as

$$\gamma^5 \equiv i\gamma^0\gamma^1\gamma^2\gamma^3 = \begin{pmatrix} 0 & 1 \\ 1 & 0 \end{pmatrix}. \tag{Appendix A.6}$$

The δ-function in D dimensions reads

$$\delta^{(D)}(x - y) = \int \frac{d^D p}{(2\pi)^D} e^{ip\cdot(x-y)}. \tag{Appendix A.7}$$

Appendix B β-function coefficients

In the following, the colour factors for $SU(N)$ with generators under the standard normalization and fermions transforming according to the fundamental representation are

$$T_F = \frac{1}{2}, \quad C_A = N, \quad C_F = \frac{N_A}{2N} = \frac{N^2-1}{2N}, \quad \frac{d_A^{abcd}d_A^{abcd}}{N_A} = \frac{N^2(N^2+36)}{24},$$
$$\frac{d_F^{abcd}d_A^{abcd}}{N_A} = \frac{N(N^2+6)}{48}, \quad \frac{d_F^{abcd}d_F^{abcd}}{N_A} = \frac{N^4-6N^2+18}{96N^2}. \tag{Appendix B.1}$$

With these results, the first five coefficients of the β-function, in our definition, read[32]

$$\beta_0 = \beta_{0,NA} + \beta_{0,f} = -\frac{1}{4\pi}\left(\frac{11}{3}C_A - \frac{4}{3}T_F n_f\right), \tag{Appendix B.2}$$

$$\beta_1 = -\frac{1}{(4\pi)^2}\left(\frac{34}{3}C_A^2 - \frac{20}{3}C_A T_F n_f - 4C_F T_F n_f\right), \tag{Appendix B.3}$$

$$\begin{aligned}\beta_2 = -\frac{1}{(4\pi)^3}\Bigg(&\frac{2857}{54}C_A^3 - \frac{1415}{27}C_A^2 T_F n_f - \frac{205}{9}C_F C_A T_F n_f + 2C_F^2 T_F n_f \\ &+ \frac{44}{9}C_F T_F^2 n_f^2 + \frac{158}{27}C_A T_F^2 n_f^2\Bigg),\end{aligned} \tag{Appendix B.4}$$

$$\begin{aligned}\beta_3 = -\frac{1}{(4\pi)^4}\Bigg(&C_A^4\left[\frac{150653}{486} - \frac{44}{9}\zeta_3\right] + \frac{d_A^{abcd}d_A^{abcd}}{N_A}\left[-\frac{80}{9} + \frac{704}{3}\zeta_3\right] \\ &+ C_A^3 T_F n_f\left[-\frac{39143}{81} + \frac{136}{3}\zeta_3\right] + C_A^2 C_F T_F n_f\left[\frac{7073}{243} - \frac{656}{9}\zeta_3\right] \\ &+ C_A C_F^2 T_F n_f\left[-\frac{4204}{27} + \frac{352}{9}\zeta_3\right] + \frac{d_F^{abcd}d_A^{abcd}}{N_A}n_f\left[\frac{512}{9} - \frac{1664}{3}\zeta_3\right] \\ &+ 46C_F^3 T_F n_f + C_A^2 T_F^2 n_f^2\left[\frac{7930}{81} + \frac{224}{9}\zeta_3\right] + C_F^2 T_F^2 n_f^2\left[\frac{1352}{27} - \frac{704}{9}\zeta_3\right] \\ &+ C_A C_F T_F^2 n_f^2\left[\frac{17152}{243} + \frac{448}{9}\zeta_3\right] + \frac{d_F^{abcd}d_F^{abcd}}{N_A}n_f^2\left[-\frac{704}{9} + \frac{512}{3}\zeta_3\right] \\ &+ \frac{424}{243}C_A T_F^3 n_f^3 + \frac{1232}{243}C_F T_F^3 n_f^3\Bigg)\end{aligned} \tag{Appendix B.5}$$

and

$$\begin{aligned}
\beta_4 = -\frac{1}{(4\pi)^5}\Bigg(& C_A^5\left[\frac{8296235}{3888} - \frac{1630}{81}\zeta_3 + \frac{121}{6}\zeta_4 - \frac{1045}{9}\zeta_5\right] \\
&+ \frac{d_A^{abcd}d_A^{abcd}}{N_A}C_A\left[-\frac{514}{3} + \frac{18716}{3}\zeta_3 - 968\zeta_4 - \frac{15400}{3}\zeta_5\right] \\
& C_A^4T_Fn_f\left[-\frac{5048959}{972} + \frac{10505}{81}\zeta_3 - \frac{583}{3}\zeta_4 + 1230\zeta_5\right] \\
& + C_A^3C_FT_Fn_f\left[\frac{8141995}{1944} + 146\zeta_3 + \frac{902}{3}\zeta_4 - \frac{8720}{3}\zeta_5\right] \\
& C_A^2C_F^2T_Fn_f\left[-\frac{548732}{81} - \frac{50581}{27}\zeta_3 - \frac{484}{3}\zeta_4 + \frac{12820}{3}\zeta_5\right] \\
& + C_AC_F^3T_Fn_f\left[3717 + \frac{5696}{3}\zeta_3 - \frac{7480}{3}\zeta_5\right] - C_F^4T_Fn_f\left[\frac{4157}{6} + 128\zeta_3\right] \\
& \frac{d_A^{abcd}d_A^{abcd}}{N_A}T_Fn_f\left[\frac{904}{9} - \frac{20752}{9}\zeta_3 + 352\zeta_4 + \frac{4000}{9}\zeta_5\right] \\
& \frac{d_F^{abcd}d_A^{abcd}}{N_A}C_An_f\left[\frac{11312}{9} - \frac{127736}{9}\zeta_3 + 2288\zeta_4 + \frac{67520}{9}\zeta_5\right] \\
& \frac{d_F^{abcd}d_A^{abcd}}{N_A}C_Fn_f\left[-320 + \frac{1280}{3}\zeta_3 + \frac{6400}{3}\zeta_5\right] \\
& C_A^3T_F^2n_f^2\left[\frac{843067}{486} + \frac{18446}{27}\zeta_3 - \frac{104}{3}\zeta_4 - \frac{2200}{3}\zeta_5\right] \\
& C_A^2C_FT_F^2n_f^2\left[\frac{5701}{162} + \frac{26452}{27}\zeta_3 - \frac{944}{3}\zeta_4 + \frac{1600}{3}\zeta_5\right] \\
& C_F^2C_AT_F^2n_f\left[\frac{31583}{18} - \frac{28628}{27}\zeta_3 + \frac{1144}{3}\zeta_4 - \frac{4400}{3}\zeta_5\right] \\
& C_F^3T_F^2n_f^2\left[-\frac{5018}{9} - \frac{2144}{3}\zeta_3 + \frac{4640}{3}\zeta_5\right] \\
& \frac{d_F^{abcd}d_A^{abcd}}{N_A}T_Fn_f^2\left[-\frac{3680}{9} + \frac{40160}{9}\zeta_3 - 832\zeta_4 - \frac{1280}{9}\zeta_5\right] \\
& \frac{d_F^{abcd}d_F^{abcd}}{N_A}C_An_f^2\left[-\frac{7184}{3} + \frac{40336}{9}\zeta_3 - 704\zeta_4 + \frac{2240}{9}\zeta_5\right] \\
& \frac{d_F^{abcd}d_F^{abcd}}{N_A}C_Fn_f^2\left[\frac{4160}{3} + \frac{5120}{3}\zeta_3 - \frac{12800}{3}\zeta_5\right] \\
& C_A^2T_F^3n_f^3\left[-\frac{2077}{27} - \frac{9736}{81}\zeta_3 + \frac{112}{3}\zeta_4 + \frac{320}{9}\zeta_5\right] \\
& C_AC_FT_F^3n_f^3\left[-\frac{736}{81} - \frac{5680}{27}\zeta_3 + \frac{224}{3}\zeta_4\right] \\
& C_F^2T_F^3n_f^3\left[-\frac{9922}{81} + \frac{7616}{27}\zeta_3 - \frac{352}{3}\zeta_4\right] \\
& \frac{d_F^{abcd}d_F^{abcd}}{N_A}T_Fn_f^3\left[\frac{3520}{9} - \frac{2624}{3}\zeta_3 + 256\zeta_4 + \frac{1280}{3}\zeta_5\right] \\
& C_AT_F^4n_f^4\left[\frac{916}{243} - \frac{640}{81}\zeta_3\right] - C_FT_F^4n_f^4\left[\frac{856}{243} + \frac{128}{27}\zeta_3\right]\Bigg).
\end{aligned}$$

(Appendix B.6)